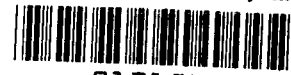# NASA TECHNICAL NOTE

$c.1$

NASA TN D-4974

PRELIMINARY INVESTIGATION OF MOMENTUM DIFFUSION BETWEEN TWO SUPERSONIC AIRSTREAMS IN THE PRESENCE OF SHOCK WAVES

by John P. Weidner and Carl A. Trexler

Langley Research Center
Langley Station, Hampton, Va.

NASA TN D-4974

PRELIMINARY INVESTIGATION OF MOMENTUM DIFFUSION

BETWEEN TWO SUPERSONIC AIRSTREAMS IN THE

PRESENCE OF SHOCK WAVES

By John P. Weidner and Carl A. Trexler

Langley Research Center
Langley Station, Hampton, Va.

NATIONAL AERONAUTICS AND SPACE ADMINISTRATION

PRELIMINARY INVESTIGATION OF MOMENTUM DIFFUSION
BETWEEN TWO SUPERSONIC AIRSTREAMS IN THE
PRESENCE OF SHOCK WAVES

By John P. Weidner and Carl A. Trexler
Langley Research Center

SUMMARY

An experimental study of compressible two-dimensional mixing between two parallel supersonic airstreams passing through oblique shock waves has been performed, and the results have been compared with those of a computerized theoretical method. This experiment was restricted to measurements of momentum diffusion in the near region, with the purpose of the study being to determine the effect of the oblique shock waves on mixing. The model consisted of a two-dimensional rectangular duct mounted in a Mach 4 airstream operating at ambient temperature. The Mach 4 stream was the primary air through the duct, while the secondary air was injected at a higher total pressure and Mach number through three isentropic nozzles set into the bottom surface of the duct. The nozzles were oriented at such an angle relative to the primary stream as to create a set of shock waves each having a turning angle of about 6.0°. Total-pressure measurements were taken across the mixing zone at several stations on either side of two crossing shock waves and were reduced to velocity profiles through the mixing zone. Average Mach numbers measured in the two streams were 3.5 and 4.4 ahead of the shock waves and 2.9 and 3.7 behind the shock waves. The theoretical solution indicated an increase in eddy viscosity in the vicinity of the shock waves. Some question remains as to whether this increased eddy viscosity is a result of the shock waves or a natural consequence of near-region mixing independent of the presence of the shock waves.

INTRODUCTION

Recent efforts in the design and development of ramjets employing subsonic and supersonic combustion have led to great interest in the turbulent mixing process in an environment typical of the ramjet combustor. The successful design of an efficient super-sonic ramjet for hypersonic speeds requires a detailed knowledge of fuel injection, mixing, and combustion of fuel with the air captured by the inlet. Adding to the complexity of such a design is the possibility of shock waves being present in the mixing and combustion region. The shock waves may result from either off-design operation of the inlet or

integration of the inlet and combustor. Analytical methods have been developed and programed for high-speed digital computers (e.g., see ref. 1) to predict diffusion between two parallel gas streams and to provide for the mixing and combustion of hydrogen and air through a diffusion-controlled combustion process.

The mixing between two parallel streams may be divided into three general regions having different mixing characteristics – the near, transition, and far regions. The length of the near region is commonly referred to as the potential core length. The potential core length begins upon contact of the two streams and ends where the smaller stream has been completely contaminated by the larger stream. Mixing in the near region proceeds at a slower rate than that in the far region, where similarity profiles exist. Also, computations in the near region are complicated by boundary-layer-induced wakes distorting the velocity profiles near the origin of injection. A theoretical treatment of the problem of an initially distorted velocity profile is given in reference 2. It has been typical of the work to date to ignore the near region, as being small compared with the overall mixing region, and to obtain correlations between the theory and experimental data (ref. 1) based only on data taken some distance from the potential core. However, reference 3 indicates that the potential core length is quite large, about 20 injector jet radii for a mass flux ratio of 1.0.

The primary purpose of this preliminary investigation was to determine the effect of shock waves when passing through a mixing region. The near-region momentum diffusion data from this experiment were correlated with results obtained by the theoretical method of reference 1 for computing mixing between two supersonic airstreams.

The present experiment employed a two-dimensional rectangular duct, having a width-height ratio of 3.85, mounted in a Mach 4 airstream operating at ambient temperature. The Mach 4 stream supplied the primary air to the duct, while the secondary air was injected at ambient temperature but at a higher total pressure and Mach number through three isentropic nozzles set into the bottom surface of the duct. The nozzles were oriented relative to the primary stream so as to create a set of shock waves each having a turning angle of about 6.0°. Pitot-pressure surveys were taken at six stations through the duct and were reduced to velocity profiles suitable for comparison with velocity profiles computed theoretically. The technique used to correlate the experimental data with the theoretical results of reference 1 was to establish input to the computer program from the first survey station 1.9 nozzle heights downstream of the injection and to compare the theoretical predictions with experimental data at other stations extending as far downstream as 16.0 nozzle heights. In this manner the mixing behavior fore and aft of the two crossing shock waves was studied.

SYMBOLS

d	exit height of first injection nozzle, 1.32 centimeters
h	duct height, 3.30 centimeters
h'	location of pitot-pressure survey probe measured from top surface of duct (see fig. 3), centimeters
h'_A	h'-location adjusted for stream-tube expansion or compression through a Prandtl-Meyer turning from p_e to p_c, centimeters
J	distance measured from the point on the velocity profile where the velocity is $0.05(V_2 - V_1)$ away from the secondary free-stream velocity to the point where the velocity is the average of the primary and secondary free-stream velocities, centimeters (see fig. 12)
K	empirical constant in eddy-viscosity model
l	length of pitot survey probe, centimeters
M	Mach number
p	local static pressure, newtons/centimeter^2
p_c	constant static pressure chosen through mixing region at a given longitudinal station, newtons/centimeter^2
p_e	static pressure estimated from measurements taken at edge of mixing region, newtons/centimeter^2
p_∞	static pressure of tunnel flow (primary airstream) ahead of model, 0.638 newtons/centimeter^2 for $p_{t,2}/p_{t,1}$ of 2.67 and 3.34, and 0.553 newtons/centimeter^2 for $p_{t,2}/p_{t,1}$ of 4.0
p_p	measured pitot pressure, newtons/centimeter^2
p_t	total pressure, newtons/centimeter^2

$p_{t,calc}$ total pressure calculated through mixing region, newtons/centimeter^2

$p_{t,\infty}$ total pressure of tunnel flow (primary airstream) ahead of model

$r_{1/2}$ distance from the injection-nozzle center line to the point on the velocity profile where the velocity is the average of the primary and secondary free-stream velocities, centimeters (see fig. 12)

S streamline axis

s distance along S-axis, centimeters

s' particular point on S-axis at which typical velocity profile is presented in figure 12

T static temperature, degrees Kelvin

T_t total temperature, degrees Kelvin

$T_{t,e}$ estimated local total temperature, degrees Kelvin

V velocity computed through the mixing region, meters/second

V_A computed velocity (V) adjusted through a Prandtl-Meyer turning from p_e to p_c, meters/second

V_∞ velocity of tunnel flow (primary airstream) ahead of model, 666 meters/second

W mixing width, centimeters

w duct width, 12.7 centimeters

w' location of static-pressure orifices (see fig. 3), centimeters

x longitudinal distance through duct originating at exit plane of first injection nozzle (see fig. 3), centimeters

y distance from streamline axis of first injection nozzle (see fig. 12), centimeters

y_i index separating velocity profiles in y-direction, centimeters

Δy width of velocity profile where the velocity is within $0.01(V_2 - V_1)$ of the free-stream velocity, centimeters

δ_b effective incident shock wave originating from second injection nozzle, degrees turning

δ_c effective reflected shock wave originating from first injection nozzle, degrees turning

ϵ eddy viscosity, newton-second/meter^2

ρ_∞ density of tunnel flow (primary airstream) ahead of model, 0.329 kilogram/meter^3 for $p_{t,2}/p_{t,1}$ of 2.67 and 3.34, and 0.285 kilogram/meter^3 for $p_{t,2}/p_{t,1}$ of 4.0

ρV mass flow per unit area, kilograms/meter^2-second

$\left(\rho V\right)_{\mathcal{C}}$ mass flow originating on center line of first injection nozzle (maximum ρV through mixing region for present experiment), kilograms/meter^2-second

$(\rho V)_{min}$ minimum mass flow within mixing region at a given longitudinal station, kilograms/meter^2-second

Subscripts:

a   conditions ahead of δ_b and δ_c

d   conditions behind δ_b and δ_c

1   primary air conditions at edge of mixing region (fig. 12)

2   secondary air conditions at edge of mixing region (fig. 12)

APPARATUS

Test Section

The model base plate (fig. 1) spanned the 22.9-cm by 22.9-cm rectangular test section of a Mach 4.05 channel which supplied the primary air. Test-section total pressures

ranged from 89.6 to 103.4 N/cm^2 with a Reynolds number per meter between 4.3×10^7 and 5.0×10^7. Test-section side windows 30.5 cm in diameter permitted visual and schlieren observation of the flow in the mixing region.

Secondary air was supplied to the model through pipes extending through both sides of the test section (see fig. 2). The secondary-air total pressure ranged between 276 and 359 N/cm^2. Both the primary and secondary streams were at approximately ambient total temperature. Operation was on a continuous-flow basis, requiring a maximum total air supply of 18 kg/sec.

Model

A simplified sketch of the model assembly is shown in figure 1. All the leading-edge surfaces were 10° wedges, with the sidewall leading edges swept 45° to the oncoming air. The primary flow passage consisted of a two-dimensional rectangular duct 12.7 cm wide and 3.3 cm high. The upper and side surfaces of the duct were corrected for an estimated boundary-layer growth to yield dimensions at the end of the duct of 13.3 cm and 3.4 cm. The basic components making up the model were a 22.9-cm-wide base plate, three two-dimensional nozzles set in a recess in the base plate to form the lower surface of the primary airflow duct, two sidewalls 1.27 cm thick containing observation windows, and a 1.27-cm-thick top plate. Photographs of the model at various stages of assembly may be seen in figure 2. The three nozzles were set at angles relative to the primary airflow of 6°, 11°, and 16°. The nozzles were attached to the sidewalls, were bolted to the base plate at two points across the 12.7-cm duct (to prevent nozzle deformation), and were vertically adjustable in order to obtain the desired Mach number at the exit of each injection nozzle.

Instrumentation

The stagnation pressure and temperature of the primary air were measured in the 40.6-cm-diameter supply pipe upstream of the test section by using a total-pressure probe and a standard iron-constantan thermocouple. The total temperature of the secondary air was measured in the 7.62-cm-diameter supply pipe upstream of the model; the stagnation pressure was measured by a pressure tube located in a region of low velocity in the settling chamber within the model (see fig. 1). Flow rates of the secondary air were measured in an upstream venturi by assuming a flow coefficient of 1.0. This coefficient was determined on the basis of calibrations of other venturis of similar design.

The model was instrumented with static-pressure orifices at the exits of the secondary-air injection nozzles (see fig. 1) and along the top plate (see fig. 3). The table in figure 3 gives the location of the static-pressure orifices along the top plate. Pitot-pressure profiles were measured across the flow field at each of the two access locations

6

indicated in figure 3. Because of the test-section construction, only two pitot-probe access locations were available through the model top plate; thus, several probes of different lengths were required to obtain pressure surveys at the desired stations. A sketch of a typical pitot-pressure probe along with a listing of probe lengths required is given in figure 4. The probe tip was flattened to an inside height of 0.013 cm. The probes were made rigid by soldering shim stocks to the undersides. The front portions of the probes were alined parallel to the predicted flow direction at the station to be surveyed.

Procedure

Tests were conducted at three combinations of primary- and secondary-airstream total pressures for each of the survey stations (x stations of 2.54, 7.62, 11.94, 18.54, 19.84, and 21.10 cm). Primary-airstream total pressures of 89.6, 103.4, and 103.4 N/cm^2 were used with secondary-airstream total pressures of 358.5, 344.8, and 275.8 N/cm^2, respectively, to yield secondary- to primary-airstream total-pressure ratios of 4.00, 3.34, and 2.67. All the pressure orifice and thermocouple data were taken before and after each pitot-pressure survey. For a constant total-pressure ratio but different survey probe locations, static orifice data in the duct upstream of the probe were compared and found to be unchanged.

RESULTS AND DISCUSSION

Theoretical and Experimental Flow Fields

The injection nozzles for the secondary flow were designed to be isentropic and fully expanded behind the shock wave at $p_{t,2}/p_{t,1} = 3.34$. The resulting shock system of the predicted inviscid flow field is shown in figure 5(a) along with a tabulation of the predicted static pressures (p), total pressures (p_t), and Mach numbers between the shock waves in the primary and secondary supersonic streams, with the mixing phenomena ignored. The primary and secondary streams are divided by the streamline originating at the upper trailing edge of the first nozzle, as indicated in figure 5(a) by a dotted line. For clarity the weaker shock and expansion waves, created by the intersection of the major shock waves with the dividing streamline, are not shown in this figure. In order to study the near-region mixing problem, data were considered no longer useful for this study when the mixing either progressed upward into the boundary layer on the top surface of the duct or downward into the wake region created by the trailing edge between the first and second nozzle. Figure 5(b) is a sketch of the experimentally determined flow field, with the mixing zone between the first injection nozzle and the primary airstream replacing the dividing streamline. Useful mixing data were taken at three stations upstream and downstream of the intersection between the second shock wave and the reflection of the first shock wave. Since the injection nozzles and subsequent shock

system were designed for a ratio of secondary- to primary-airstream total pressure of 3.34, operation at $p_{t,2}/p_{t,1}$ of 4.00 and 2.67 represented off-design conditions at which the injection nozzles were underexpanded or overexpanded.

<center>Static-Pressure Distributions</center>

An attempt was made to measure static pressure through the mixing zone by replacing the tip of the pitot probes with a tip suitable for measuring static pressure, but the accuracy was questionable upstream of the shock waves where the static pressures were low. The local static pressures above and below the mixing zone were therefore determined by using the pitot readings, the predicted total pressures listed in figure 5(a), and the tables of reference 4. It is believed that this procedure provided the most accurate prediction of the actual static pressures and Mach numbers that could be obtained. The experimental Mach numbers were not necessarily the same as the theoretical Mach numbers because extraneous expansion or compression waves passed through the mixing zone. When these waves produced a difference between the local static pressures on either side of the mixing zone at any given survey location, the static-pressure profile through the mixing zone was estimated by examining the pitot-pressure profile for discontinuities that might have caused a static-pressure change.

The estimated static pressure in the flow field on either side of the mixing zone along with the average of the static pressures measured along the center line and on either side of the center line of the top surface of the duct are plotted in figure 6 as functions of x/d (see solid and dashed curves, respectively). In addition, the static-pressure distribution predicted along the top surface of the rectangular duct from the inviscid design of figure 5(a) is given by the straight dashed lines in figure 6(a). As shown in figure 6(a), the static pressures measured on the top surface of the duct are in good agreement with the predicted pressure ahead of the first shock wave, but increase above the predicted pressure behind the first shock wave before dropping back to the predicted level. The maximum pressure rise behind the first shock, occurring at x/d = 10.5, represents the pressure rise that would be caused by an additional incident and reflected shock wave having a turning angle of 4.0°. The difference between the static pressure measured at the exit of the first nozzle and the pressure estimated on either side of the mixing region at x/d = 1.9 corresponds to the pressure rise across a shock wave having a turning angle of 3.5°. The indication is that a shock wave was formed along the lower surface of the first nozzle in the region upstream of x/d = 0, as designated in figure 5(b), and that this wave was followed by an expansion wave causing a return to the predicted static pressure behind the first shock wave.

Knowledge of the presence of this extra shock wave and expansion wave influenced the fairing of the solid curve (fig. 6(a)) through the static pressures estimated on either

8

side of the mixing zone such that the static pressure peaks between values of x/d of 7.8 and 8.8 and then drops through an expansion at a value of x/d of about 9.5 to the same pressure that existed at $x/d = 1.9$. The scatter in the static-pressure points on either side of the mixing zone at values of x/d of 5.8 and 9.0 was caused by the extra shock or expansion wave passing through the mixing zone at these stations. Repeated tests indicated that static pressures at these stations were very sensitive to slight changes in the location of the extra shock and expansion waves formed within the first nozzle. Similar trends were present at the conditions $p_{t,2}/p_{t,1} = 4.0$ and $p_{t,2}/p_{t,1} = 2.67$ in figures 6(b) and 6(c), respectively. The overstrengths of the extra shock wave and expansion wave formed within the first nozzle at values of $p_{t,2}/p_{t,1}$ of 4.00, 3.34, and 2.67 were estimated to be about 4.5°, 3.5°, and 1.5° of flow turning, respectively.

Mach Number Distributions

Mach numbers along the top surface of the duct and on either side of the mixing zone, computed from the static pressures presented in figure 6 and the predicted total pressures listed in figure 5, are shown in figure 7 as functions of x/d. Evidence of the extra shock and expansion waves developed in the first nozzle may be seen in figure 7(a) for $p_{t,2}/p_{t,1} = 3.34$; behind the first shock wave the Mach number along the top surface of the duct decreases well below the predicted Mach number and then increases to the predicted Mach number before the second shock wave is encountered. Similar results are given in figures 7(b) and 7(c) for the off-design conditions at $p_{t,2}/p_{t,1} = 4.0$ and $p_{t,2}/p_{t,1} = 2.67$. The differences between the Mach numbers in the primary and secondary airstreams at values of $p_{t,2}/p_{t,1}$ of 4.0, 3.34, and 2.67 are approximately 1.00, 0.90, and 0.75, respectively, with resulting ratios of secondary- to primary-airstream mass flux of 1.59, 1.50, and 1.38, respectively. Typical static-pressure and Mach number variations across the top surface of the duct are given in figure 8 for $p_{t,2}/p_{t,1} = 3.34$. This figure indicates little departure from two-dimensional flow. The greatest changes across the duct occur at $x/d = 8.75$ and $x/d = 17.4$, which are located close to regions of rapidly changing pressure.

Schlieren Photographs

Schlieren photographs are shown in figure 9 at the three operating conditions corresponding to values of $p_{t,2}/p_{t,1}$ of 4.00, 3.34, and 2.67 and also at $p_{t,2}/p_{t,1} = 3.34$ with three different probes installed in the model survey stations at x/d of 5.8, 9.0, and 15.0. The shock system within the duct is viewed through the first four of the five windows mounted in the sidewalls (fig. 1). The incident and reflected shock waves originating from the first nozzle appear in the most upstream window. The mixing region between the primary stream and the secondary stream of the first nozzle is indicated in figure 9(a).

Experimental Mixing Profiles

Velocity profiles were computed through the mixing zone from measured pitot-pressure surveys and from static pressures that were estimated on either side of the mixing zone (fig. 6) and faired through the mixing zone. The average measured total temperatures used in the calculations were 289° K in the primary stream and 297° K, 295° K, and 293° K at values of $p_{t,2}/p_{t,1}$ of 4.00, 3.34, and 2.67, respectively, in the secondary stream. The total temperature profile through the mixing zone was assumed to have a shape similar to a near-region concentration profile predicted by reference 1.

Since the computer program of reference 1 required a constant static pressure normal to the flow direction, it was desirable to have each experimentally derived velocity profile correspond to a constant static pressure. Therefore, each point of each experimentally derived velocity profile was subjected to an isentropic expansion or compression sufficient to adjust the original static pressure to a constant static pressure shown by the symbols in figure 10. To maintain the conservation of mass, this adjustment yielded a change in both the velocity at each point and the distance between each point. The data reduction process was computerized from equations in reference 4, and the results are tabulated in appendix A. This static-pressure adjustment had only a small effect on the velocity profiles, as shown by the small difference in V and V_A in appendix A.

The velocity profiles adjusted to a constant static pressure are plotted in figure 11 for values of $p_{t,2}/p_{t,1}$ of 4.00, 3.34, and 2.67 for all the survey stations. The dashed lines indicate the adjusted velocities ascribed to the primary and secondary streams outside the mixing region. The decrease in velocity between the primary and secondary streams is a result of the boundary-layer wake formed on the upper and lower surfaces of the top portion of the first injection nozzle. This wake was large enough to produce a decrease in velocity from the primary-stream velocity at the most downstream survey station of $x/d = 16.0$. There was little difference noted between the mixing rates at values of $p_{t,2}/p_{t,1}$ of 4.0, 3.34, and 2.67. However, all three conditions are presented here and the data are subsequently compared with the theoretical results in order to better validate the repeatability of the data and to aid in establishing trends between the data and theoretical calculations.

Theoretical Mixing Models

A method for predicting two-dimensional or axisymmetric mixing between two gases was developed and programed to operate on a high-speed digital computer. A detailed description of the theoretical method is given in reference 1. The program was intended to predict diffusion-controlled equilibrium combustion between hydrogen and air for supersonic combustion applications, but will calculate the mixing between two airstreams by providing for a mixture of oxygen and nitrogen in both streams. A schematic of the

flow field used by the computer program is given in figure 12. Input parameters required by the computer program are the initial velocity, temperature, and concentration profiles extending from the center of the injected gas stream to the free-stream conditions of the primary fluid. The axial static pressure is specified by a third-order polynomial written along the S-axis while the static pressure in the y-direction (at any particular value of s) is required to be constant. (See fig. 12.) The S-axis lies along the streamline originating at the center of the injection nozzle. Constant input parameters required are the turbulent Prandtl number, the Lewis number, and an empirical eddy-viscosity coefficient (K). The basic operation of the program solution is to separate the flow field into stream tubes equal to the number of input points along the velocity profile and to perform the required computations on each stream tube in the axial direction at small increments of s.

For a given set of initial input conditions, the parameter that controls the rate of mixing between the two parallel streams is the eddy viscosity ϵ. The eddy-viscosity model employed by the computer program as described in reference 1 is given by

$$\epsilon = Kr_{1/2}(\rho V)_{\mathbb{C}}$$

where K is the empirical eddy-viscosity coefficient and is input to the computer program as a constant. The parameter $r_{1/2}$ is a distance measured in the y-direction and is defined and computed by the computer program as the distance measured from the streamline originating at the center of the injection nozzle (S-axis) to the point on the velocity profile where the velocity is the average of the primary and secondary free-stream velocities. The factor $(\rho V)_{\mathbb{C}}$ is taken along the S-axis (at y = 0) and is initially computed from the input velocity and temperature profiles. Within the near region the value of $(\rho V)_{\mathbb{C}}$ is not affected by the mixing process but is only a function of the axial static pressure. In using this viscosity model for the two-dimensional near-region mixing solution, the initial value of $r_{1/2}$ can be selected arbitrarily; however, then a value of the constant K must be selected which is compatible with the value of $r_{1/2}$ in order to obtain a correct prediction of the mixing rate. Thus, the solution is dependent on the initial value of the product $Kr_{1/2}$. Therefore, for a given mixing situation and with $r_{1/2}$ defined by the radius or half-height of the injection nozzle, the required value of K becomes a function of the geometric size of the injection nozzle. It should be noted that this viscosity model was formulated from considerations of the far-region mixing only by ignoring the near region as being small.

Unpublished results of a Langley Research Center investigation of the axisymmetric mixing between two airstreams within the near and far regions without shock waves indicate that theoretical solutions based on the viscosity model defined by the parameter $r_{1/2}$ will not allow for the required increase in ϵ to predict the experimental mixing data for both near and far regions by the use of a constant value of K. A mixing parameter

11

J has been suggested as a replacement for $r_{1/2}$ to provide a more reasonable solution for both the near- and far-region mixing. The parameter J, shown in figure 12, is defined as the distance measured from the point where the velocity is $0.05\left(V_2 - V_1\right)$ away from the secondary free-stream velocity to the point where the velocity is the average of the primary and secondary free-stream velocities. The immediately obvious difference between the parameters J and $r_{1/2}$ is that within the near region the parameter J is dependent only on the shape of the velocity profile through the mixing region while the parameter $r_{1/2}$ is a function of both the velocity profile and the height or radius of the injection nozzle. Thus, the viscosity model defined by the parameter J is considered to be more consistent with the near-region mixing phenomena. The experimental data of this investigation have been correlated with theoretical solutions based on both the parameters $r_{1/2}$ and J.

Computer Program Input

To adapt the theoretical flow model to the present experiment, the s-coordinate was located along the center streamline of the secondary-stream nozzle, with a resulting value of $r_{1/2}$ at x/d of 0 equal to the half-height of the nozzle (0.66 cm). Experimental velocity and temperature profiles at the most upstream survey station of x/d = 1.9 were used as input to the computer program, and the experimental data at the downstream stations were correlated with the theoretical predictions. At x/d = 1.9 the computed value of $r_{1/2}$ was 0.592 cm, while the computed value of J at $p_{t,2}/p_{t,1} = 3.34$ was 0.061 cm. Figure 13 gives the experimental velocity data from which the input to the computer program was derived. The velocity profile generated by the computer solution at the initial station is also presented for comparison. With a good estimation of the velocity profile through the boundary-layer wake at x/d = 0, the computer solution could be initiated at that station. However, for the purpose of determining as accurately as possible the appropriate value of the empirical eddy-viscosity coefficient from the experimental data and the subsequent quality of the theoretical predictions at the downstream survey stations, the solution was initiated by using the most upstream experimentally derived velocity profiles. All the mixing data were correlated with the theory by comparing the velocity profiles in the nondimensionalized form as given in figure 13. It should be noted that the origin of the y_i-coordinate is arbitrary and that the velocity profiles corresponding to the three values of $p_{t,2}/p_{t,1}$ are arbitrarily positioned relative to each other to facilitate comparison at the different total-pressure ratios. For these correlations the Prandtl number and Lewis number were set equal to 0.7 to yield a Schmidt number equal to unity.

The axial static-pressure distributions used in the theoretical mixing calculations are given in figure 10. The symbols represent the constant static pressures across the

mixing zone associated with the velocity profiles of figure 11. Two sets of static-pressure distributions were considered in attempts to correlate the theoretical method with the data for the purpose of determining the sensitivity of the theoretical calculations to the pressure path. These static-pressure distributions are presented in figure 10 as methods A and B. Method A utilized a continuous static-pressure rise throughout the duct, whereas in method B the static pressure was held constant starting at $x/d = 6.1$, then underwent a step change at $x/d = 12.5$ where the shock waves crossed in figure 5(a), and was again held constant behind the shock system. The step change of method B at $x/d = 12.5$ represents the pressure rise through the two shock waves separating bays 2 and 3 from bays 6 and 7 (fig. 5(a)). The pressure rise was negotiated by taking each point of the flow field from the computer program output at $x/d = 12.5$ and calculating across two shock waves of sufficient strength to accomplish the desired static-pressure rise. The procedure for these calculations and a table of results obtained are given in appendix B.

Method B of handling the theoretical calculations through the duct having internal shock waves is considered to be the more realistic, particularly since figure 6 indicates that the static pressure ahead of the shock system is about the same as the pressure occurring at $x/d = 1.9$. Method A is considered a simplified means of effecting the theoretical calculations. In both methods at each survey station where the static pressure used in the theoretical computations differed from the static pressure associated with the experimental data (symboled data of fig. 10), the velocity profiles computed by the theory were isentropically adjusted to correspond to the static pressure indicated by the symboled data. This operation is similar to that performed on the data of figure 11 and results in a slight change in both the velocity and the y_i-coordinates of the velocity profile.

Correlations of Theoretical Mixing Computations

With Experimental Data

Correlating the theoretical solutions based on the parameter $r_{1/2}$ with the data ahead of the shock system (at stations x/d of 5.8 and 9.0) yielded a value for the empirical eddy-viscosity constant K of 0.0013. The eddy viscosities computed from methods A and B were essentially the same, and no plottable difference was noted between the velocity profiles from the two methods upstream or downstream of the shock system. The theoretical velocity profiles computed from method B ahead of the shock system and the velocity profiles computed behind the shock waves as given in appendix B are shown in figure 14. The stream-tube compression and associated decrease in mixing width caused by crossing the shock waves may be seen by comparing the velocity profiles to either side of the shock system. The tables of appendix B indicate an average turning through each

of the two shock waves of about 5.1°. If the static pressure ahead of the shock waves (fig. 10) had been held constant and equal to the static pressure at $x/d = 1.9$ the computed turning through each of the two shock waves would have been increased by 0.75° to 1.0°. The similar results obtained from the theoretical solutions using the axial static-pressure distributions of methods A and B (fig. 10) could be attributed to the low entropy gain associated with the shock waves. If higher entropy gains were encountered through stronger shock waves, the solutions of methods A and B might not agree as well.

Comparisons between the theoretical velocity profiles and the experimental data points based on the parameter $r_{1/2}$ in the eddy-viscosity model and a value of K of 0.0013 upstream, downstream, and through the shock wave region are given in figure 15. Satisfactory agreement was obtained between the theory and experimental data upstream of the shock waves (figs. 15(a) and 15(b)) with respect to both the mixing width and the velocity decrement. However, poor correlations were obtained between the theoretical velocity profiles and experimental data at stations of x/d of 14.0, 15.0, and 16.0 downstream of the shock waves (figs. 15(c), 15(d), and 15(e)) because the theoretical solution did not provide for enough mixing to match either the velocity decrement or the mixing width of any of the experimental velocity profiles behind the shock waves. The immediate conclusion that may be drawn is that the rate of mixing is influenced by the shock waves. This influence could either extend downstream of the shock waves or be locally confined to the area of the interaction between the shock waves and the mixing region.

Two additional attempts were made to correlate the data behind the shock waves with the theoretical solution based on the parameter $r_{1/2}$ in the eddy-viscosity model. The first assumed an influence of the shock waves on the rate of mixing extending downstream of the shock waves. The empirical eddy-viscosity coefficient K was thus increased, starting at $x/d = 12.5$, to the value required to obtain the best correlation at the survey station of $x/d = 15.0$. The resultant K increased by a factor of about 5 from 0.0013 to 0.0061, with a corresponding increase occurring in the eddy viscosity ϵ behind the shock waves. The resulting axial eddy-viscosity distributions are given in figure 16 by the solid lines up to $x/d = 10.2$ and by the dashed curves beyond $x/d = 10.2$. However, the resultant theoretical velocity profiles, compared with the experimental data in figure 17, underpredicted the mixing width at $x/d = 14.0$ (fig. 17(a)) and overpredicted the mixing width at x/d of 16.0 (fig. 17(c)). It appears that the value of K, and thus the mixing rate in the region of the survey stations, is too high to simultaneously correlate the data at stations x/d of 14.0, 15.0, and 16.0.

The final attempt to correlate the data behind the shock waves with the theoretical solution based on $r_{1/2}$ assumed only a local influence of the shock waves on the rate of mixing confined to the area where the shock waves cross the mixing region. The empirical eddy-viscosity coefficient K was thus increased for a distance corresponding to the

14

sum of the lengths of the two segments of mixing region intercepted by the two shock waves (a distance x/d of about 3.6), while K remained equal to 0.0013 on each side of this region. The increased value of K over the interaction region x/d of 3.6 was determined so as to again obtain the best correlation at the survey station of $x/d = 15.0$. The required value of K increased by a factor of 3.5 from 0.0013 to 0.0046, with a similar increase occurring in the eddy viscosity over the region of interaction. The theoretical solution yielded axial eddy-viscosity distributions as given in figure 16 by the solid curves. The resulting theoretical velocity profiles are compared with the experimental data at values of x/d of 14.0, 15.0, and 16.0 in figure 18. It is believed that these correlations represent the best that may be obtained from a theoretical solution as given by the method of reference 1. The localized increase in mixing rate in the vicinity of the shock waves thus appears to be the most correct representation for the extent of the effect of the shock waves on the mixing based on the parameter $r_{1/2}$ in the eddy-viscosity model. In this regard, reference 5 represents an early attempt to determine the effect of shock waves on mixing; a localized increase in mixing through a normal shock wave was found.

The theoretical solutions employing the eddy-viscosity model based on the parameter J produced acceptable correlations with the data both upstream and downstream of the shock system at a constant value of K in the eddy-viscosity model. The resulting axial eddy-viscosity distributions obtained with $K = 0.0065$ are given in figure 19 and show a continuously increasing eddy viscosity with axial distance through the duct, the implication being that the shock waves have no effect on mixing. This solution is in contrast to the optimum theoretical solution based on the parameter $r_{1/2}$ given by the solid lines of figure 16. The parameter $r_{1/2}$ had allowed little change in eddy viscosity with x/d, other than that imposed by a change in the constant K, to account for a localized increase in the mixing rate attributed to the presence of the shock waves. At $p_{t,2}/p_{t,1} = 3.34$ the two solutions yield eddy viscosities from about 3.4×10^{-3} to 12×10^{-3} N-sec$/$m^2, while solutions correlated with the subsonic data of reference 6 and the supersonic data of reference 7 (both being two-dimensional near-region air-in-air mixing data) yield eddy viscosities of 7×10^{-3} and 4×10^{-3} N-sec$/$m^2, respectively.

The velocity profiles from the theoretical solutions based on the parameter J are given in figure 20 by the solid curves and are also compared with the best previous theoretical solution based on the parameter $r_{1/2}$ from figures 15(a) and (b) and figure 18. Little difference was noted between the two theoretical solutions at stations of x/d of 9.0 and 15.0. It is believed that the dashed curves provided the better correlations with the experimental data at x/d of 5.8, 14.0, and 16.0; however, the overall correlations represented by the solid curves are good and the parameter J should be considered in further investigations.

The integral of the eddy viscosity is a measure of the amount of mixing that has taken place to a point along the path of mixing and is given for the solutions based on the parameters J and $r_{1/2}$ in figure 21. The similarity between the velocity profiles of the two solutions given in figure 20 is reflected by the proximity of the solid and dashed curves given in figure 21; where the solid and dashed curves come together, velocity profiles from the two solutions are essentially the same. The nearly constant eddy viscosities of the solution based on the parameter $r_{1/2}$ are reflected by the straight-line segments forming the dashed curves.

Having obtained the aforementioned theoretical solutions, it is possible to predict eddy-viscosity distributions as given by other viscosity models. As a matter of interest, integrated eddy viscosity and eddy-viscosity distributions corresponding to several eddy-viscosity models are presented in figure 22. Because a value of the integrated eddy viscosity represents a unique solution of the velocity profile for a given flow condition, it is possible to define the data points in figure 22(a) as the predicted integrated eddy viscosity required to correlate the experimental velocity profiles. The third model is a classical form of the viscosity model and gives the eddy viscosity as proportional to the product of the mixing width (W) and the difference between the maximum and minimum values of ρV within the mixing region. The correlation obtained for this model is poor when compared with the results for the first, second, or fourth viscosity model. The fourth viscosity model was formulated by assuming the viscosity to be proportional to x/d raised to some power and solving for the exponent of x/d and the constant K to obtain the best agreement with the data. This model correlated the data well because of the two variables within the equation. The fifth model is of the simplest form and assumes the eddy viscosity to be a constant; this model yields the poorest correlation with the data points. The fifth eddy-viscosity model could approach the results of the first eddy-viscosity model by setting the eddy viscosity equal to a constant of 0.0036 upstream and downstream of the shock region, with a step increase to 0.011 in the region of the shock waves.

Summary of Mixing Correlations

Theoretical mixing solutions based on different eddy-viscosity models have been presented and successfully correlated with experimental velocity data upstream and downstream of two shock waves. The first solution, based on the parameter $r_{1/2}$ in the eddy-viscosity model, yields a near-constant eddy viscosity for a given value of the empirical constant K in the eddy-viscosity model and requires an increase in K and thus in eddy viscosity in the region of the shock waves to correlate with the experimental data. This result implies a contribution of the shock waves on the local rate of mixing

possibly brought about by highly distorted velocity profiles in the region where the shock waves pass through the mixing zone. However, the second solution, based on the parameter J in the eddy-viscosity model, and the fourth viscosity model presented in figure 22 yield a continuously increasing eddy viscosity at a constant value of K to produce velocity profiles that will correlate with the experimental data. These solutions thus indicate a need for an increase in eddy viscosity, but not necessarily an increase that is brought about by shock waves. The question that remains is whether the increase in eddy viscosity given in figures 16 and 19 is required by the presence of the shock waves or is a normal consequence of the near-region mixing phenomena. It is believed that comparison between experimental mixing data taken in a similar flow field with and without shock waves is required to resolve this question.

A summary of the theoretical solutions and experimental data is given in figure 23 in the form of the width of the velocity profile as a function of the distance through the duct. In order to isolate the effect of static pressure on the width of the velocity profiles, the mixing widths predicted by the theoretical curves and experimental data of figures 13, 15, and 20 were isentropically adjusted, satisfying the conservation of mass, to the constant static pressures given by the solid curves of figure 10 upstream and downstream of $x/d = 12.5$. The solid curve of figure 23 upstream of the shock region and the lower solid curve downstream of the shock region correspond to the average theoretical mixing width based on the parameter $r_{1/2}$ and a constant value of K. The upper solid curve downstream of the shock region represents the solution obtained by increasing the value of K in the region of the shock waves (see fig. 16). The dashed curve represents the theoretical solution based on the parameter J in the eddy-viscosity model. The difference between the two solid curves downstream of the shock region corresponds to a 40-percent increase in the mixing width which was required to correlate the data; this result implies that the shock waves accelerate the mixing. However, as was stated previously and is supported in this figure, the solution based on J in the eddy-viscosity model provides a reasonable correlation with the experimental data when K is held constant over the full length of the mixing region; this result implies that the shock waves had no effect on the mixing.

CONCLUSIONS

The experimental investigation of near-region momentum diffusion between two supersonic streams in the presence of shock waves and subsequent correlations with computerized theoretical predictions yielded the following results:

1. Good correlations were obtained between the experimental data ahead of the shock waves and the theoretical solution based on the eddy-viscosity model involving the

distance from the injection-nozzle center line to the point where the velocity is the average of the primary and secondary free-stream velocities. A value of 0.0013 was required for the empirical constant in the eddy-viscosity model. The solution yielded a nearly constant eddy viscosity upstream of the shock waves. In order to correlate this theoretical solution with the experimental data downstream of the shock waves, it was necessary to increase the eddy-viscosity constant by a factor of 3.5 over the total longitudinal distance within the mixing region intercepted by the two shock waves (3.6 nozzle-exit heights). This increase in the eddy-viscosity constant produced a 40-percent increase in the mixing width and resulted in a correlation with measured values.

2. An acceptable correlation was obtained between the experimental data and the theoretical solution based on a second eddy-viscosity model involving the distance measured from the edge of the mixing region next to the secondary flow to the point where the velocity is the average of the primary and secondary free-stream velocities. This solution required a value of eddy-viscosity constant of 0.0065, which was held constant throughout the full length of the mixing region without regard to the presence of the shock waves. The second model yielded a continuously increasing eddy viscosity throughout the length of the duct.

3. The two theoretical solutions based on different eddy-viscosity models yield an increase in eddy viscosity, but place contradicting emphasis on the presence of the shock waves. The first solution yields a relatively constant eddy viscosity with a local increase in eddy viscosity required by the presence of the shock waves, while the second solution implies a general requirement of increasing eddy viscosity within the near region independent of the shock waves.

4. The two theoretical solutions yielded an average eddy viscosity upstream of the shock waves of about 3.4×10^{-3} N-sec/m^2 and in the vicinity of the shock waves of about 12.0×10^{-3} N-sec/m^2. Theoretical solutions correlated with supersonic and subsonic data of two previous investigations yielded eddy viscosities of about 4×10^{-3} and 7×10^{-3} N-sec/m^2, respectively.

Langley Research Center,
National Aeronautics and Space Administration,
Langley Station, Hampton, Va., August 6, 1968,
722-03-00-04-23.

APPENDIX A

TABULATION OF DATA THROUGH MIXING REGION

(a) Region ahead of shock waves; $x/d = 1.9$

h'	p_p	p_e	$T_{t,e}$	$p_{t,calc}$	M	V	V_A	$\dfrac{V_A - V_{A,1}}{V_{A,2} - V_{A,1}}$	h'_A
$p_{t,2}/p_{t,1} = 4.00$; $p_{t,1} = 88.3$, $p_{t,2} = 353.7$, $T_{t,1} = 288.1$, $T_{t,2} = 296.4$, $p_c = 1.16$									
2.580	18.75	1.18	288.1	85	3.46	641	642	-0.007	2.580
2.625	18.75	1.18	288.1	85	3.46	641	642	-.007	2.625
2.671	18.75	1.18	288.1	85	3.46	641	642	-.007	2.674
2.717	18.48	1.18	288.1	82	3.43	640	640	-.034	2.719
2.768	17.17	1.18	288.2	68	3.31	632	633	-.172	2.770
2.844	13.20	1.18	289.2	36	2.88	604	605	-.702	2.846
2.895	10.55	1.18	290.5	22	2.56	578	579	-1.211	2.897
2.935	9.24	1.18	291.8	17	2.39	561	562	-1.529	2.939
2.976	8.69	1.18	293.1	15	2.31	553	555	-1.670	2.981
3.027	10.45	1.18	294.6	22	2.55	580	581	-1.157	3.032
3.062	14.00	1.18	295.5	42	2.97	618	619	-.447	3.067
3.149	28.68	1.18	296.4	266	4.30	687	687	.866	3.154
3.174	30.89	1.18	296.4	328	4.47	692	693	.968	3.182
3.199	31.34	1.18	296.4	342	4.50	693	694	.987	3.207
3.245	31.37	1.18	296.4	343	4.50	693	694	.988	3.253
3.291	31.20	1.18	296.4	337	4.49	693	693	.981	3.298
$p_{t,2}/p_{t,1} = 3.34$; $p_{t,1} = 102.7$, $p_{t,2} = 342.0$, $T_{t,1} = 288.1$, $T_{t,2} = 294.2$, $p_c = 1.20$									
2.605	20.68	1.25	288.1	99	3.52	644	646	-0.015	2.605
2.656	20.82	1.25	288.1	101	3.54	645	647	-.001	2.658
2.712	20.82	1.25	288.1	101	3.54	645	647	-.001	2.717
2.757	20.62	1.25	288.1	98	3.52	644	646	-.021	2.763
2.834	18.89	1.25	288.2	79	3.36	636	637	-.209	2.841
2.879	16.41	1.25	288.6	56	3.13	621	623	-.528	2.887
2.935	13.31	1.25	289.5	34	2.80	598	600	-1.046	2.945
2.991	10.34	1.25	290.6	20	2.45	566	569	-1.746	3.001
3.042	9.27	1.25	291.8	16	2.32	552	556	-2.058	3.055
3.093	11.24	1.25	292.8	24	2.56	580	583	-1.447	3.105
3.138	16.72	1.25	293.6	58	3.16	629	631	-.361	3.154
3.184	25.72	1.25	294.0	176	3.94	671	672	.572	3.199
3.225	31.37	1.25	294.2	306	4.36	686	687	.921	3.243
3.281	32.27	1.25	294.2	331	4.43	688	689	.967	3.298
3.316	32.06	1.25	294.2	325	4.41	688	689	.956	3.337
3.367	31.58	1.25	294.2	311	4.38	687	688	.932	3.390
$p_{t,2}/p_{t,1} = 2.67$; $p_{t,1} = 102.7$, $p_{t,2} = 275.8$, $T_{t,1} = 288.1$, $T_{t,2} = 292.5$, $p_c = 1.06$									
2.707	19.31	1.10	288.1	102	3.64	650	651	-0.000	2.707
2.757	19.31	1.10	288.1	102	3.64	650	651	-.000	2.760
2.808	19.10	1.10	288.1	99	3.62	649	650	-.028	2.811
2.859	18.13	1.10	288.1	87	3.52	644	646	-.161	2.864
2.905	16.82	1.10	288.2	72	3.39	637	638	-.359	2.910
2.956	14.41	1.10	288.6	49	3.13	621	623	-.795	2.963
3.017	11.30	1.10	289.4	28	2.75	594	596	-1.555	3.024
3.067	9.03	1.10	290.1	17	2.45	565	568	-2.340	3.077
3.113	7.93	1.10	290.8	13	2.28	548	550	-2.826	3.123
3.154	8.76	1.10	291.4	16	2.41	562	565	-2.424	3.166
3.204	14.27	1.10	292.0	48	3.11	624	626	-.722	3.217
3.255	22.93	1.10	292.4	161	3.97	670	671	.551	3.271
3.291	27.03	1.10	292.5	254	4.32	683	684	.910	3.300
3.331	27.57	1.10	292.5	268	4.36	684	685	.950	3.349
3.372	27.44	1.10	292.5	265	4.35	684	685	.941	3.390
3.433	27.03	1.10	292.5	254	4.32	683	684	.910	3.453

TABULATION OF DATA THROUGH MIXING REGION — Continued

(b) Region ahead of shock waves; x/d = 5.8

h'	p_p	p_e	$T_{t,2}$	$p_{t,calc}$	M	V	V_A	$\dfrac{V_A - V_{A,1}}{V_{A,2} - V_{A,1}}$	h'_A
$p_{t,2}/p_{t,1}$ = 4.00; $p_{t,1}$ = 80.3, $p_{t,2}$ = 357.2, $T_{t,1}$ = 288.1, $T_{t,2}$ = 296.4, p_c = 1.33									
1.773	20.34	1.34	288.1	85	3.37	636	636	0.000	1.773
1.818	20.10	1.34	288.1	83	3.35	635	635	-.021	1.818
1.874	19.13	1.34	288.3	73	3.27	630	630	-.109	1.874
1.915	17.89	1.34	288.7	62	3.16	623	624	-.232	1.915
1.966	16.51	1.34	289.5	51	3.03	615	616	-.380	1.968
2.017	15.48	1.34	290.5	44	2.93	609	609	-.497	2.019
2.067	15.17	1.41	291.7	40	2.82	602	605	-.580	2.072
2.123	16.20	1.50	293.0	43	2.83	604	610	-.485	2.133
2.174	18.06	1.61	294.2	50	2.89	610	619	-.313	2.189
2.225	22.20	1.77	295.1	71	3.06	624	636	.002	2.250
2.276	27.96	1.84	295.9	118	3.38	645	657	.386	2.314
2.332	35.06	1.84	296.3	212	3.80	667	677	.749	2.382
2.387	40.27	1.84	296.4	309	4.08	679	688	.943	2.453
2.428	41.58	1.84	296.4	337	4.14	681	690	.985	2.502
2.474	41.37	1.84	296.4	333	4.13	681	690	.979	2.560
$p_{t,2}/p_{t,1}$ = 3.34; $p_{t,1}$ = 102.0, $p_{t,2}$ = 342.0, $T_{t,1}$ = 288.1, $T_{t,2}$ = 294.2, p_c = 1.41									
1.834	22.20	1.38	288.1	103	3.48	642	641	0.027	1.834
1.900	21.82	1.38	288.1	98	3.45	640	640	-.010	1.900
1.986	21.03	1.38	288.1	89	3.39	637	636	-.091	1.984
2.067	19.17	1.38	288.2	71	3.23	627	627	-.297	2.065
2.138	17.41	1.41	288.7	55	3.04	615	615	-.542	2.136
2.215	16.24	1.45	289.8	45	2.89	605	607	-.736	2.212
2.321	17.79	1.54	291.6	51	2.93	611	615	-.549	2.326
2.398	23.96	1.65	292.8	94	3.30	637	643	.070	2.410
2.464	30.10	1.70	293.7	162	3.66	658	664	.520	2.486
2.525	35.03	1.70	294.1	243	3.96	671	677	.803	2.555
2.606	39.13	1.70	294.2	330	4.19	680	685	.987	2.649
2.667	39.47	1.70	294.2	338	4.21	681	686	1.001	2.718
$p_{t,2}/p_{t,1}$ = 2.67; $p_{t,1}$ = 102.7, $p_{t,2}$ = 276.5, $T_{t,1}$ = 288.1, $T_{t,2}$ = 292.5, p_c = 1.21									
2.093	21.03	1.28	288.1	101	3.53	644	646	-0.000	2.093
2.169	21.03	1.28	288.1	101	3.53	644	646	-.000	2.171
2.230	19.79	1.28	288.1	86	3.42	639	640	-.160	2.235
2.286	18.03	1.28	288.1	68	3.26	629	631	-.415	2.293
2.347	16.38	1.38	288.5	49	2.97	610	617	-.820	2.359
2.408	15.27	1.40	289.3	41	2.85	601	609	-1.038	2.426
2.479	16.41	1.40	290.5	48	2.95	611	618	-.780	2.504
2.545	19.96	1.40	291.6	77	3.27	634	640	-.181	2.578
2.606	25.13	1.40	292.3	138	3.68	657	662	.432	2.646
2.667	30.20	1.40	292.5	226	4.05	673	677	.854	2.713
2.723	32.27	1.40	292.5	272	4.19	678	682	.991	2.773
2.789	32.41	1.40	292.5	275	4.20	679	682	1.000	2.847

APPENDIX A

TABULATION OF DATA THROUGH MIXING REGION — Continued

(c) Region ahead of shock waves; x/d = 9.0

h'	p_p	p_e	$T_{t,e}$	$p_{t,calc}$	M	V	V_A	$\dfrac{V_A - V_{A,1}}{V_{A,2} - V_{A,1}}$	h'_A
$p_{t,2}/p_{t,1} = 3.34$; $p_{t,1} = 102.7$, $p_{t,2} = 342.7$, $T_{t,1} = 288.1$, $T_{t,2} = 294.2$, $p_c = 1.88$
1.118	23.65	1.55	288.1	100	3.39	637	629	0.000	1.118
1.173	23.30	1.55	288.1	97	3.36	635	627	-.032	1.166
1.240	22.61	1.55	288.1	90	3.31	632	624	-.098	1.224
1.300	21.58	1.55	288.3	80	3.23	628	619	-.201	1.278
1.346	20.72	1.55	288.6	73	3.16	624	615	-.288	1.318
1.427	19.17	1.55	289.6	60	3.04	616	607	-.455	1.389
1.483	18.20	1.55	290.5	53	2.96	611	601	-.566	1.440
1.544	18.48	1.55	291.5	55	2.98	614	604	-.507	1.494
1.590	19.51	1.55	292.3	63	3.06	621	612	-.354	1.534
1.651	22.10	1.55	293.1	85	3.27	635	627	-.040	1.587
1.732	27.10	1.55	293.9	143	3.63	656	649	.418	1.659
1.798	31.06	1.48	294.2	221	3.99	673	665	.740	1.714
1.849	31.79	1.37	294.2	272	4.21	681	672	.875	1.755
1.915	31.92	1.25	294.2	321	4.40	688	677	.975	1.806
$p_{t,2}/p_{t,1} = 2.67$; $p_{t,1} = 103.4$, $p_{t,2} = 277.2$, $T_{t,1} = 288.1$, $T_{t,2} = 292.5$, $p_c = 1.69$
1.427	22.96	1.52	288.1	97	3.37	636	632	-0.030	1.427
1.483	22.27	1.53	288.1	88	3.31	632	628	-.124	1.481
1.529	21.44	1.53	288.1	80	3.24	628	624	-.224	1.521
1.580	19.86	1.53	288.1	67	3.11	620	615	-.436	1.570
1.641	18.48	1.57	288.2	54	2.96	609	605	-.683	1.628
1.692	17.10	1.57	288.5	45	2.84	600	596	-.909	1.676
1.758	16.48	1.62	288.9	40	2.74	592	590	-1.063	1.740
1.824	17.10	1.62	289.6	44	2.80	598	595	-.932	1.808
1.880	18.55	1.62	290.2	53	2.92	608	606	-.672	1.864
1.930	20.96	1.62	290.7	70	3.11	622	620	-.308	1.915
1.991	24.79	1.65	291.3	103	3.36	639	638	.120	1.976
2.052	29.89	1.69	291.9	160	3.66	655	655	.553	2.037
2.123	33.92	1.72	292.3	217	3.86	665	666	.815	2.108
2.179	36.54	1.76	292.5	257	3.97	670	671	.947	2.164
2.240	37.44	1.76	292.5	274	4.02	672	673	.996	2.225
2.276	37.89	1.76	292.5	283	4.04	673	674	1.020	2.261
2.316	37.89	1.76	292.5	283	4.04	673	674	1.020	2.301

TABULATION OF DATA THROUGH MIXING REGION – Continued

(d) Region behind shock waves; x/d = 14.0

h'	p_p	p_e	$T_{t,e}$	$p_{t,calc}$	M	V	V_A	$\dfrac{V_A - V_{A,1}}{V_{A,2} - V_{A,1}}$	h'_A
$p_{t,2}/p_{t,1} = 4.00$; $\quad p_{t,1} = 88.9$, $\quad p_{t,2} = 356.5$, $\quad T_{t,1} = 288.1$, $\quad T_{t,2} = 296.4$, $\quad p_c = 3.52$									
0.747	33.72	3.41	288.1	80	2.70	588	586	-0.065	0.747
.798	34.30	3.41	288.1	83	2.73	590	588	-.034	.798
.843	34.34	3.41	288.1	83	2.73	590	588	-.032	.841
.884	34.13	3.41	288.1	82	2.72	589	588	-.043	.881
.935	33.34	3.41	288.1	78	2.68	586	585	-.086	.930
.986	32.58	3.41	288.3	74	2.65	584	582	-.125	.981
1.052	32.41	3.41	289.0	73	2.65	584	582	-.125	1.044
1.087	32.78	3.41	289.6	75	2.66	586	584	-.095	1.080
1.143	34.47	3.41	290.7	84	2.73	593	592	.013	1.135
1.199	38.75	3.52	292.0	105	2.86	605	605	.209	1.191
1.255	43.23	3.59	293.4	131	3.00	617	618	.395	1.247
1.311	48.06	3.62	294.6	167	3.15	629	631	.573	1.303
1.362	53.37	3.62	295.5	216	3.33	641	643	.744	1.356
1.423	59.16	3.62	296.2	280	3.51	653	654	.901	1.417
1.499	61.71	3.62	296.4	312	3.59	657	658	.962	1.496
1.529	62.19	3.62	296.4	319	3.60	658	659	.972	1.527
1.565	62.85	3.62	296.4	327	3.62	659	660	.986	1.562
1.621	63.50	3.62	296.4	336	3.64	660	661	1.000	1.621
1.677	63.50	3.62	296.4	336	3.64	660	661	1.000	1.677
1.732	63.43	3.62	296.4	335	3.64	659	660	.999	1.735
1.809	62.60	3.62	296.4	324	3.61	658	659	.981	1.811
$p_{t,2}/p_{t,1} = 3.34$; $\quad p_{t,1} = 102.7$, $\quad p_{t,2} = 274.8$, $\quad T_{t,1} = 288.1$, $\quad T_{t,2} = 292.5$, $\quad p_c = 3.28$									
0.782	36.13	3.52	288.1	89	2.76	593	591	-0.105	0.782
.848	36.92	3.52	288.1	94	2.79	595	593	-.059	.846
.920	37.09	3.52	288.1	95	2.80	596	594	-.050	.917
.986	36.85	3.52	288.1	93	2.79	595	593	-.063	.981
1.026	35.72	3.52	288.1	87	2.74	591	589	-.128	1.019
1.067	34.51	3.52	288.3	81	2.69	587	585	-.199	1.059
1.123	33.78	3.52	288.8	77	2.66	585	583	-.236	1.113
1.163	33.96	3.52	289.4	78	2.67	586	584	-.215	1.153
1.224	36.27	3.52	290.5	90	2.76	596	594	-.055	1.212
1.280	40.37	3.59	291.6	112	2.89	607	606	.163	1.268
1.341	46.95	3.76	292.7	150	3.05	621	622	.425	1.331
1.382	50.61	3.76	293.3	179	3.18	630	631	.574	1.372
1.433	55.92	3.76	293.9	229	3.34	641	642	.759	1.423
1.478	59.36	3.76	294.1	266	3.45	647	648	.865	1.471
1.544	62.09	3.76	294.2	299	3.53	651	652	.939	1.537
1.605	63.60	3.76	294.2	318	3.57	654	655	.977	1.600
1.661	64.40	3.76	294.2	329	3.60	655	656	.997	1.656
1.707	64.54	3.76	294.2	330	3.60	655	656	1.000	1.702
1.758	64.26	3.76	294.2	327	3.59	655	656	.993	1.755
1.814	63.57	3.76	294.2	318	3.57	654	655	.976	1.811
$p_{t,2}/p_{t,1} = 2.67$; $\quad p_{t,1} = 102.7$, $\quad p_{t,2} = 342.7$, $\quad T_{t,1} = 288.1$, $\quad T_{t,2} = 294.2$, $\quad p_c = 3.65$									
0.772	32.92	3.17	288.1	82	2.77	594	592	-0.229	0.772
.859	34.99	3.17	288.1	95	2.86	601	600	-.072	.856
.975	35.51	3.17	288.1	98	2.88	603	601	-.034	.970
1.062	34.23	3.17	288.1	90	2.83	599	597	-.127	1.054
1.108	33.13	3.17	288.2	84	2.78	595	593	-.210	1.108
1.174	30.89	3.17	288.6	72	2.68	587	585	-.389	1.174
1.235	30.34	3.17	289.2	69	2.66	585	583	-.424	1.232
1.275	31.34	3.17	289.7	74	2.70	588	588	-.326	1.273
1.326	33.96	3.17	290.4	88	2.82	600	598	-.099	1.321
1.367	37.58	3.28	290.9	107	2.92	609	609	.124	1.362
1.412	41.44	3.34	291.5	131	3.04	618	619	.345	1.410
1.453	45.54	3.34	291.9	164	3.19	629	630	.572	1.450
1.494	48.54	3.34	292.2	192	3.30	636	637	.721	1.491
1.534	50.95	3.34	292.4	216	3.38	642	642	.829	1.532
1.590	53.47	3.34	292.5	244	3.47	646	647	.931	1.590
1.656	54.54	3.34	292.5	257	3.51	648	649	.972	1.656
1.687	54.88	3.34	292.5	261	3.52	649	650	.984	1.687
1.727	55.19	3.34	292.5	265	3.53	649	650	.996	1.730
1.778	55.33	3.34	292.5	267	3.53	650	650	1.001	1.781
1.844	55.37	3.34	292.5	267	3.53	650	651	1.002	1.847
1.885	54.64	3.34	292.5	258	3.51	648	649	.976	1.890

APPENDIX A

TABULATION OF DATA THROUGH MIXING REGION — Continued

(e) Region behind shock waves; x/d = 15.0

h'	p_p	p_e	$T_{t,e}$	$p_{t,calc}$	M	V	V_A	$\dfrac{V_A - V_{A,1}}{V_{A,2} - V_{A,1}}$	h'_A
$p_{t,2}/p_{t,1}$ = 4.00; $p_{t,1}$ = 90.0, $p_{t,2}$ = 360.6, $T_{t,1}$ = 288.1, $T_{t,2}$ = 296.4, p_c = 3.24									
0.625	33.51	3.24	288.1	84	2.77	593	593	-0.004	0.625
.727	33.58	3.24	288.1	84	2.77	594	594	.000	.727
.793	33.37	3.24	288.1	83	2.76	593	593	-.011	.793
.839	33.06	3.24	288.1	81	2.75	592	592	-.027	.839
.890	32.34	3.24	288.4	77	2.72	589	589	-.063	.890
.940	31.75	3.24	288.9	74	2.69	588	588	-.087	.940
.976	31.65	3.24	289.5	74	2.68	588	588	-.086	.976
1.017	31.92	3.24	290.3	75	2.70	590	590	-.058	1.017
1.062	32.82	3.24	291.3	80	2.74	594	594	.007	1.062
1.139	36.20	3.24	293.1	99	2.88	608	608	.206	1.139
1.189	39.58	3.24	294.3	122	3.02	620	620	.373	1.189
1.240	42.47	3.03	295.2	159	3.24	636	633	.562	1.238
1.301	47.57	3.03	296.0	211	3.44	648	646	.746	1.296
1.357	52.12	3.03	296.4	267	3.60	658	655	.881	1.352
1.408	54.23	3.03	296.4	296	3.68	661	659	.935	1.400
1.464	55.33	3.03	296.4	312	3.71	663	661	.962	1.453
1.509	56.26	3.03	296.4	326	3.75	665	662	.984	1.497
1.565	57.78	3.03	296.4	350	3.80	667	665	1.019	1.553
1.616	59.33	3.03	296.4	376	3.85	669	667	1.053	1.601
1.662	60.78	3.03	296.4	401	3.90	671	669	1.083	1.644
1.718	65.40	3.03	296.4	489	4.05	677	675	1.172	1.697
1.779	68.36	3.03	296.4	553	4.14	681	679	1.224	1.756
$p_{t,2}/p_{t,1}$ = 3.34; $p_{t,1}$ = 103.4, $p_{t,2}$ = 343.4, $T_{t,1}$ = 288.1, $T_{t,2}$ = 294.2, p_c = 3.31									
0.544	36.13	3.31	288.1	96	2.85	600	600	0.000	0.544
.686	36.09	3.31	288.1	96	2.85	600	600	-.002	.686
.788	35.47	3.31	288.1	92	2.82	598	598	-.037	.788
.829	35.06	3.31	288.2	90	2.80	597	597	-.059	.829
.905	34.34	3.31	288.6	86	2.77	594	594	-.095	.905
.971	33.20	3.31	289.2	80	2.72	591	591	-.155	.971
1.042	32.34	3.31	290.1	75	2.69	588	588	-.197	1.042
1.098	32.20	3.31	290.8	75	2.68	589	589	-.193	1.098
1.149	33.03	3.31	291.5	79	2.72	593	593	-.127	1.149
1.199	34.47	3.31	292.2	87	2.78	599	599	-.025	1.199
1.255	37.75	3.31	292.8	107	2.91	610	610	.172	1.255
1.321	42.92	3.31	293.5	144	3.11	626	626	.431	1.321
1.372	47.26	3.31	293.9	182	3.27	636	636	.613	1.372
1.418	50.09	3.14	294.1	228	3.46	648	646	.771	1.418
1.464	53.23	3.14	294.2	266	3.57	654	652	.874	1.461
1.509	55.02	3.14	294.2	290	3.64	657	655	.927	1.507
1.565	57.64	3.14	294.2	328	3.72	661	659	1.000	1.560
1.631	58.43	3.14	294.2	340	3.75	662	661	1.021	1.626
1.672	58.54	3.14	294.2	342	3.75	662	661	1.024	1.664
1.702	59.05	3.14	294.2	350	3.77	663	662	1.037	1.692
1.733	59.98	3.14	294.2	365	3.80	665	663	1.061	1.723
1.779	63.09	3.14	294.2	417	3.90	669	667	1.135	1.766
$p_{t,2}/p_{t,1}$ = 2.67; $p_{t,1}$ = 103.4, $p_{t,2}$ = 276.5, $T_{t,1}$ = 288.1, $T_{t,2}$ = 292.5, p_c = 3.03									
0.676	34.92	3.03	288.1	100	2.93	606	606	0.002	.676
.813	34.89	3.03	288.1	100	2.93	606	606	-.000	.813
.864	34.78	3.03	288.1	99	2.92	606	606	-.007	.864
.940	34.58	3.03	288.1	98	2.91	605	605	-.022	.940
.996	33.89	3.03	288.1	93	2.88	603	603	-.073	.996
1.067	32.16	3.03	288.3	83	2.80	597	597	-.203	1.067
1.144	30.23	3.03	288.8	72	2.71	590	590	-.355	1.144
1.215	29.92	3.03	289.5	71	2.70	589	589	-.367	1.215
1.271	30.58	3.03	290.2	74	2.73	592	592	-.295	1.271
1.311	32.68	3.03	290.6	86	2.83	601	601	-.109	1.311
1.372	36.47	3.03	291.3	110	2.99	615	615	.184	1.372
1.418	39.99	3.03	291.8	137	3.14	626	626	.414	1.418
1.464	43.44	3.02	292.1	169	3.29	635	635	.618	1.464
1.520	47.64	3.02	292.4	213	3.45	645	645	.825	1.520
1.570	49.92	3.02	292.5	241	3.53	650	649	.926	1.570
1.626	51.02	3.02	292.5	254	3.57	652	652	.970	1.626
1.697	52.57	3.02	292.5	275	3.63	654	654	1.030	1.697
1.748	54.33	3.02	292.5	300	3.69	657	657	1.095	1.748
1.804	55.02	3.02	292.5	310	3.71	659	658	1.120	1.804
1.855	54.68	3.02	292.5	305	3.70	658	658	1.107	1.855

APPENDIX A

TABULATION OF DATA THROUGH MIXING REGION — Concluded

(f) Region behind shock waves; $x/d = 16.0$

h'	p_p	p_e	$T_{t,e}$	$p_{t,calc}$	M	V	V_A	$\dfrac{V_A - V_{A,1}}{V_{A,2} - V_{A,1}}$	h'_A

$p_{t,2}/p_{t,1} \approx 4.00$; $p_{t,1} = 89.6$, $p_{t,2} = 358.5$, $T_{t,1} = 288.1$, $T_{t,2} \approx 296.4$, $p_c = 3.24$

h'	p_p	p_e	$T_{t,e}$	$p_{t,calc}$	M	V	V_A	$\dfrac{V_A - V_{A,1}}{V_{A,2} - V_{A,1}}$	h'_A
0.701	31.85	3.17	288.5	77	2.72	590	589	-0.062	0.701
.762	31.89	3.17	289.2	77	2.73	591	590	-.050	.762
.813	33.30	3.17	290.0	85	2.79	597	596	.039	.810
..864	35.85	3.17	291.0	100	2.90	607	606	.182	.861
.930	39.99	3.17	292.3	129	3.07	621	620	.384	.927
.991	45.30	3.17	293.5	175	3.27	636	635	.598	.986
1.052	50.95	3.24	294.6	227	3.44	647	647	.769	1.047
1.102	53.99	3.24	295.4	263	3.54	654	654	.862	1.097
1.163	56.33	3.24	296.1	294	3.62	658	658	.930	1.158
1.224	57.71	3.24	296.4	313	3.67	661	661	.967	1.219
1.285	59.16	3.24	296.4	334	3.72	663	663	1.000	1.280
1.351	60.40	3.24	296.4	353	3.76	665	665	1.027	1.346
1.427	60.88	3.24	296.4	361	3.77	666	666	1.037	1.422
1.478	60.64	3.24	296.4	357	3.76	665	665	1.032	1.473

$p_{t,2}/p_{t,1} = 3.34$; $p_{t,1} = 102.0$, $p_{t,2} = 340.6$, $T_{t,1} = 288.1$, $T_{t,2} = 294.2$, $p_c = 3.31$

h'	p_p	p_e	$T_{t,e}$	$p_{t,calc}$	M	V	V_A	$\dfrac{V_A - V_{A,1}}{V_{A,2} - V_{A,1}}$	h'_A
0.691	34.68	3.31	288.2	88	2.79	595	595	-0.081	0.691
.752	33.85	3.31	288.6	83	2.75	593	593	-.125	.752
.798	34.27	3.31	289.0	86	2.77	595	595	-.092	.798
.833	35.30	3.31	289.4	91	2.81	599	599	-.024	.833
.884	36.34	3.31	290.1	98	2.85	603	603	.047	.884
.904	37.85	3.31	290.4	107	2.92	608	608	.135	.904
.965	40.75	3.17	291.3	135	3.10	622	620	.342	.965
1.052	47.23	3.17	292.6	194	3.34	639	638	.633	1.049
1.168	53.99	3.17	293.8	272	3.58	654	652	.882	1.163
1.224	54.88	3.17	294.1	284	3.61	656	654	.914	1.217
1.275	55.85	3.17	294.2	298	3.65	657	656	.943	1.265
1.361	57.99	3.17	294.2	328	3.72	661	659	1.002	1.349
1.473	59.09	3.17	294.2	345	3.75	663	661	1.031	1.458
1.554	57.99	3.17	294.2	328	3.72	661	659	1.002	1.537

$p_{t,2}/p_{t,1} = 2.67$; $p_{t,1} = 102.0$, $p_{t,2} = 272.3$, $T_{t,1} = 288.1$, $T_{t,2} = 292.5$, $p_c = 3.03$

h'	p_p	p_e	$T_{t,e}$	$p_{t,calc}$	M	V	V_A	$\dfrac{V_A - V_{A,1}}{V_{A,2} - V_{A,1}}$	h'_A
0.620	32.03	2.76	288.1	93	2.94	607	603	-0.024	0.620
.686	31.92	2.76	288.1	92	2.93	607	602	-.032	.683
.747	31.44	2.76	288.1	89	2.91	605	600	-.068	.739
.803	30.82	2.76	288.1	85	2.88	603	598	-.117	.792
.874	29.72	2.76	288.4	78	2.83	599	594	-.202	.859
.930	29.96	2.76	288.7	79	2.84	600	595	-.175	.909
.991	30.89	2.76	289.3	85	2.88	604	599	-.088	.965
1.052	33.75	2.76	289.9	105	3.02	615	611	.141	1.024
1.123	38.61	2.90	290.6	135	3.16	626	623	.401	1.090
1.194	43.64	2.96	291.3	176	3.33	637	636	.651	1.161
1.275	47.44	2.96	292.0	217	3.47	646	645	.836	1.240
1.341	49.44	2.96	292.3	241	3.55	650	649	.926	1.303
1.407	50.75	2.96	292.5	258	3.59	653	652	.980	1.369
1.463	50.81	2.96	292.5	259	3.60	653	652	.982	1.422
1.519	51.57	2.96	292.5	269	3.62	654	654	1.010	1.478

APPENDIX B

PROCEDURE FOR COMPUTATIONS ACROSS A TWO-WAVE SHOCK SYSTEM

AND TABULATION OF RESULTS

At the design operating condition of $p_{t,2}/p_{t,1}$ = 3.34, the inviscid shock system (see fig. 5(a)) consists of two intersecting oblique shock waves, namely, the reflection of the initial shock wave and the second shock wave. Since the Mach numbers of the primary and secondary airstreams differ, an additional weak expansion or compression wave is required wherever the inviscid dividing streamline passes through a shock wave in order to achieve equilibrium of both the static pressures and the flow directions downstream of the shock waves. In actuality, the inviscid dividing streamline has degenerated into a mixing region about 0.8 cm wide, across which the upstream Mach number varies from about 3.2 to 4.3. In order to achieve equilibrium this flow pattern requires a complicated system of weak expansion and compression waves originating within the mixing region.

The required system of weak waves becomes cumbersome to calculate, so a simplified procedure was devised to compute the shock system necessary to produce the downstream flow field starting from the mixing zone ahead of the shock system. This procedure consisted of combining the effects of the two effective shock waves of approximately equal strength. These shock waves were chosen, by using tables of reference 8, to accomplish the required static-pressure rise from p_a to p_d. Using measured flow conditions at upstream survey stations as input, the computer mixing program provided velocity, temperature, and Mach number profiles at the x/d station of 12.5 immediately upstream of the shock system. The computer program also divided the cross-sectional area of the overall mixing field into a number of sections each containing equal mass flow. A different set of shock waves was required for each streamline within the mixing region in order to maintain a constant value of p_d. The equal-mass-flow sections provided a convenient set of streamlines for the shock-wave calculations. Each section was compressed by the appropriate shock waves to produce p_d, and the associated flow properties, including a new flow area for each section, were calculated. The result is a one-dimensional calculation for each stream tube crossing the effective shock system which is located at about the middle of the region that includes the inviscid shock system (fig. 5(a)) and mixing zone. By using these new profiles as representative of the flow immediately downstream of the two effective shock waves, mixing calculations were made for the region downstream of x/d = 12.5. Since the effective shock waves themselves were relatively weak, between 4.4° and 6.0° at $p_{t,2}/p_{t,1}$ = 3.34, and produced little total pressure loss, it is believed that little error

was engendered by using this simplified procedure to determine the flow field across the shock system.

The tables included in this appendix give the conditions from the computer solution at $x/d = 12.5$ before the effective shock waves were negotiated, the turning through the two effective shock waves δ_b and δ_c, and the conditions across the mixing zone after the effective shock waves were negotiated. The origin of the y_i-coordinate was arbitrarily picked to be at the lower edge of the mixing zone.

APPENDIX B

TABULATION OF FLOW-FIELD PROPERTIES AT $x/d = 12.5$ BEFORE AND AFTER A TWO-WAVE SHOCK SYSTEM

(a) $p_{t,2}/p_{t,1} = 4.0$; $p_a/p_\infty = 2.31$; $p_c/p_\infty = 5.65 \pm 0.03$

$y_{i,a}$	V_a	T_a	M_a	δ_b	δ_c	V_d	T_d	M_d	$y_{i,d}$
1.008	637.3	49.6	3.37	5.6	5.7	594.1	64.4	2.76	0.570
.937	635.5	50.5	3.33	5.7	5.7	591.3	65.5	2.72	.530
.866	632.3	51.7	3.27	5.8	5.9	586.6	67.2	2.66	.489
.790	627.7	53.1	3.20	5.9	6.0	580.2	69.0	2.60	.446
.714	622.6	54.5	3.14	6.0	6.1	573.5	70.7	2.54	.403
.635	620.1	55.0	3.11	6.0	6.2	570.0	71.4	2.51	.357
.556	624.3	54.1	3.16	6.0	6.0	575.8	70.2	2.56	.311
.480	635.8	51.6	3.29	5.7	5.9	589.3	67.0	2.68	.268
.409	651.1	48.2	3.49	5.4	5.5	610.2	62.4	2.87	.227
.348	665.4	44.6	3.71	5.1	5.2	628.6	57.8	3.08	.192
.290	676.4	41.5	3.91	4.8	5.0	642.4	53.8	3.26	.161
.236	683.8	39.1	4.07	4.7	4.8	652.1	50.8	3.41	.131
.185	688.2	37.4	4.19	4.6	4.6	658.3	48.5	3.52	.103
.137	690.7	36.2	4.27	4.5	4.5	661.8	47.0	3.59	.075
.091	692.0	35.5	4.32	4.4	4.5	664.2	46.1	3.64	.050
.046	692.6	35.2	4.35	4.4	4.5	664.7	45.7	3.66	.024
0	693.1	34.6	4.38	4.3	4.5	665.3	44.9	3.69	0

TABULATION OF FLOW-FIELD PROPERTIES AT x/d = 12.5 BEFORE

AND AFTER A TWO-WAVE SHOCK SYSTEM – Continued

(b) $p_{t,2}/p_{t,1}$ = 3.34; p_a/p_∞ = 2.09; p_c/p_∞ = 5.00 ± 0.03

$y_{i,a}$	V_a	T_a	M_a	δ_b	δ_c	V_d	T_d	M_d	$y_{i,d}$
0.995	641.6	48.2	3.44	5.4	5.4	661.5	62.1	2.84	0.570
.926	639.9	49.1	3.40	5.5	5.5	661.3	63.3	2.80	.530
.856	636.6	50.4	3.34	5.5	5.6	661.0	64.9	2.74	.489
.783	631.4	52.0	3.26	5.6	5.8	659.5	67.1	2.67	.447
.706	625.3	53.6	3.18	5.7	5.9	657.4	69.0	2.60	.403
.628	622.0	54.2	3.15	5.8	6.0	652.7	69.9	2.56	.357
.549	626.1	53.1	3.20	5.7	5.9	644.7	68.5	2.61	.312
.475	638.3	50.3	3.35	5.5	5.6	632.6	64.8	2.75	.269
.407	653.6	46.6	3.56	5.2	5.3	614.8	60.1	2.95	.230
.345	667.0	43.0	3.79	4.9	5.0	595.6	55.4	3.16	.195
.289	676.6	40.1	3.98	4.6	4.8	579.9	51.7	3.34	.163
.237	682.5	38.0	4.12	4.5	4.6	574.5	49.0	3.47	.133
.187	685.8	36.6	4.22	4.4	4.5	580.0	47.2	3.56	.105
.139	687.4	35.8	4.28	4.3	4.5	586.8	46.1	3.61	.078
.093	688.2	35.3	4.31	4.2	4.5	593.9	45.5	3.65	.052
.046	688.5	35.1	4.33	4.2	4.5	598.2	45.2	3.66	.026
0	688.6	35.0	4.33	4.2	4.5	601.0	45.2	3.66	0

APPENDIX B

TABULATION OF FLOW-FIELD PROPERTIES AT x/d = 12.5   BEFORE

AND AFTER A TWO-WAVE SHOCK SYSTEM – Concluded

(c) $p_{t,2}/p_{t,1}$ = 2.67; p_a/p_∞ = 1.83; p_c/p_∞ = 4.55 ± 0.03

$y_{i,a}$	V_a	T_a	M_a	δ_b	δ_c	V_d	T_d	M_d	$y_{i,d}$
0.964	647.8	46.9	3.52	5.5	5.5	607.3	61.0	2.89	0.541
.893	645.8	47.8	3.47	5.6	5.6	603.9	62.4	2.85	.501
.819	642.1	49.3	3.40	5.6	5.8	598.6	64.2	2.78	.459
.743	636.0	51.2	3.31	5.8	5.9	590.4	66.6	2.69	.416
.662	628.4	53.1	3.21	6.0	6.0	580.5	69.1	2.60	.370
.579	623.5	54.0	3.16	6.1	6.2	573.8	70.5	2.54	.323
.495	627.2	53.1	3.20	6.0	6.0	579.1	69.1	2.59	.275
.415	639.7	50.2	3.36	5.7	5.8	595.2	65.4	2.74	.230
.342	655.1	46.5	3.57	5.4	5.5	615.0	60.6	2.94	.189
.276	668.0	43.0	3.79	5.1	5.2	632.0	56.1	3.14	.152
.216	676.5	40.3	3.96	4.8	5.0	642.9	52.5	3.30	.119
.159	681.4	38.5	4.09	4.7	4.9	649.7	50.2	3.41	.087
.105	683.8	37.4	4.16	4.7	4.7	653.4	48.7	3.49	.058
.052	684.9	36.7	4.20	4.6	4.7	654.7	47.9	3.52	.029
0	685.3	36.4	4.23	4.6	4.7	655.3	47.5	3.54	0

REFERENCES

1. Edelman, R.: Diffusion Controlled Combustion for Scramjet Application. Part I — Analysis & Results of Calculations. Tech. Rep. 569 (Contract No. NAS 1-5117), Gen. Appl. Sci. Lab., Inc., Dec. 1965.

2. Korst, H. H.; and Chow, W. L.: Non-Isoenergetic Turbulent ($Pr_t = 1$) Jet Mixing Between Two Compressible Streams at Constant Pressure. NASA CR-419, 1966.

3. Zakkay, Victor; Krause, Egon; and Woo, Stephen D. L.: Turbulent Transport Properties for Axisymmetric Heterogeneous Mixing. ARL 64-103, U.S. Air Force, June 1964. (Available from DDC as AD 604 008.)

4. Ames Research Staff: Equations, Tables, and Charts for Compressible Flow. NACA Rep. 1135, 1953. (Supersedes NACA TN 1428.)

5. Wilder, John G., Jr.; and Hindersinn, Kenneth: Spreading of Supersonic Jets in Supersonic Streams. Aeronaut. Eng. Rev., vol. 12, no. 10, Oct. 1953, pp. 54-68.

6. Weinstein, Alvin S.: Diffusion of Momentum From Free and Confined Slot Jets Into Moving Secondary Streams. AFCRC-TN-55-476, U.S. Air Force, May 4, 1955.

7. Bailey, Harry E.; and Kuethe, Arnold M.: Supersonic Mixing of Jets and Turbulent Boundary Layers. WADC Tech. Rep. 57-402, ASTIA Doc. No. AD 150992, U.S. Air Force, June 1957.

8. Dennard, John S.; and Spencer, Patricia B.: Ideal-Gas Tables for Oblique-Shock Flow Parameters in Air at Mach Numbers From 1.05 to 12.0. NASA TN D-2221, 1964.

22.9 cm

Base plate

Top view

0   5

Scale: cm

Sidewall

Top plate

Glass windows

Base plate

10°

Total-pressure
orifice

Secondary air
settling chamber

Pressure orifice ₵
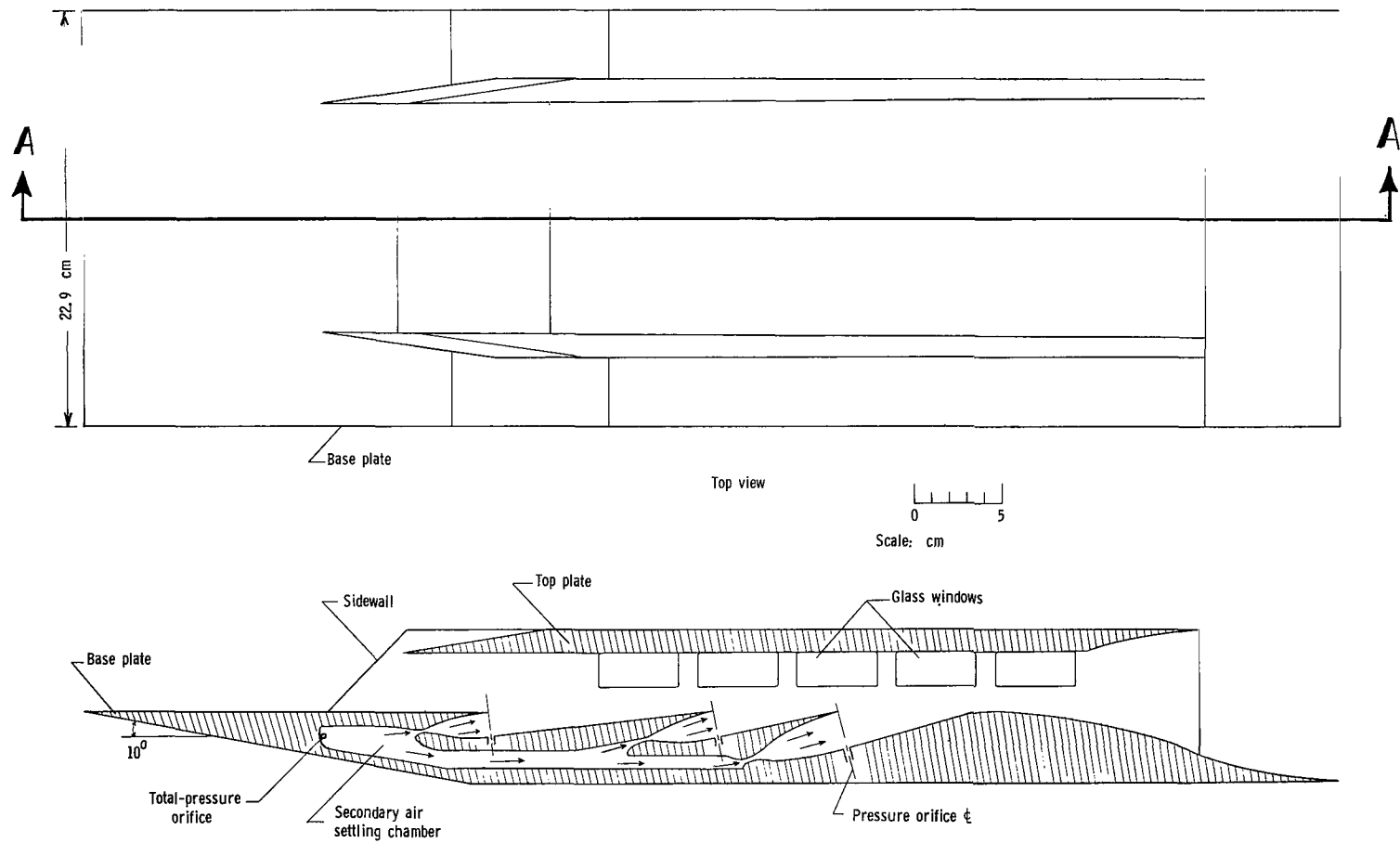
Figure 1.- Sketch of model assembly.
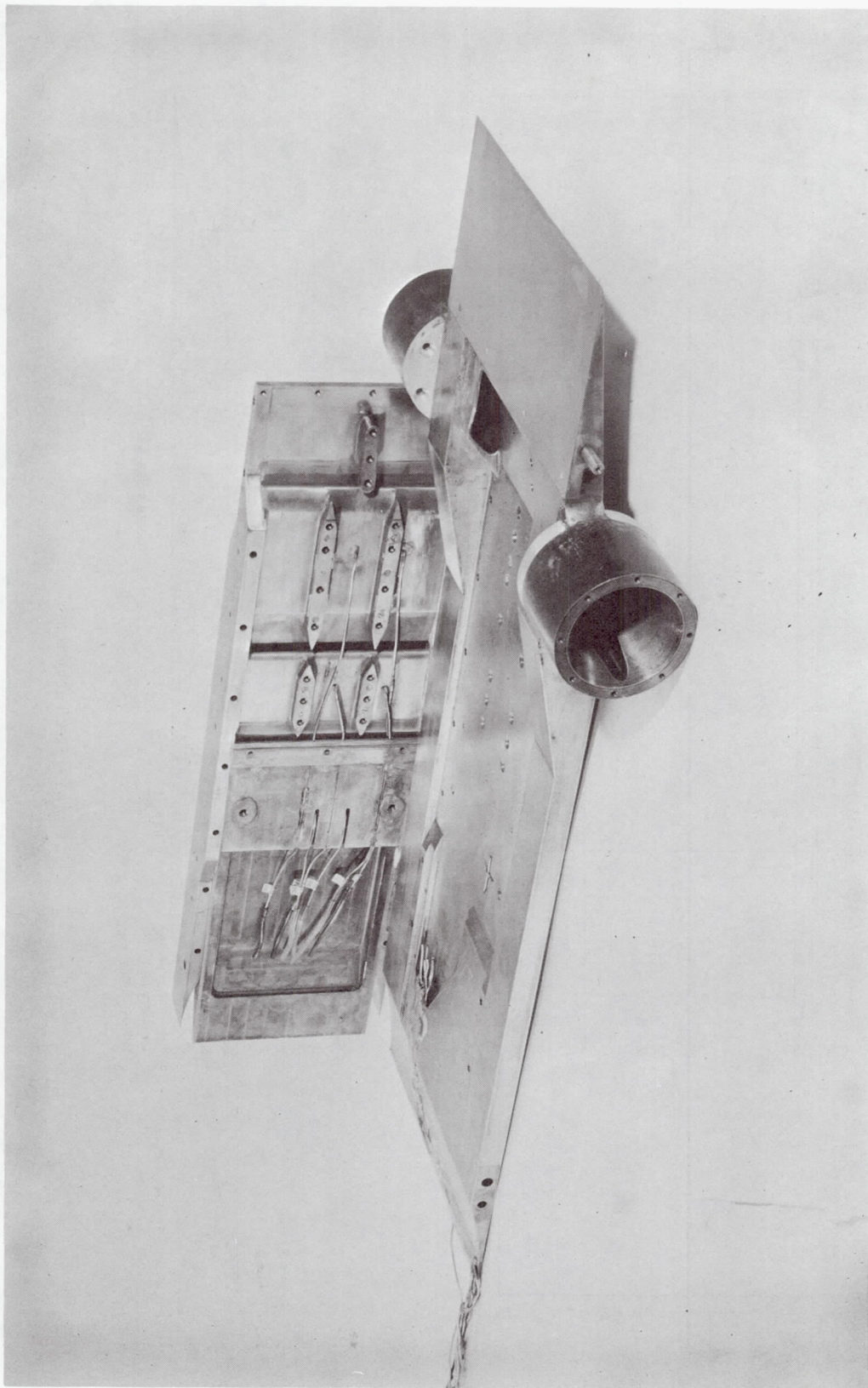
(a) Base plate and vane box assembly.

Figure 2.- Model at different stages of assembly.

L-67-4694
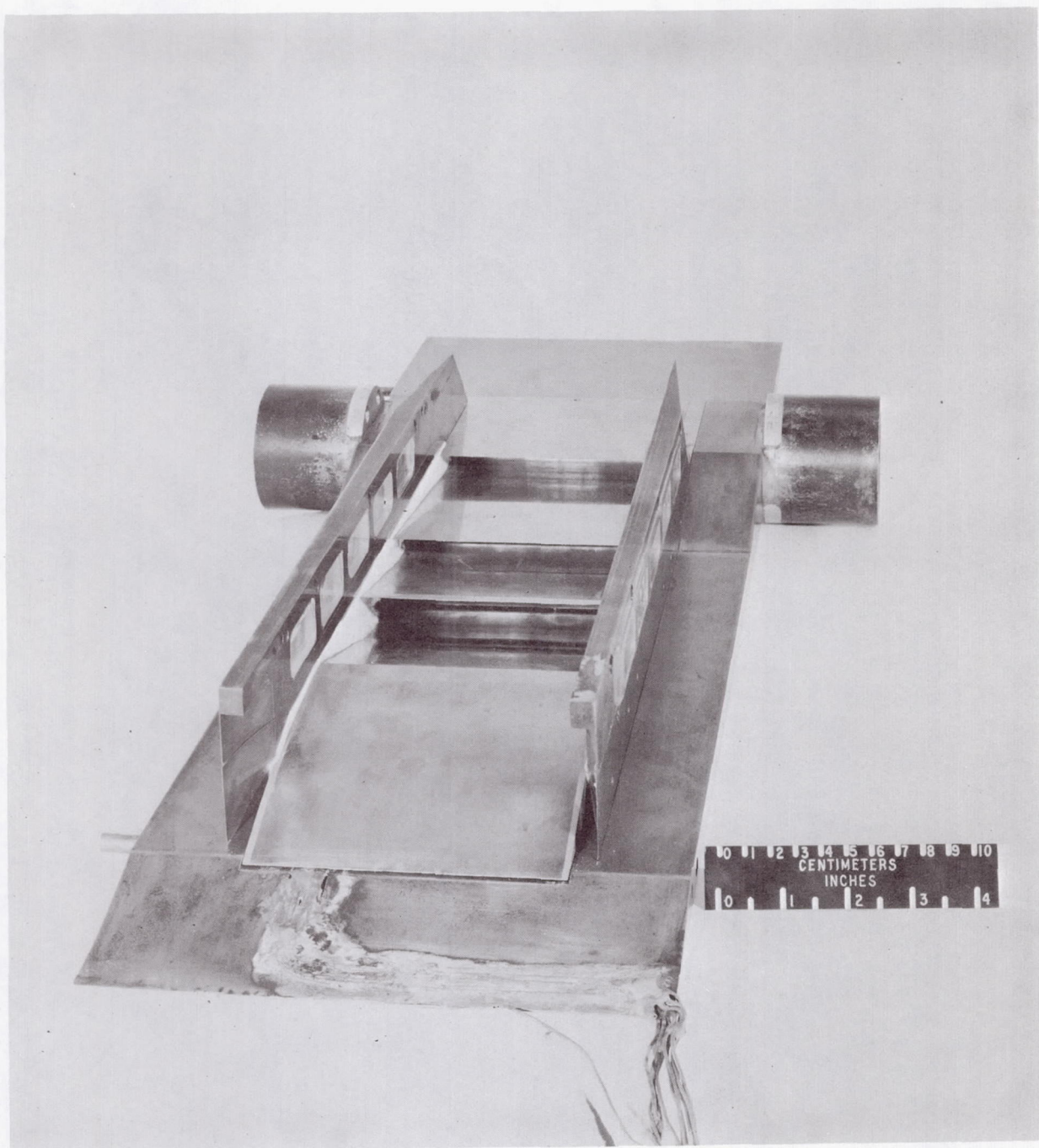
(b) Back view of model less top plate.

Figure 2.- Continued.
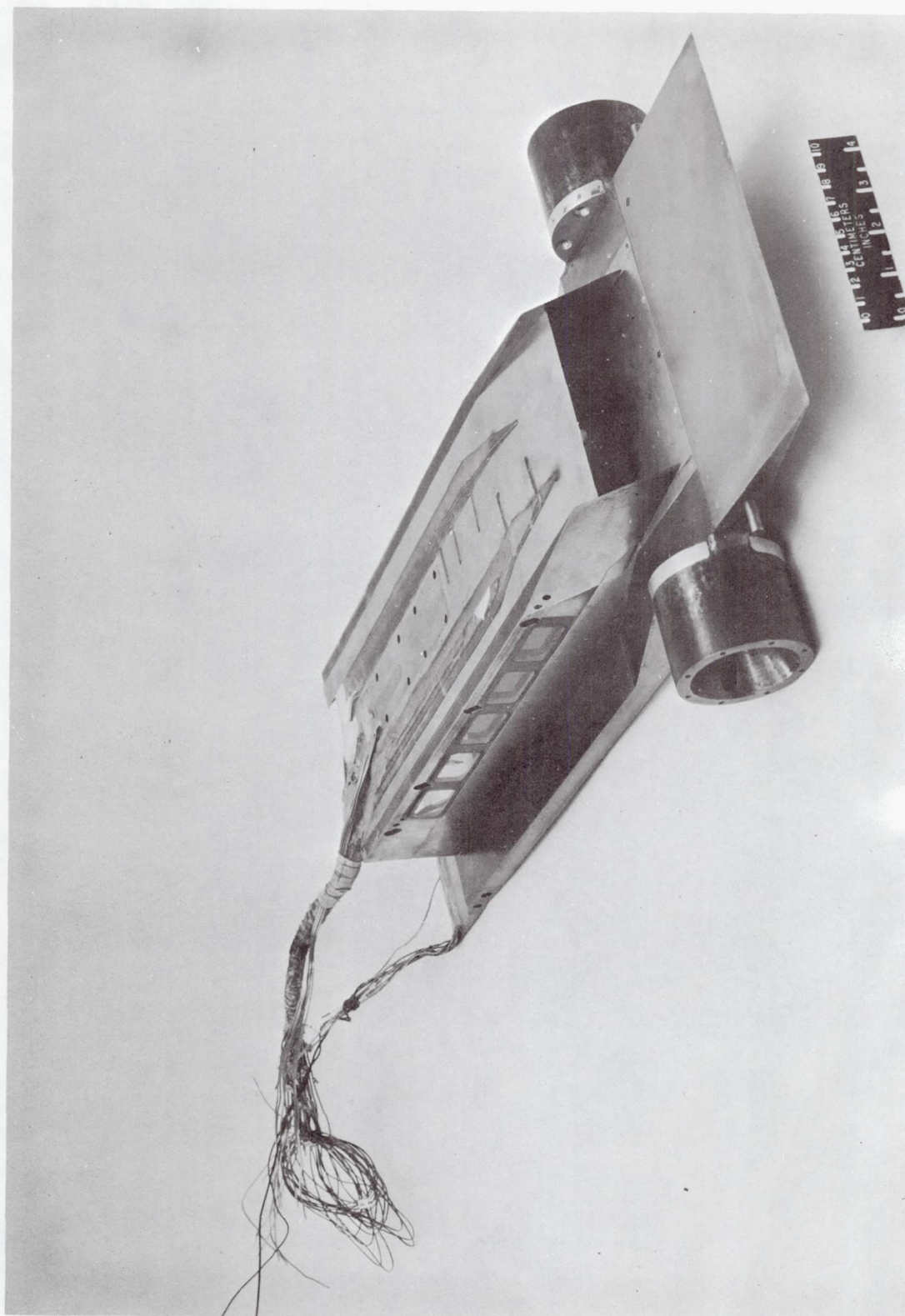
L-67-4693

(c) Front view of complete model.

Figure 2.- Concluded.

L-67-4697

34

Figure 3.- Static-pressure-orifice locations on top surface of duct.
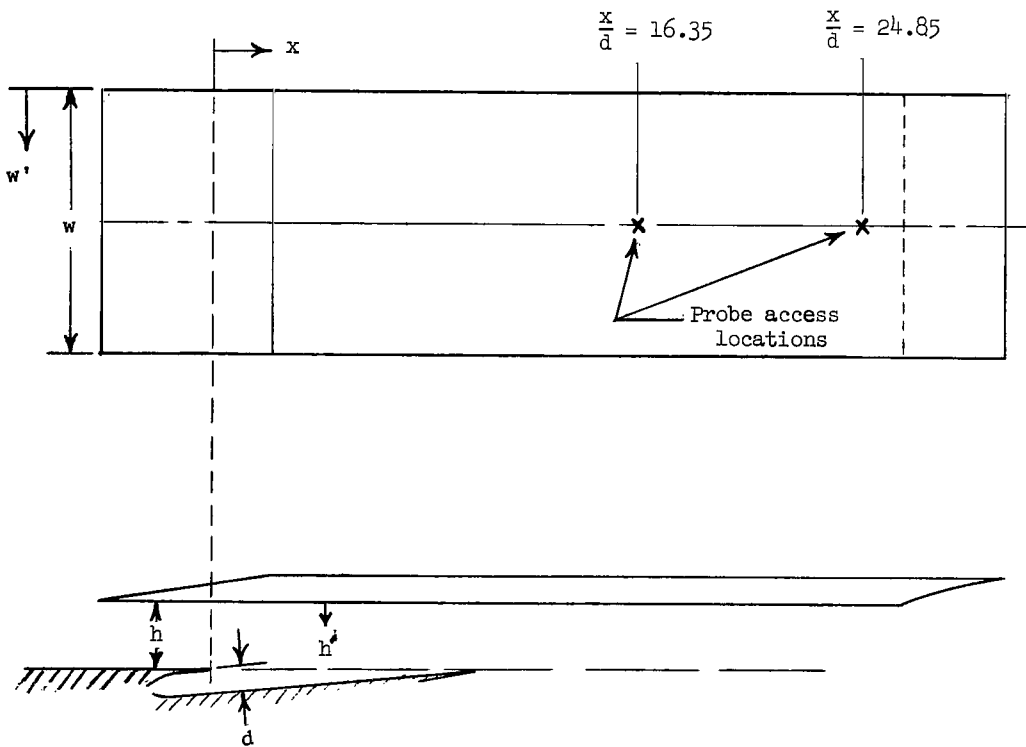
$\frac{x}{d}$	w'/w		
	0.3	0.5	0.7
.10	*	*	*
2.98	*	*	*
5.88	*	*	*
8.75	*	*	*
10.68		*	
11.63	*		*
14.53	*		*
17.40	*		*
20.30	*		*
23.18	*		*
26.05	*		*

* Orifice present

Survey station (x)	Probe length (l)
cm	cm
2.54	19.05
7.62	13.97
11.94	9.65
18.54	3.05
19.82	1.78
21.10	11.69

0.102-cm stainless-steel tip flattened to inside height of 0.013 cm

0.153-cm continuous length monel tubing

0.317-cm-thick wall stainless-steel tubing

Key for yaw alinement

0.159-cm flat shim stock

l
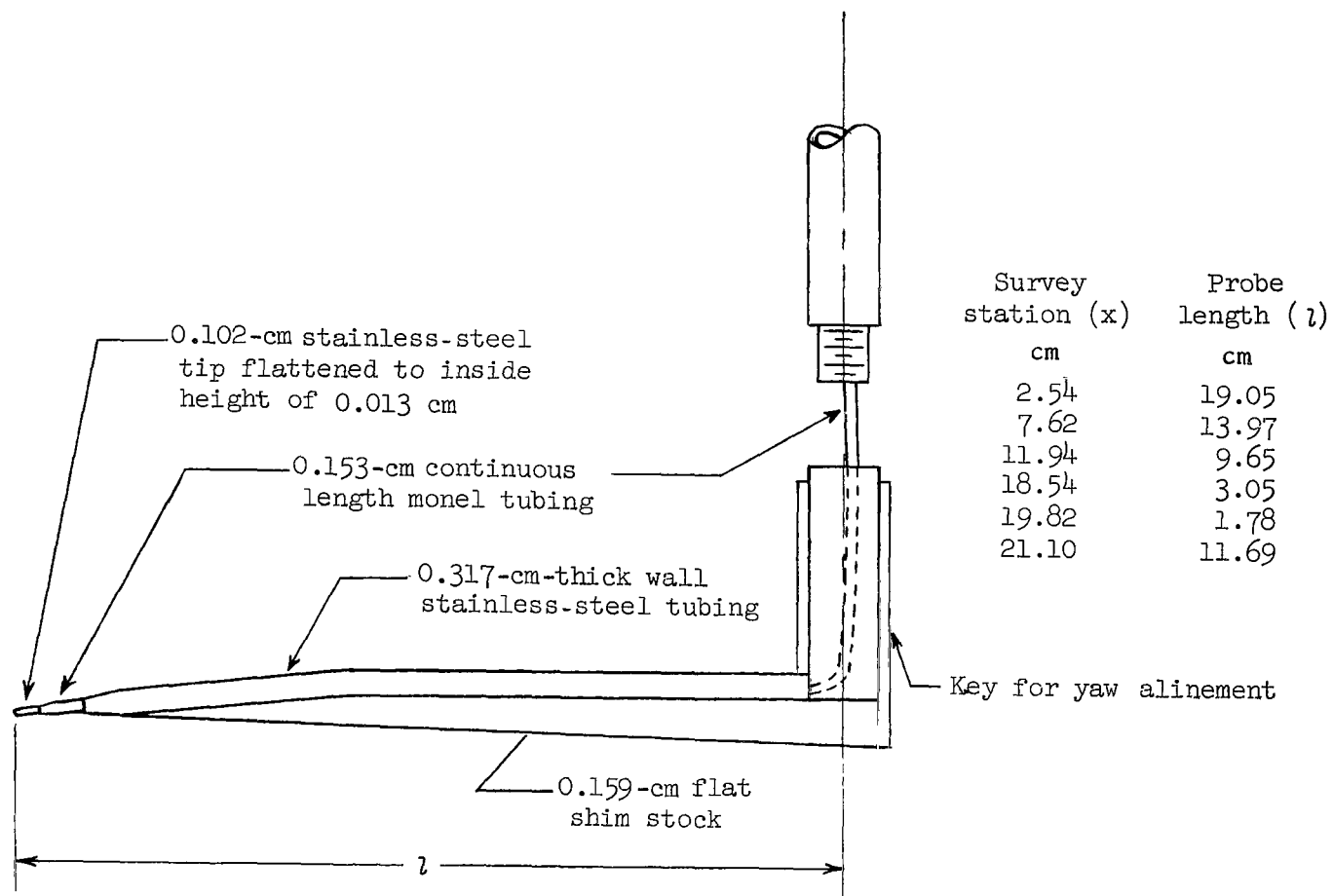
Figure 4.- Sketch of pitot-pressure survey probe.

Pitot-pressure survey stations

x/d = 1.9   x/d = 5.8   x/d = 9.0   x/d = 14.0, 15.0, 16.0
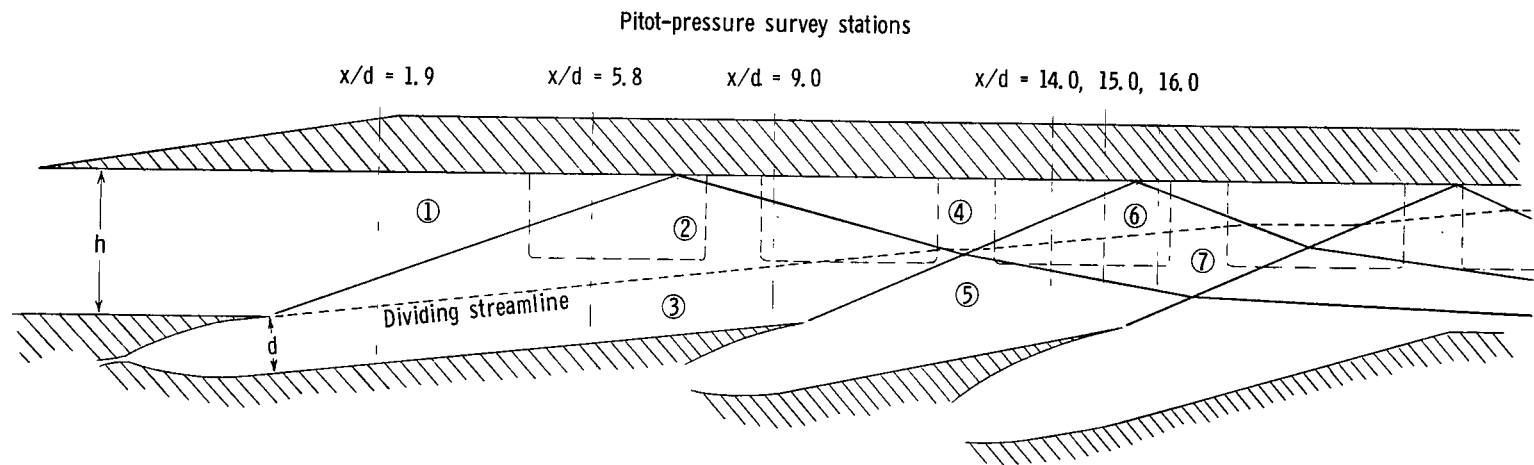
Bay	p/p_∞	$p_t/p_{t,\infty}$	M
①	1.00	1.000	4.00
②	1.75	0.986	3.57
③	1.75	3.333	4.49
④	2.94	0.975	3.19
⑤	2.94	3.280	4.06
⑥	4.78	0.970	2.86
⑦	4.78	3.240	3.70

(a) Theoretical flow field at $p_{t,2}/p_{t,1} = 3.34$.

Figure 5.- Sketch of two-dimensional duct.

Pitot-pressure survey stations

x/d = 1.9   x/d = 5.8   x/d = 9.0   x/d = 14.0, 15.0, 16.0

Mixing zone

Area of extra shock-
wave formation
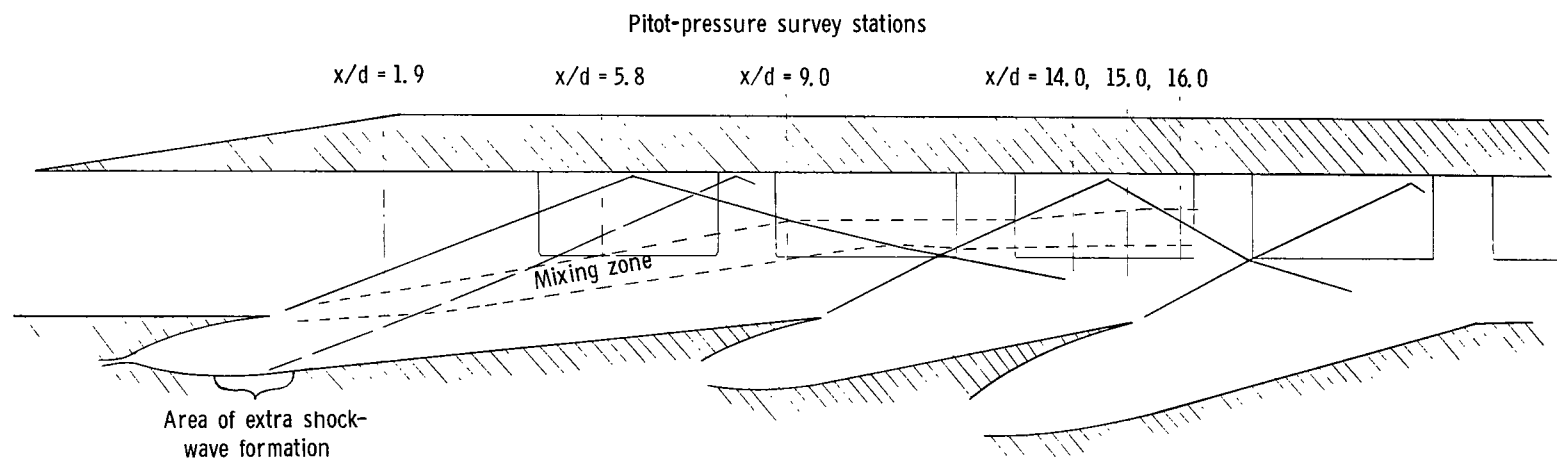
(b) Experimentally determined flow field at $p_{t,2}/p_{t,1} = 3.34$.

Figure 5.- Concluded.
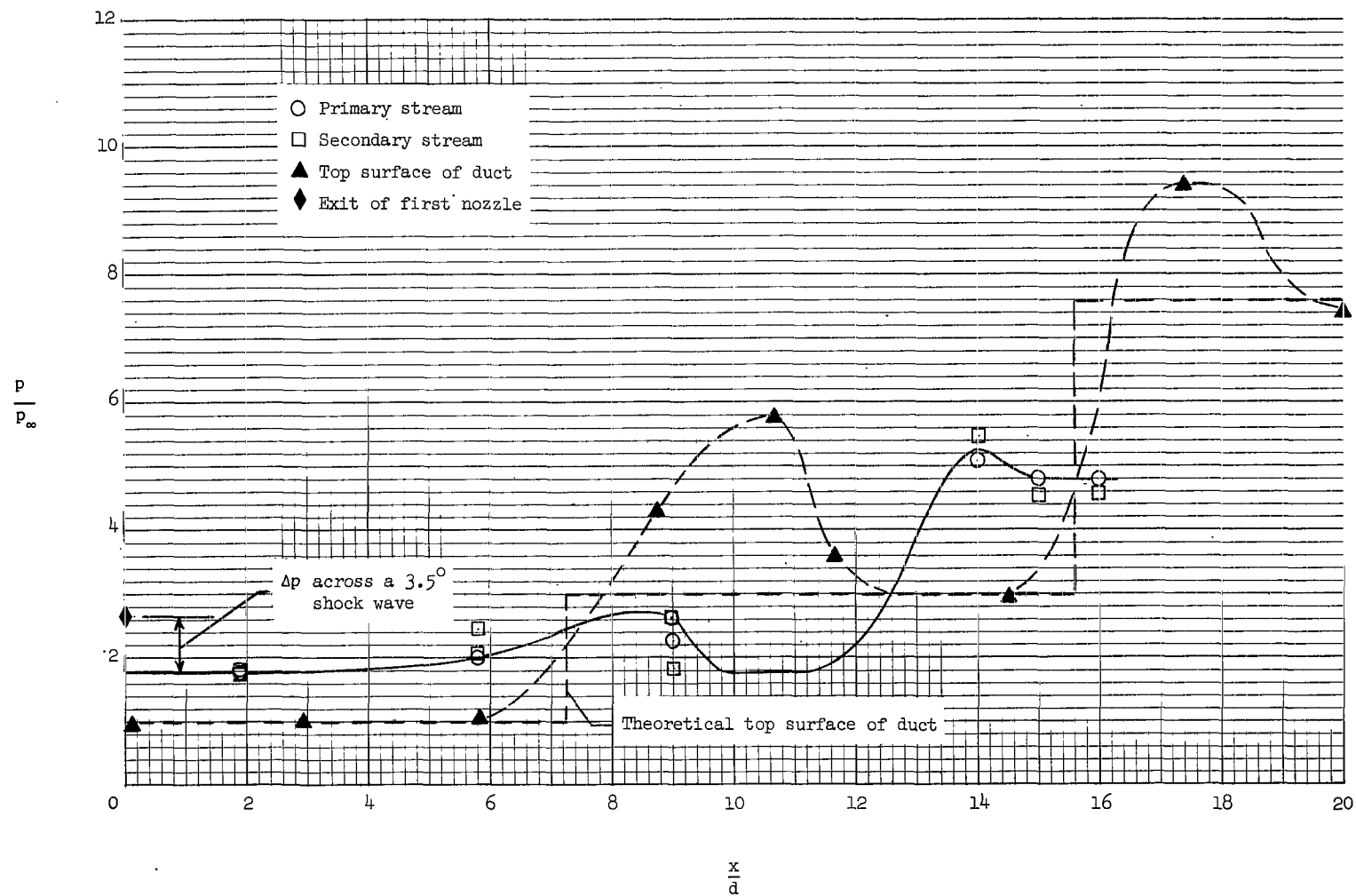
(a) $p_{t,2}/p_{t,1} = 3.34$.

Figure 6.- Static pressure through the two-dimensional duct.
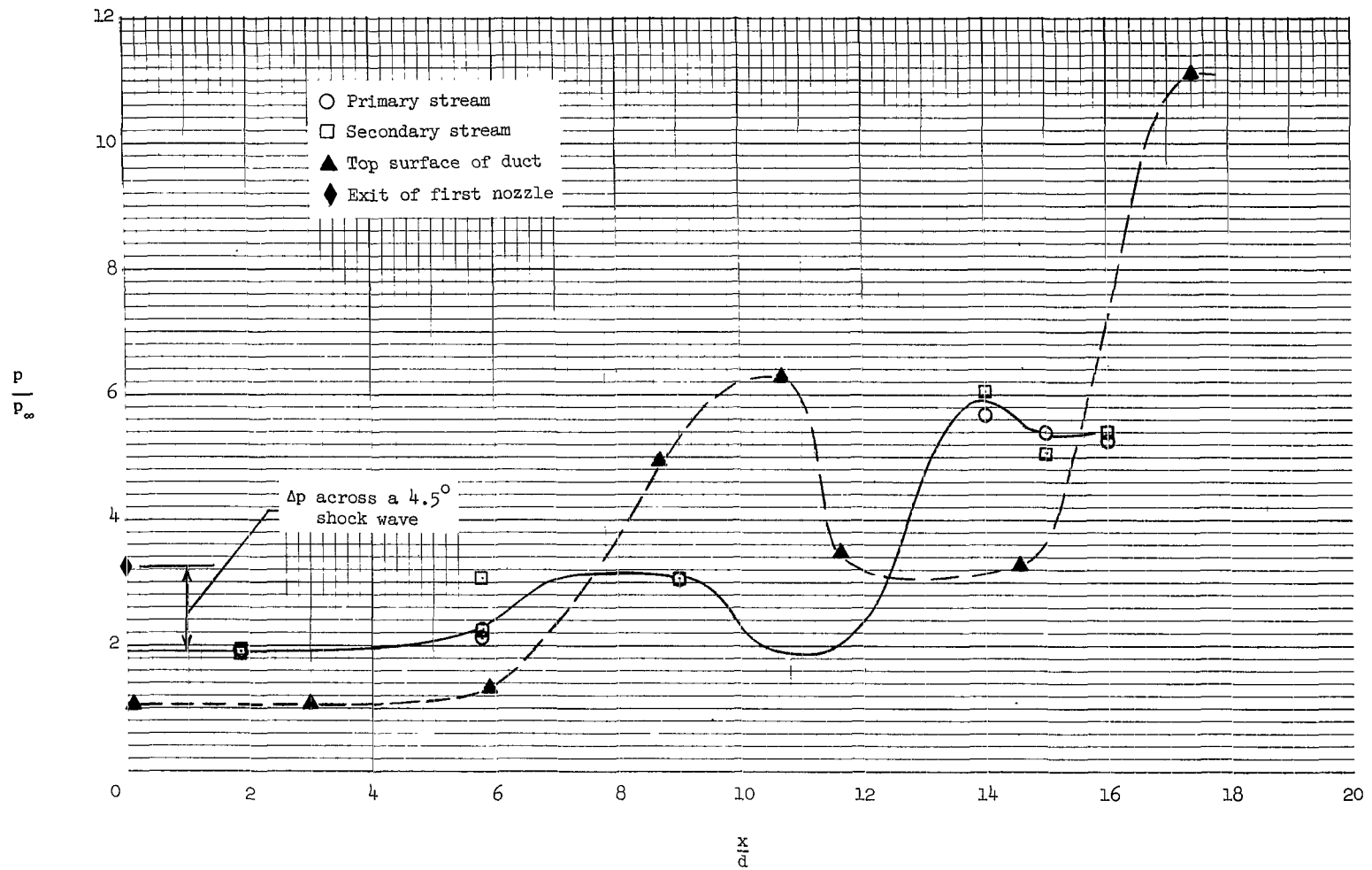
(b) $p_{t,2}/p_{t,1} = 4.0$.

Figure 6.- Continued.
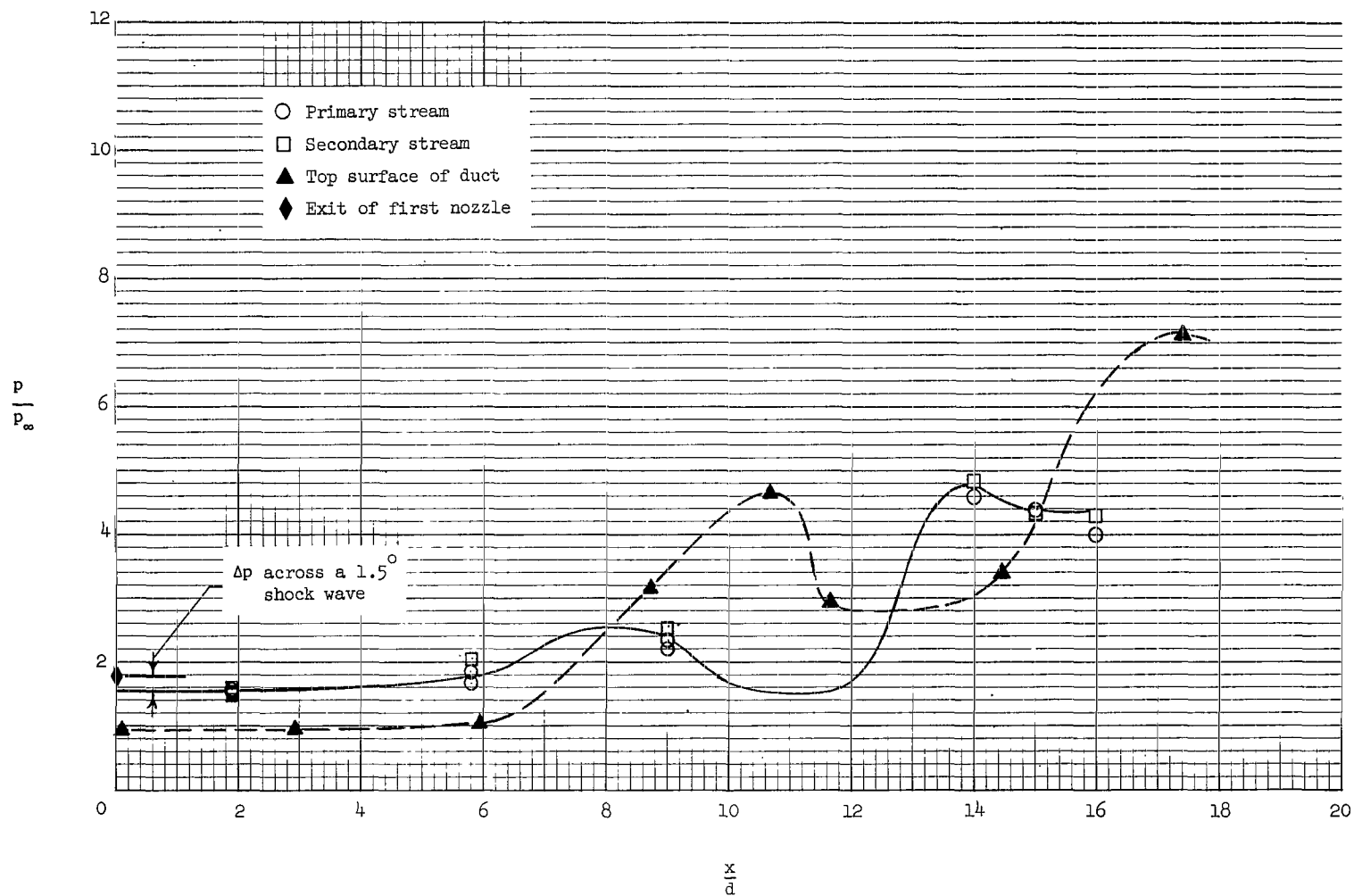
(c) $p_{t,2}/p_{t,1} = 2.67$.

Figure 6.- Concluded.
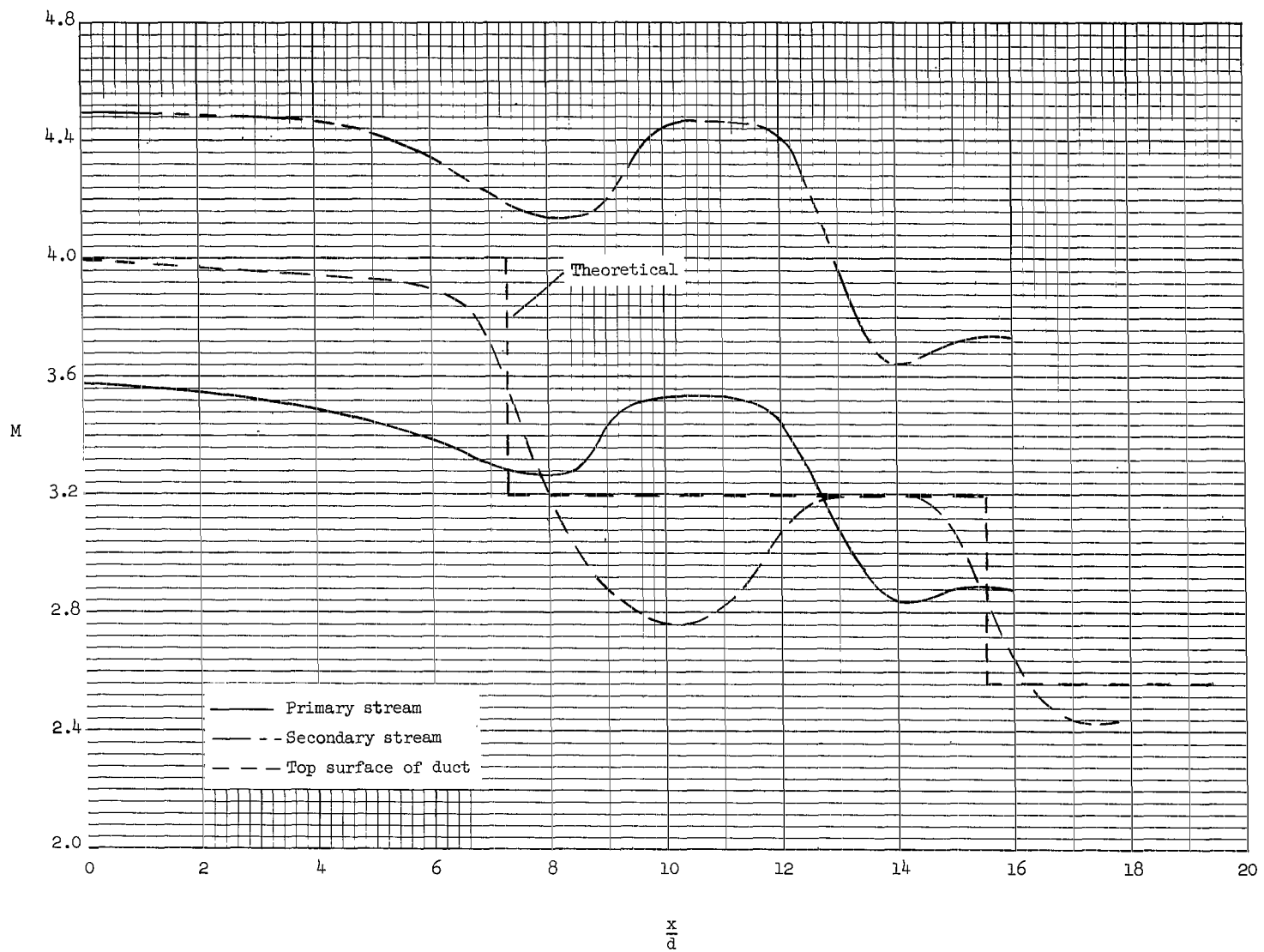
(a) $p_{t,2}/p_{t,1} = 3.34$.

Figure 7.- Mach number through the two-dimensional duct.
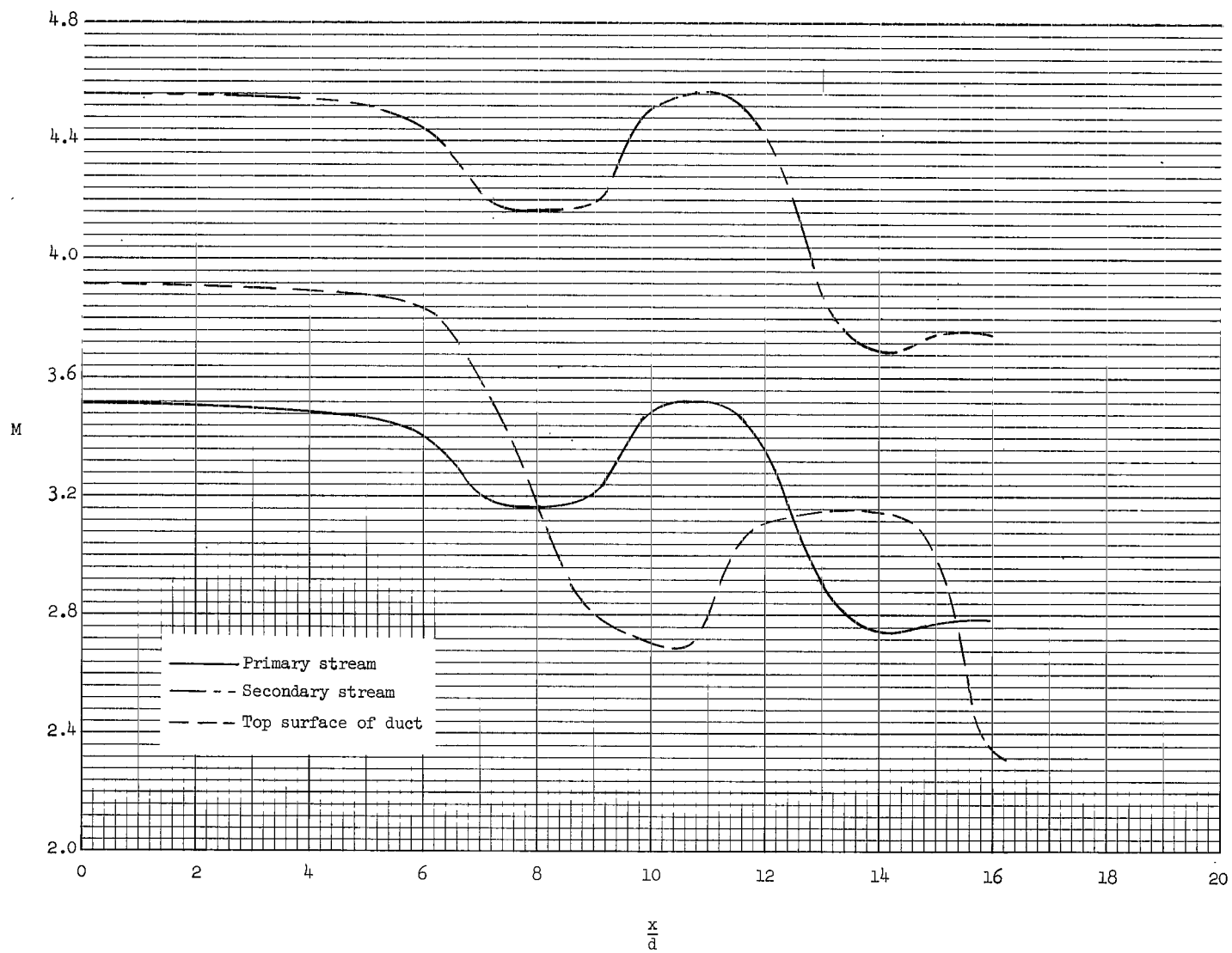
(b) $p_{t,2}/p_{t,1} = 4.0$.

Figure 7.- Continued.
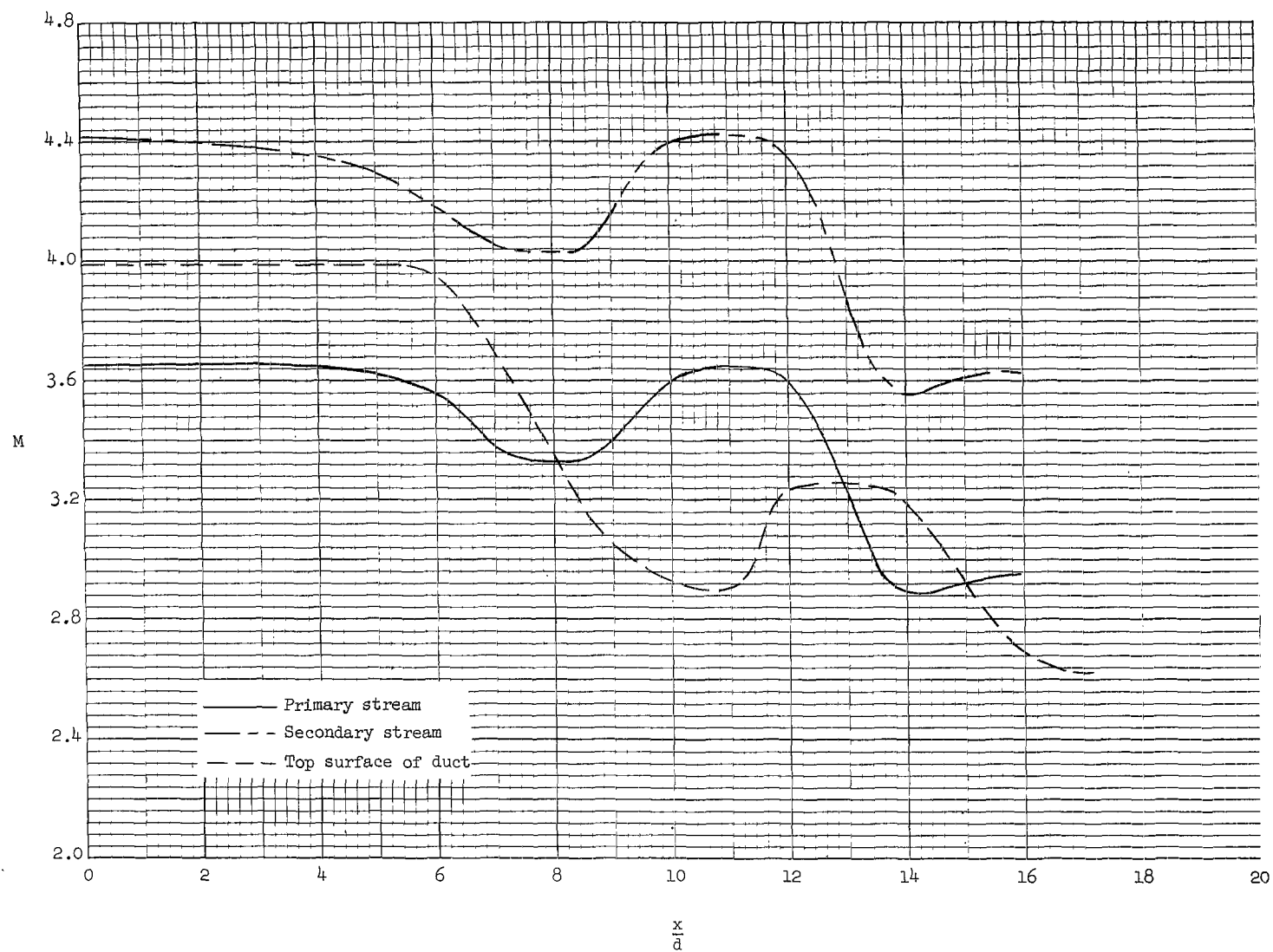
(c) $p_{t,2}/p_{t,1} = 2.67$.

Figure 7.- Concluded.
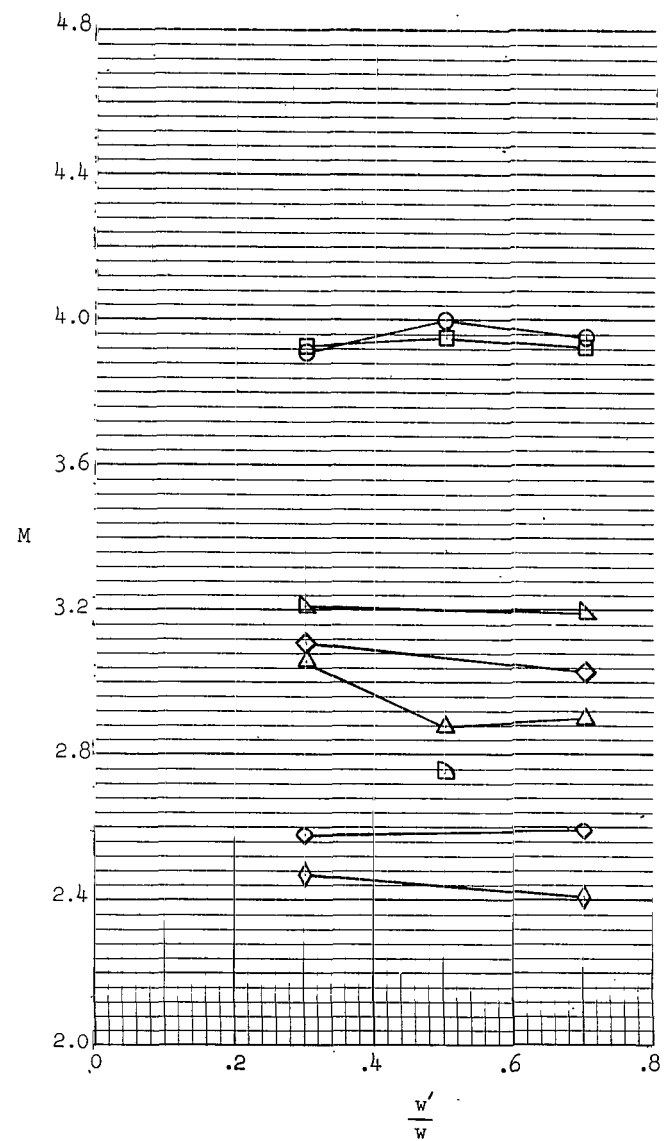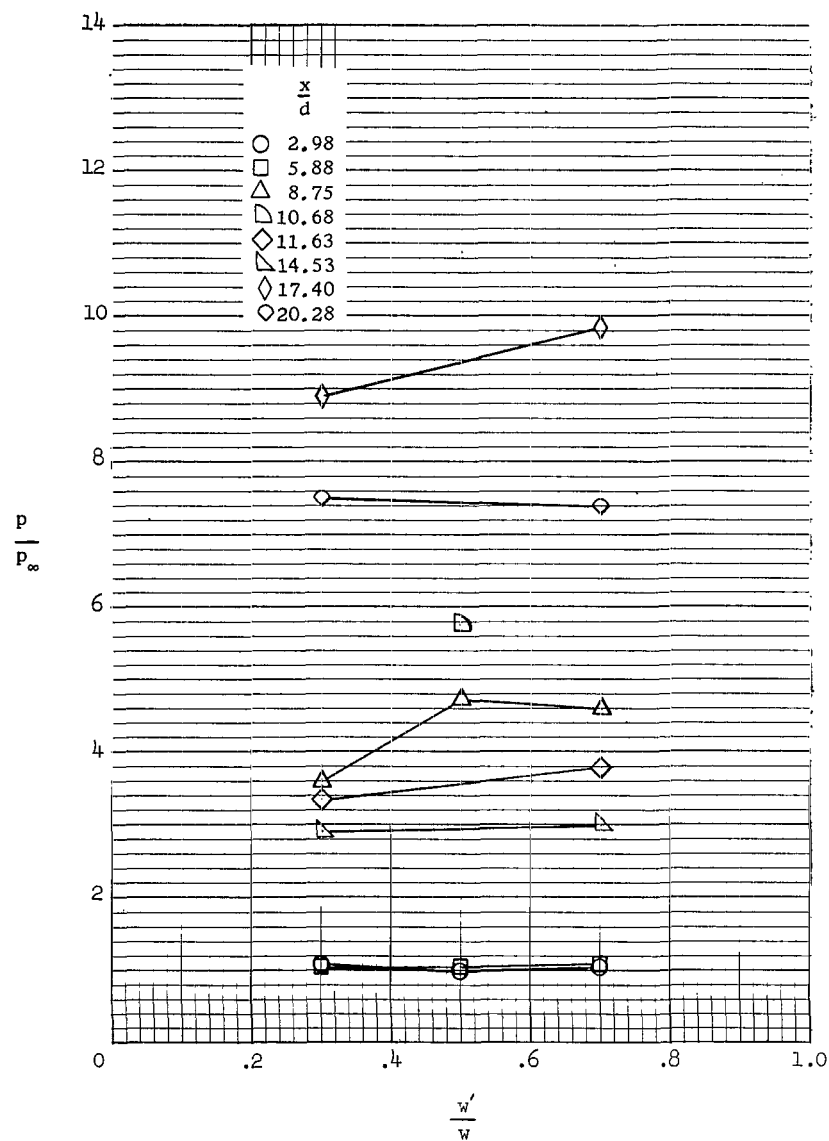
Figure 8.- Static pressure and Mach number across top surface of two-dimensional duct at $p_{t,2}/p_{t,1} = 3.34$.

46
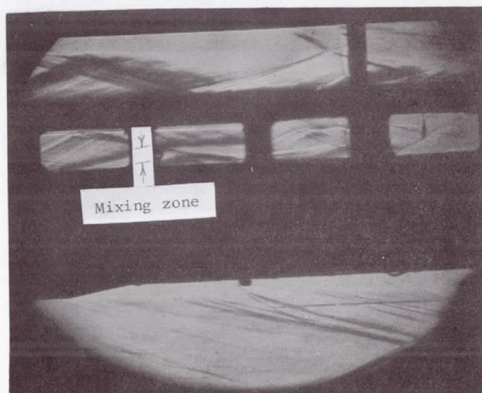
(a) $p_{t,2}/p_{t,1} = 4.00$; $l = 1.78$ cm.
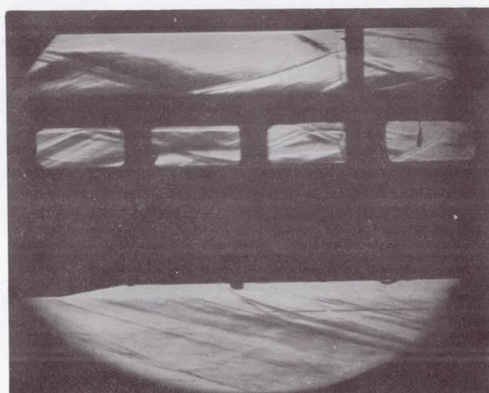
(b) $p_{t,2}/p_{t,1} = 3.34$; $l = 1.78$ cm.
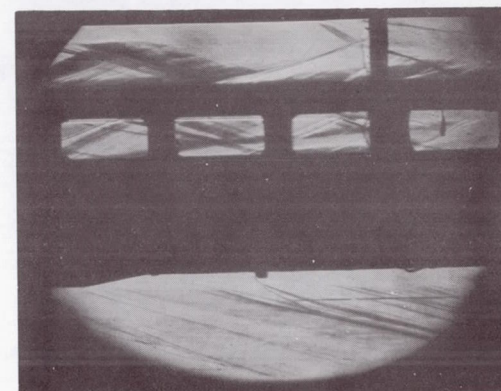
(c) $p_{t,2}/p_{t,1} = 2.67$; $l = 1.78$ cm.
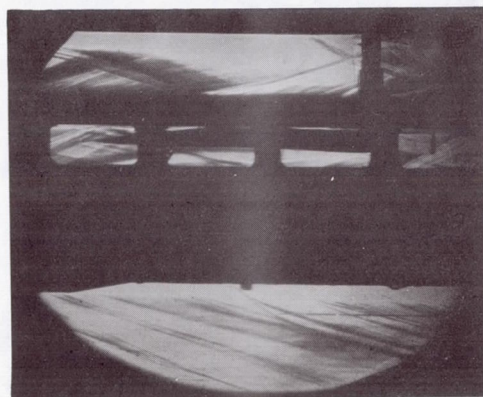
(d) $l = 13.97$ cm; $p_{t,2}/p_{t,1} = 3.34$.
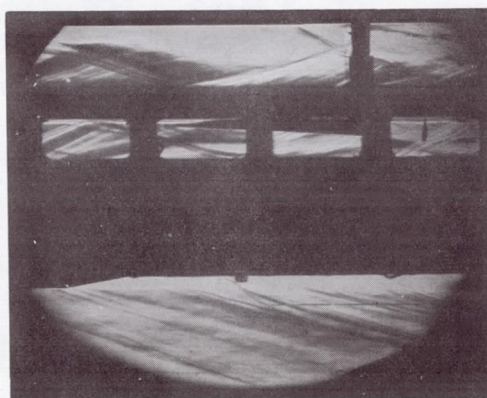
(e) $l = 9.65$ cm; $p_{t,2}/p_{t,1} = 3.34$.
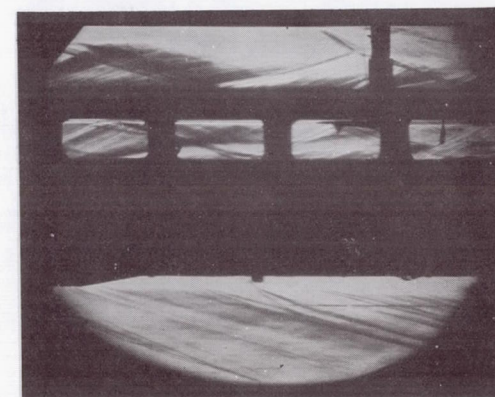
(f) $l = 1.78$ cm; $p_{t,2}/p_{t,1} = 3.34$.

Figure 9.- Schlieren photographs.

L-68-8588
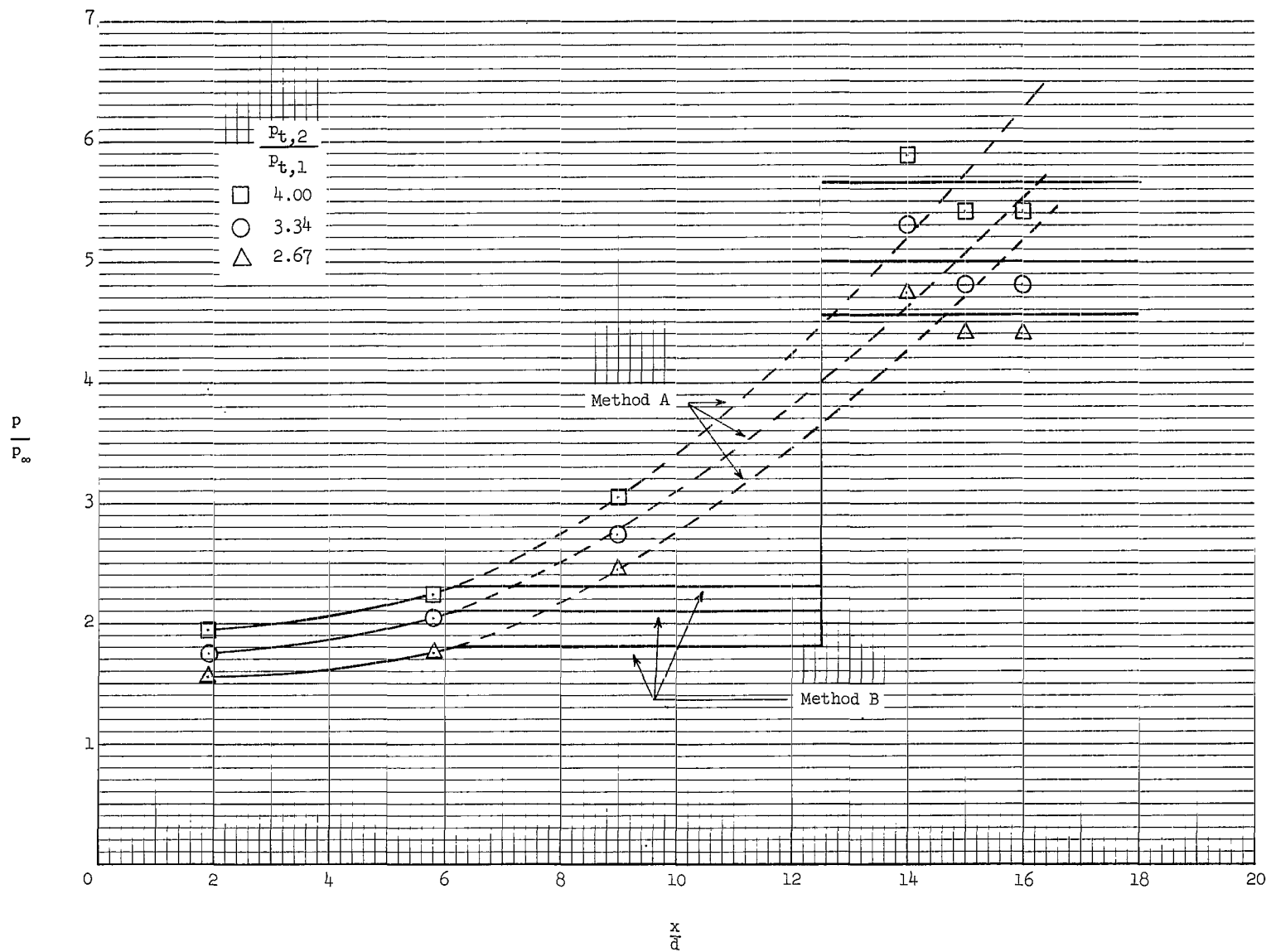
Figure 10.- Static-pressure distributions along mixing path used for theoretical mixing calculations.

h'_A, cm

V_A, m/sec

$\dfrac{p_{t,2}}{p_{t,1}}$	$\dfrac{p}{p_\infty}$
□ 4.00	1.94
○ 3.34	1.74
△ 2.67	1.54
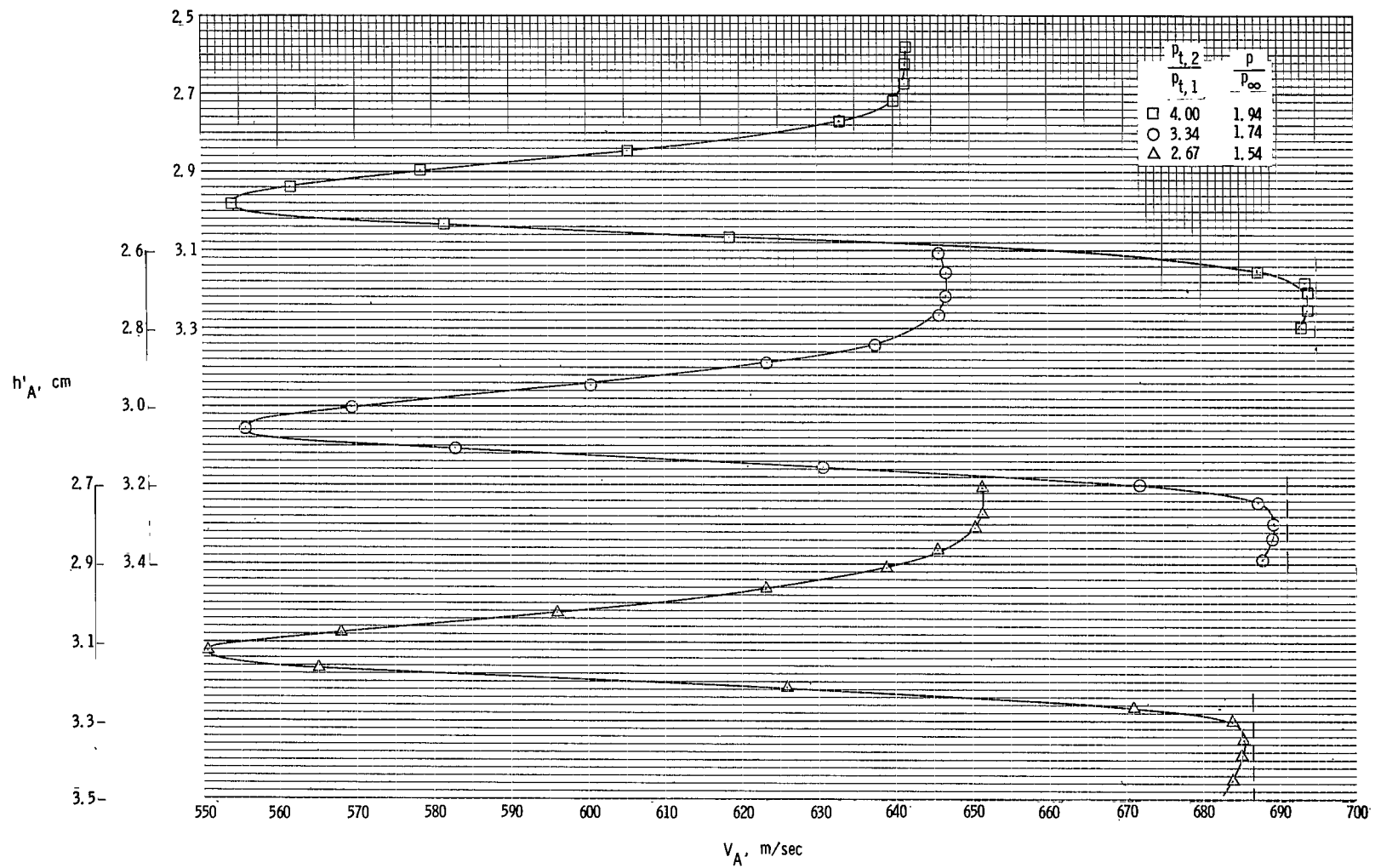
(a) x/d = 1.9.

Figure 11. Velocity profiles through the mixing region.
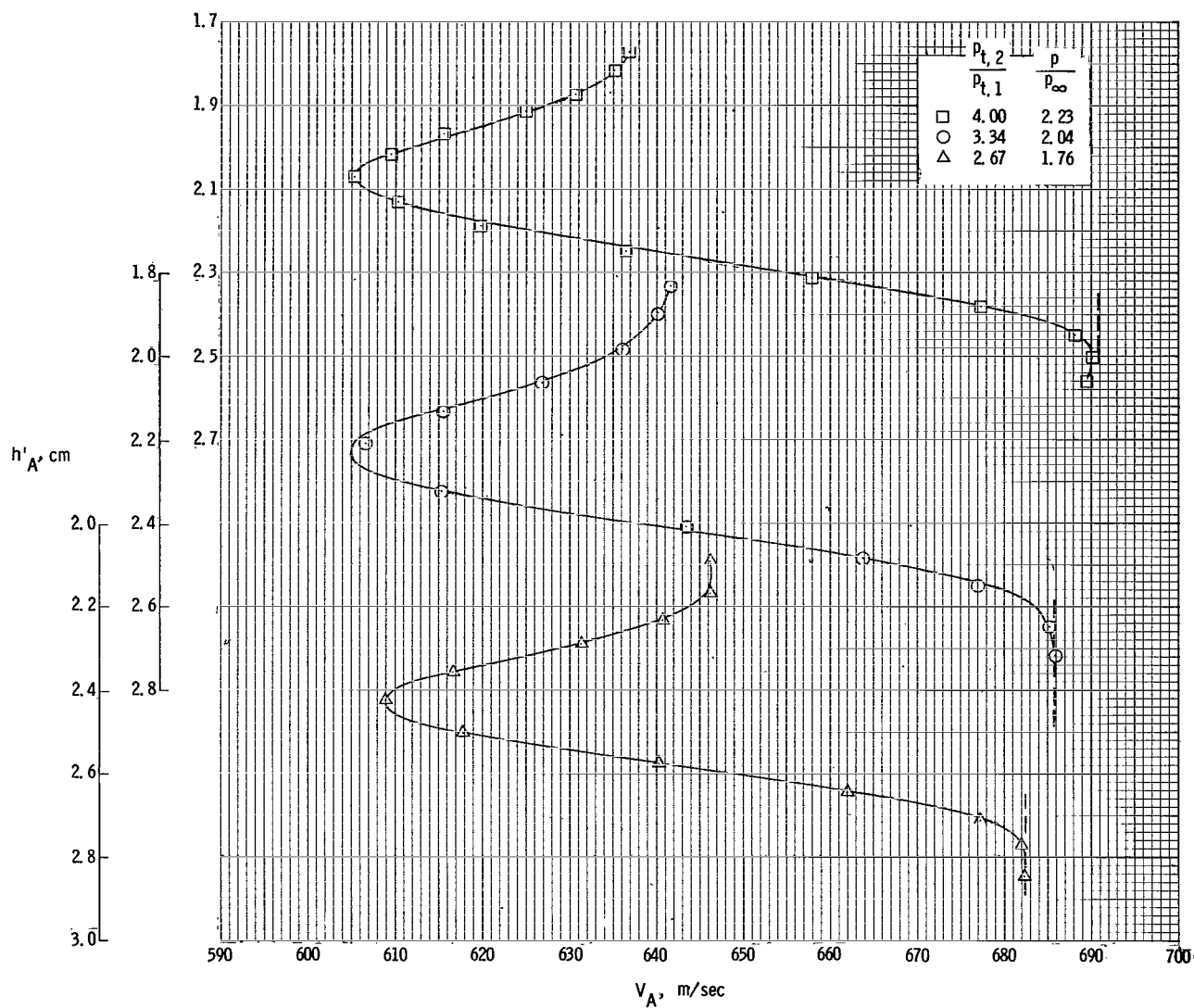
(b) x/d = 5.8.

Figure 11.- Continued.
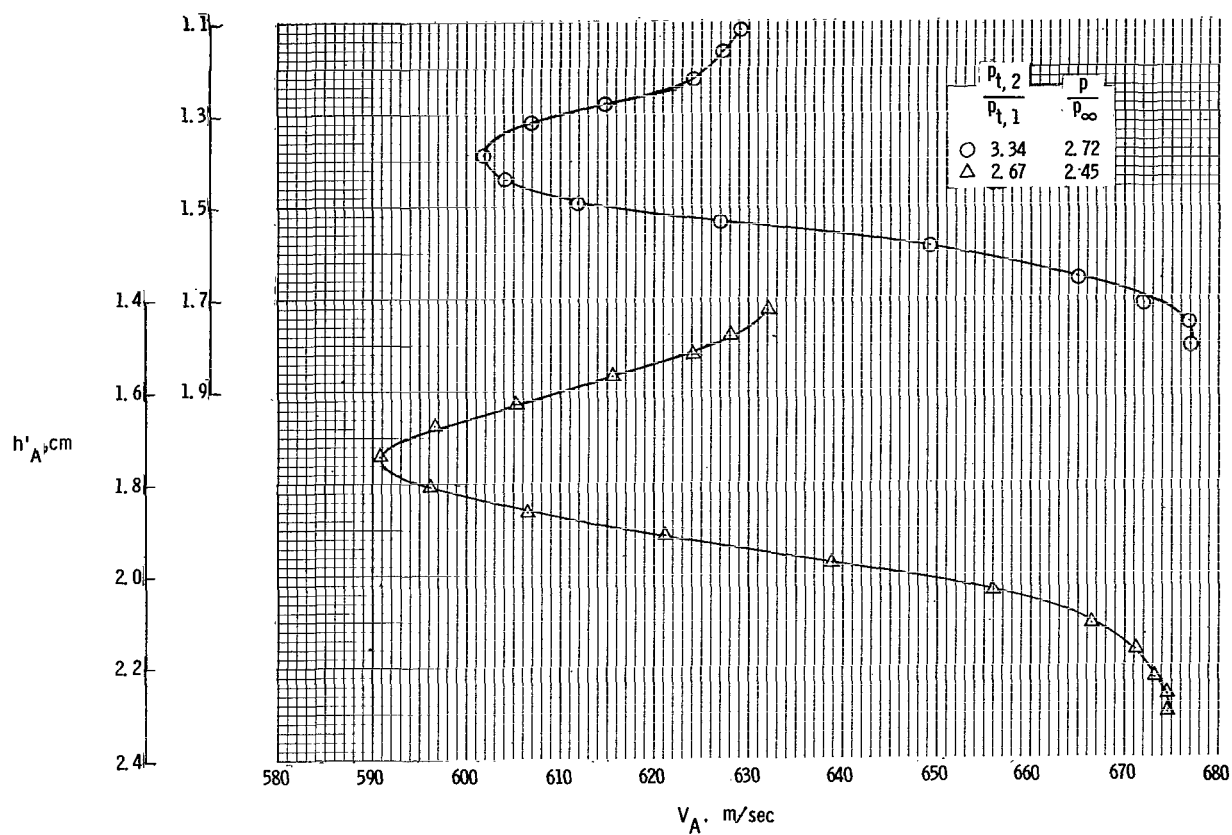
(c) x/d = 9.0.

Figure 11.- Continued.
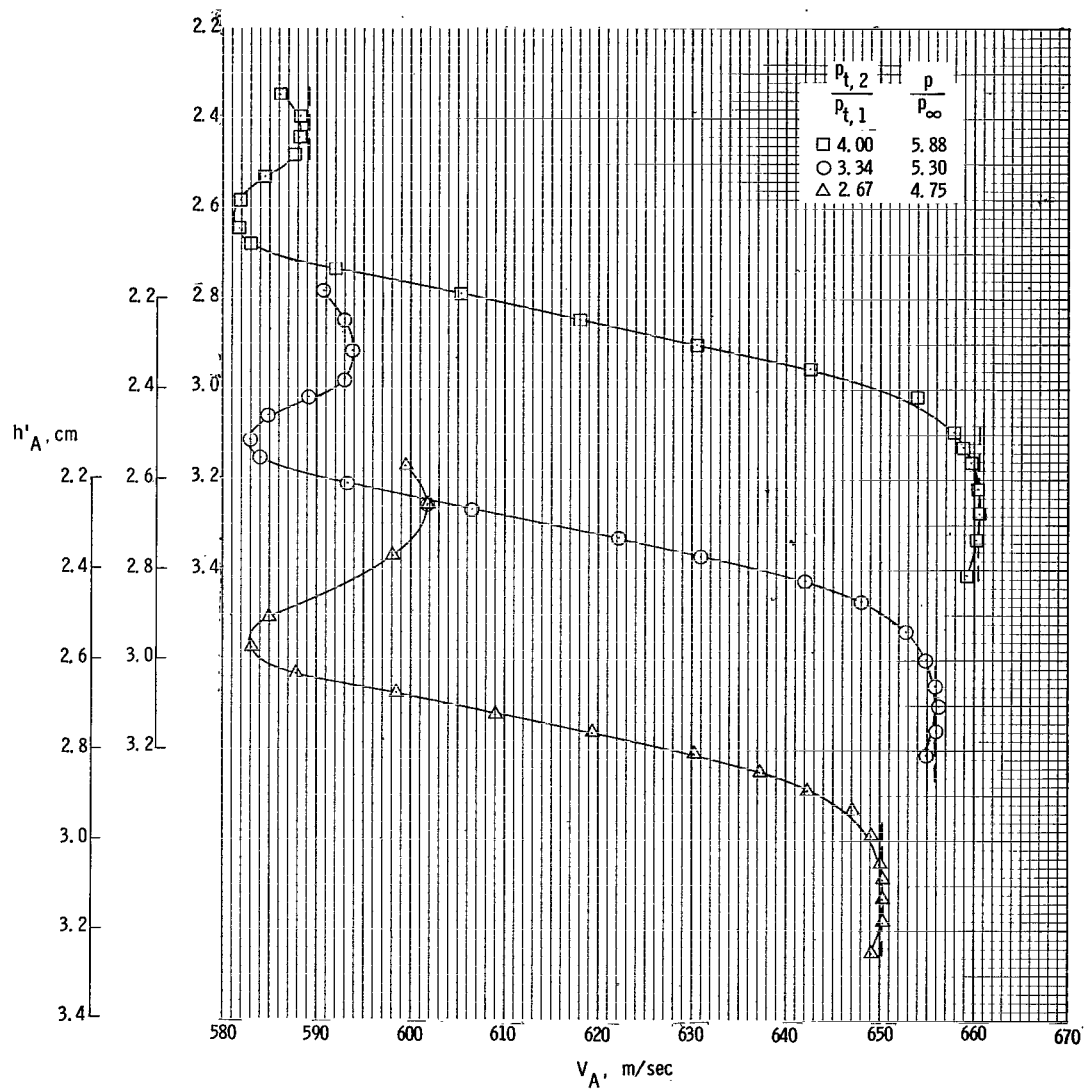
(d) x/d = 14.0.
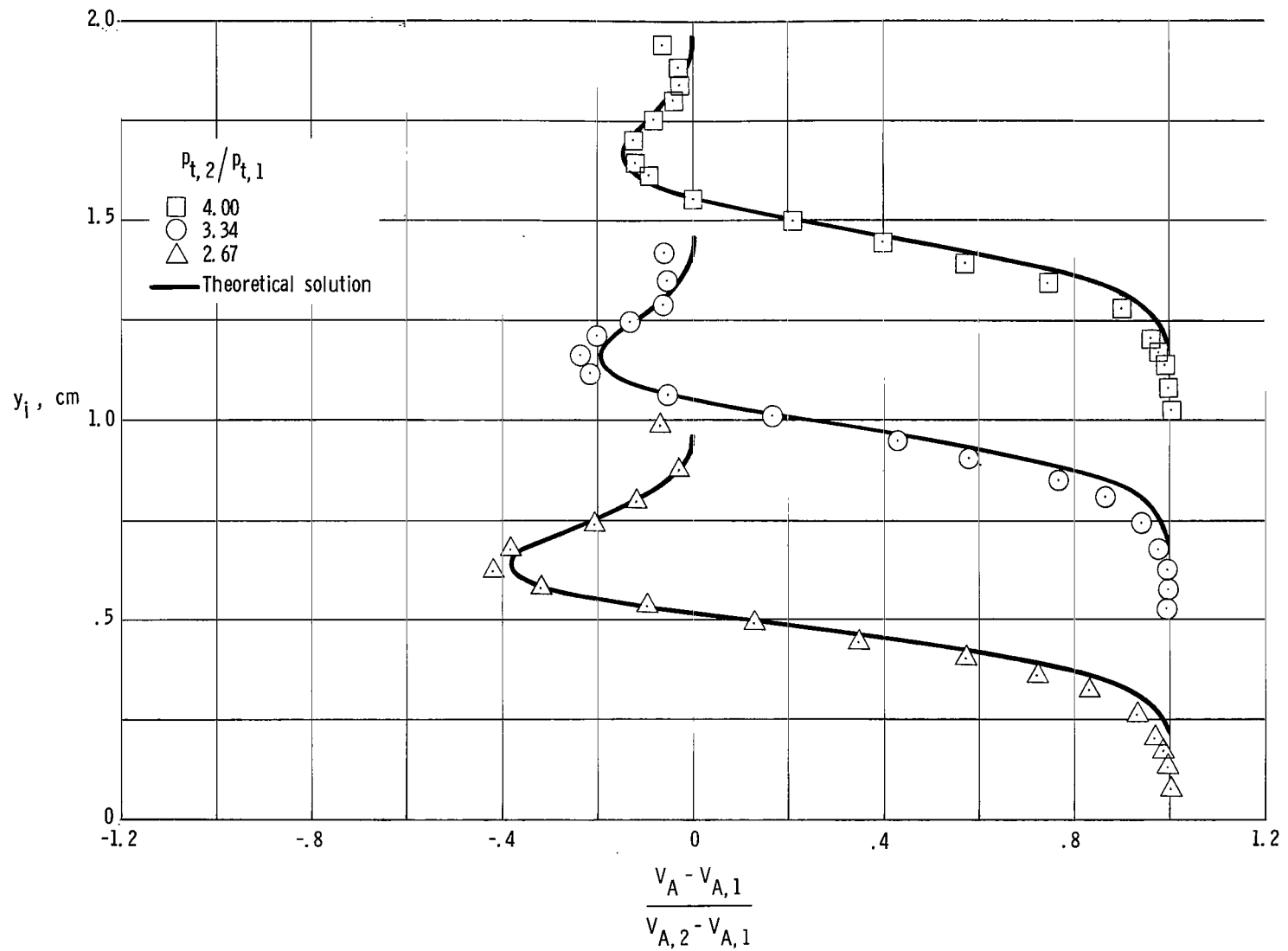
Figure 11.- Continued.
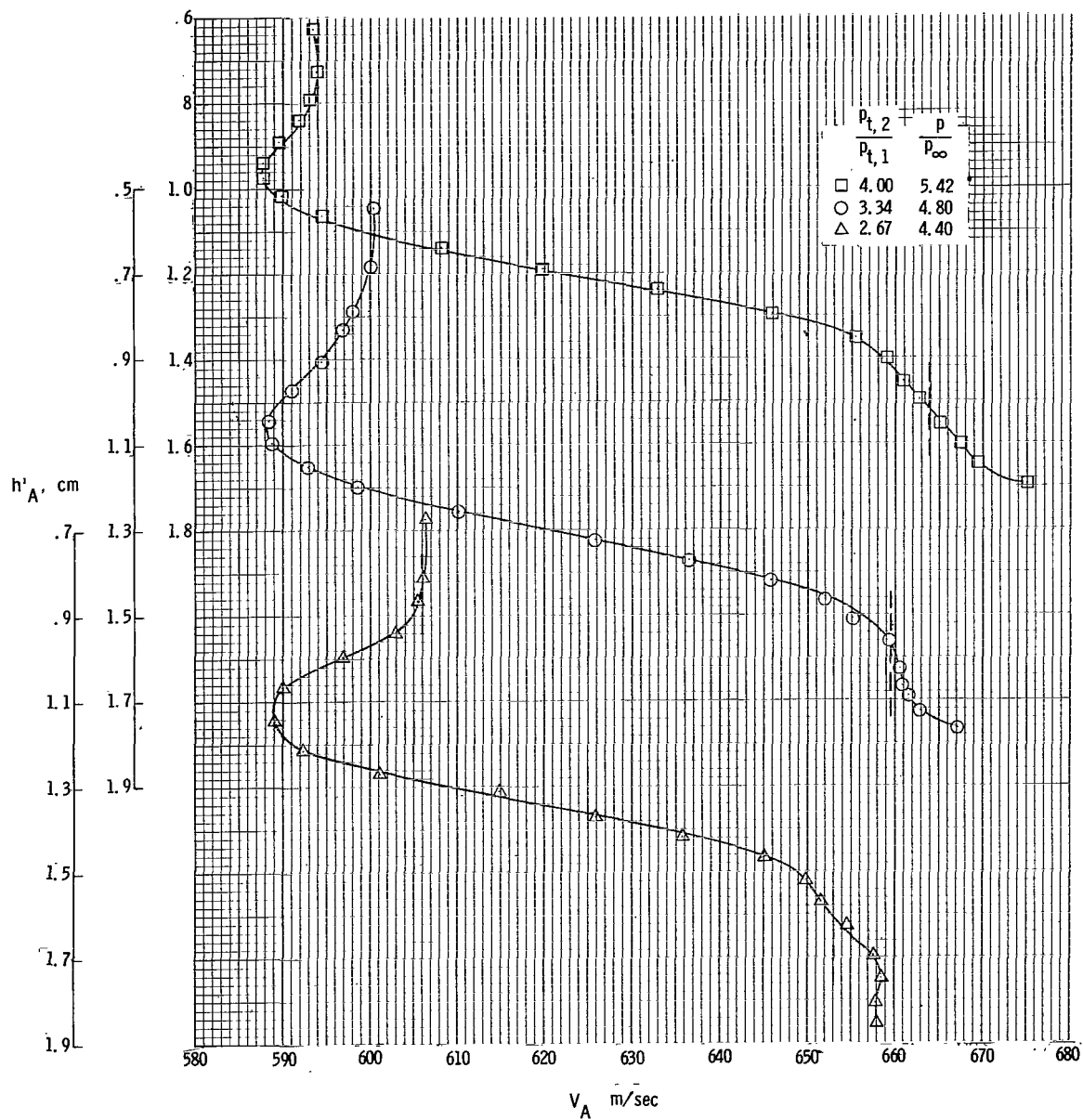
(e) x/d = 15.0.

Figure 11.- Continued.
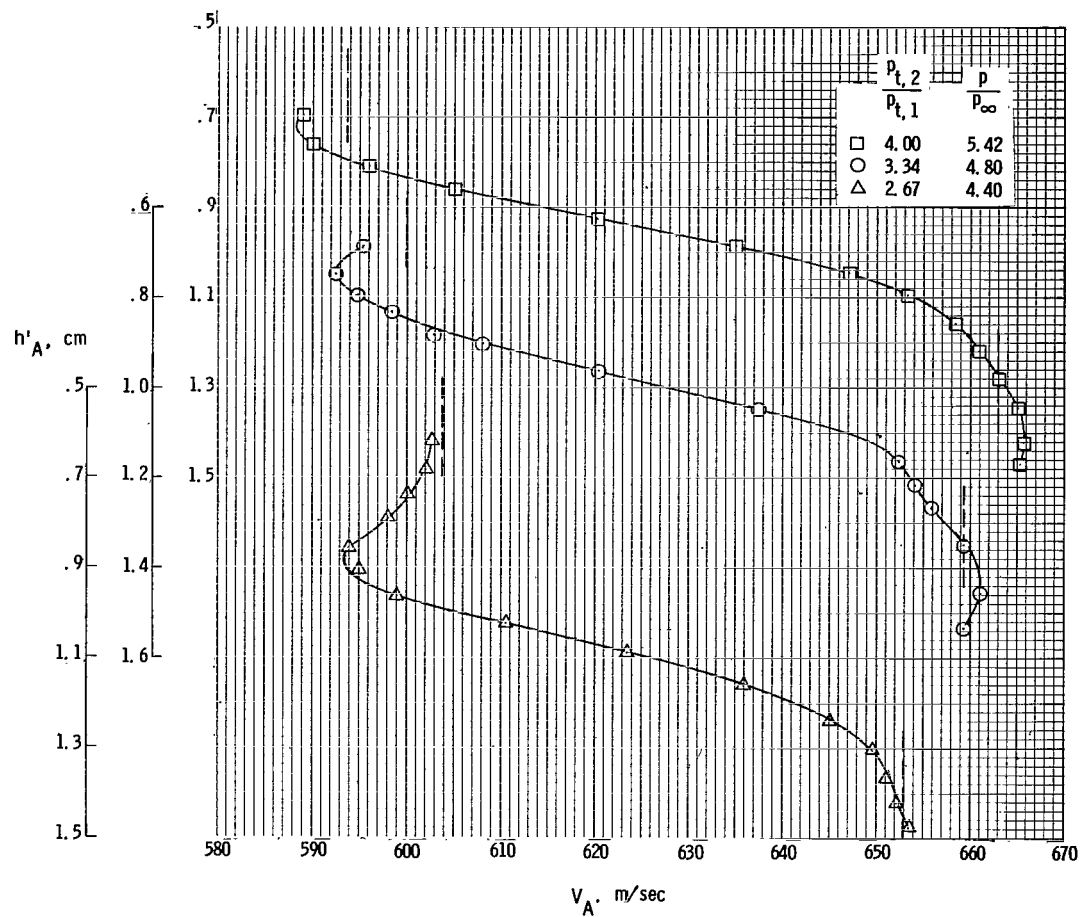
(f) x/d = 16.0.

Figure 11.- Concluded.

Eddy-viscosity models

$$\epsilon = K \; r_{1/2} \; (\rho V)_{\mathbb{C}}$$

$$\epsilon = K \; J \; (\rho V)_{\mathbb{C}}$$
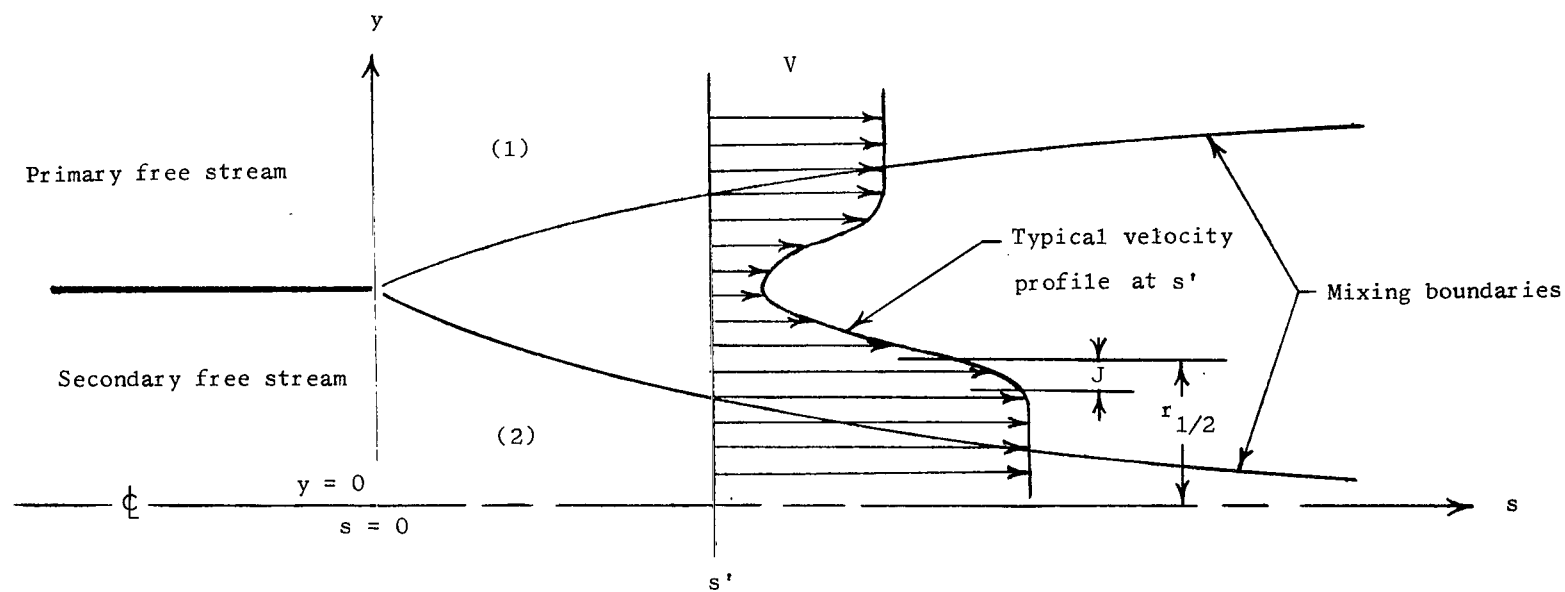
Figure 12.- Schematic of flow field for the theoretical solution.
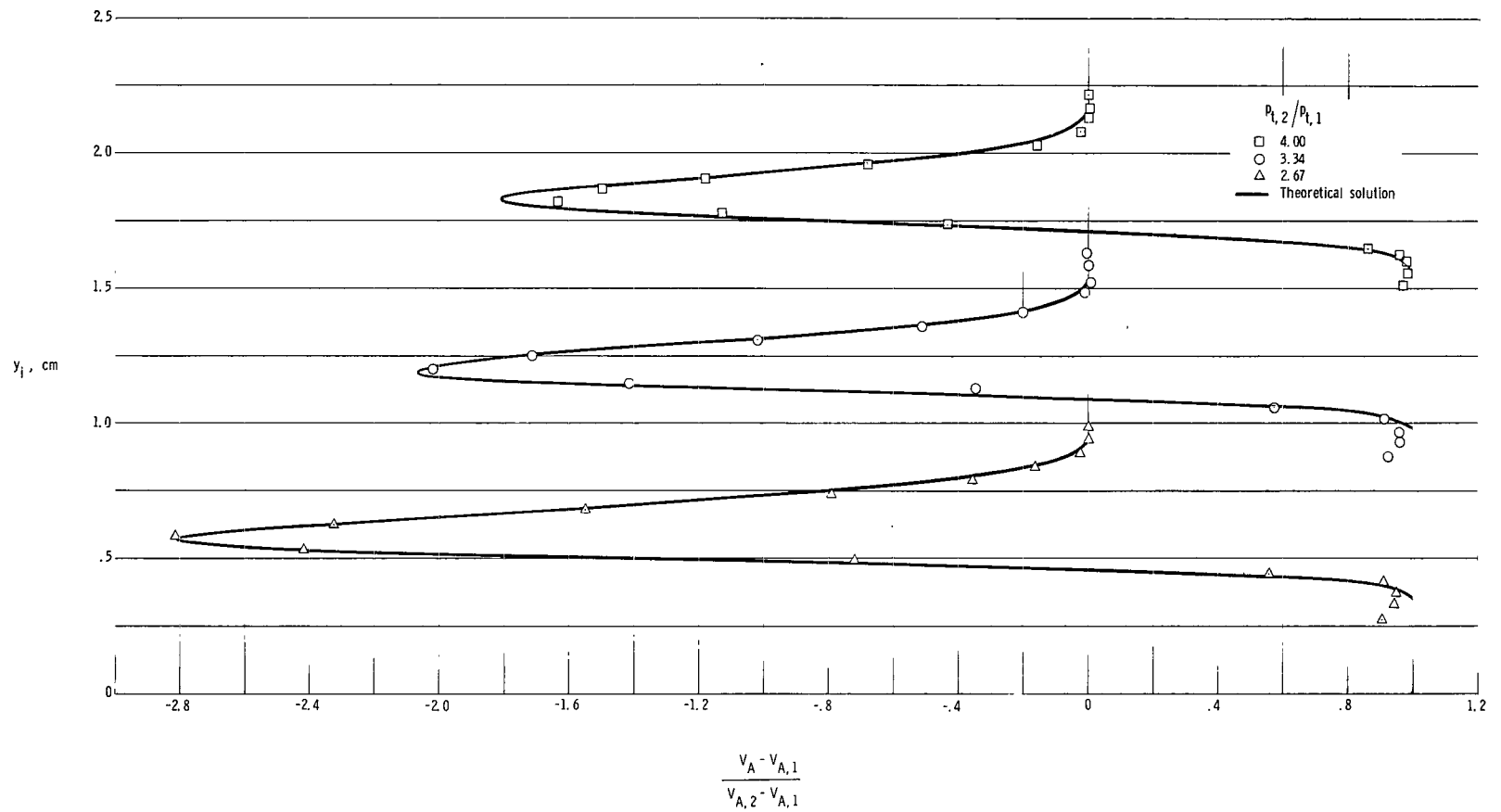
Figure 13.- Velocity data at $x/d = 1.9$.
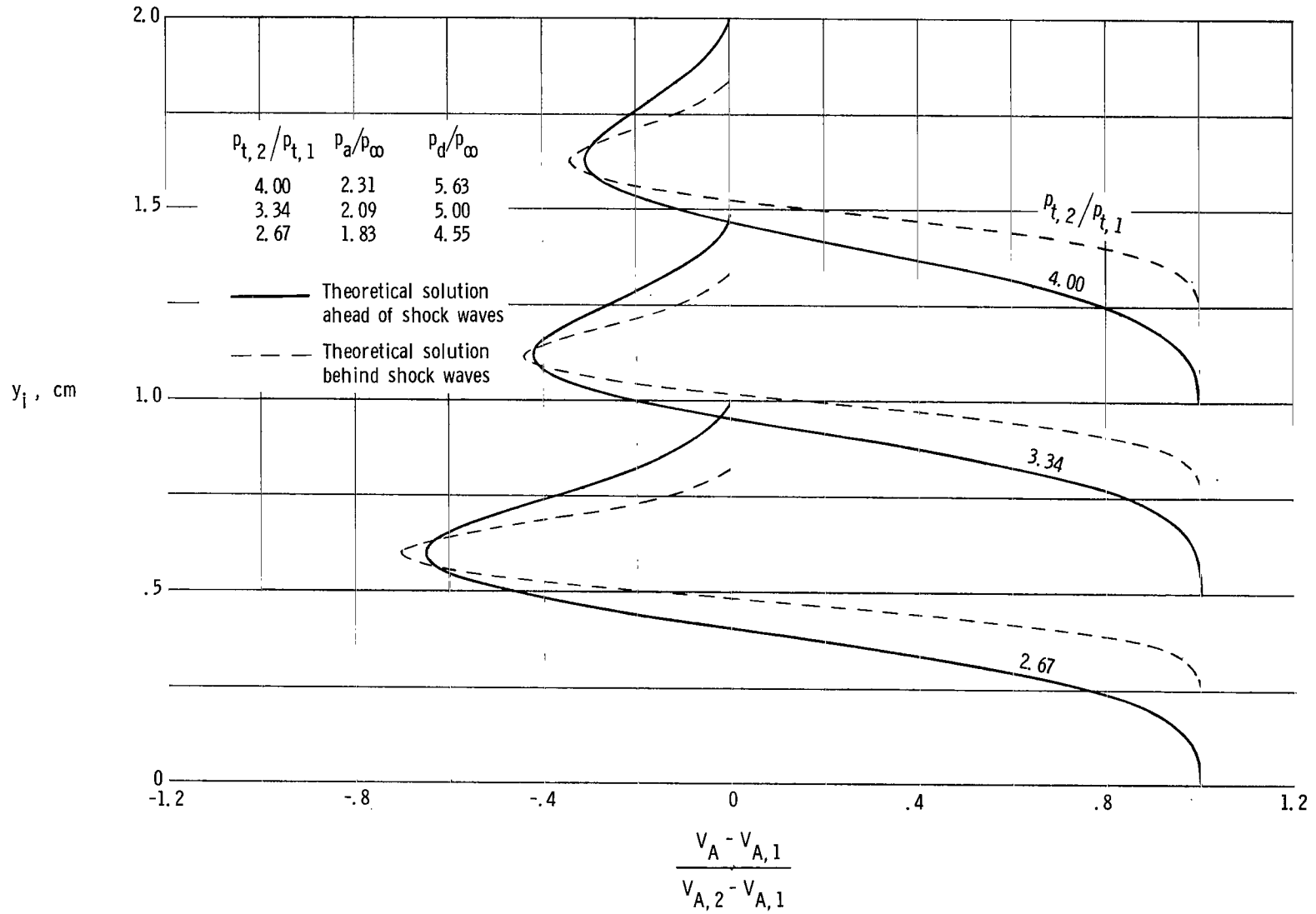
Figure 14.- Computed velocity profiles at $x/d = 12.5$ before and after crossing two shock waves. $\varepsilon = Kr_{1/2}(\rho V)_{\mathfrak{k}}$.
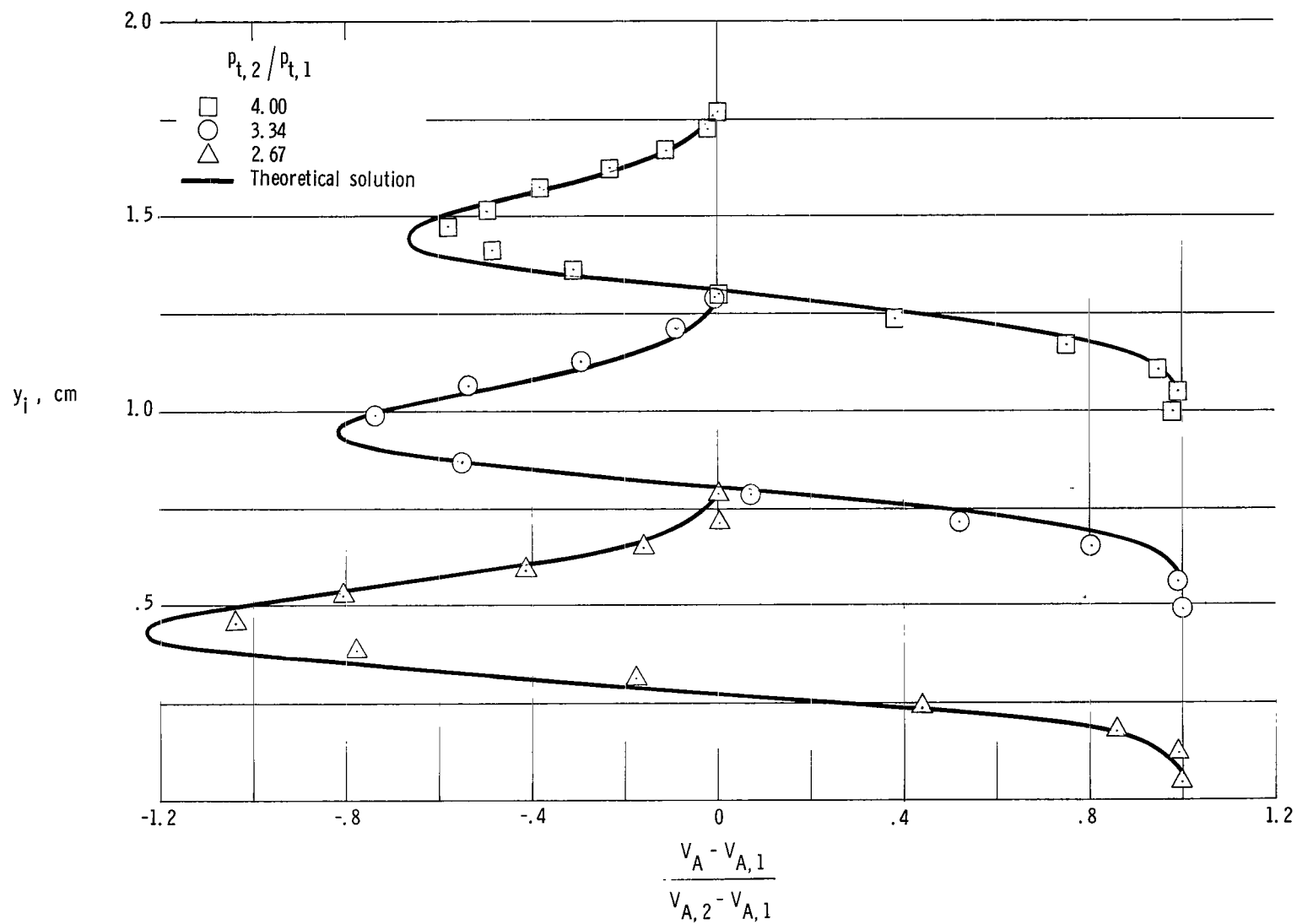
(a) x/d = 5.8.

Figure 15.- Correlation of theoretical velocity profiles with data. $\varepsilon = Kr_{1/2}(\rho V)_{\dot{c}}$, with K = 0.0013.
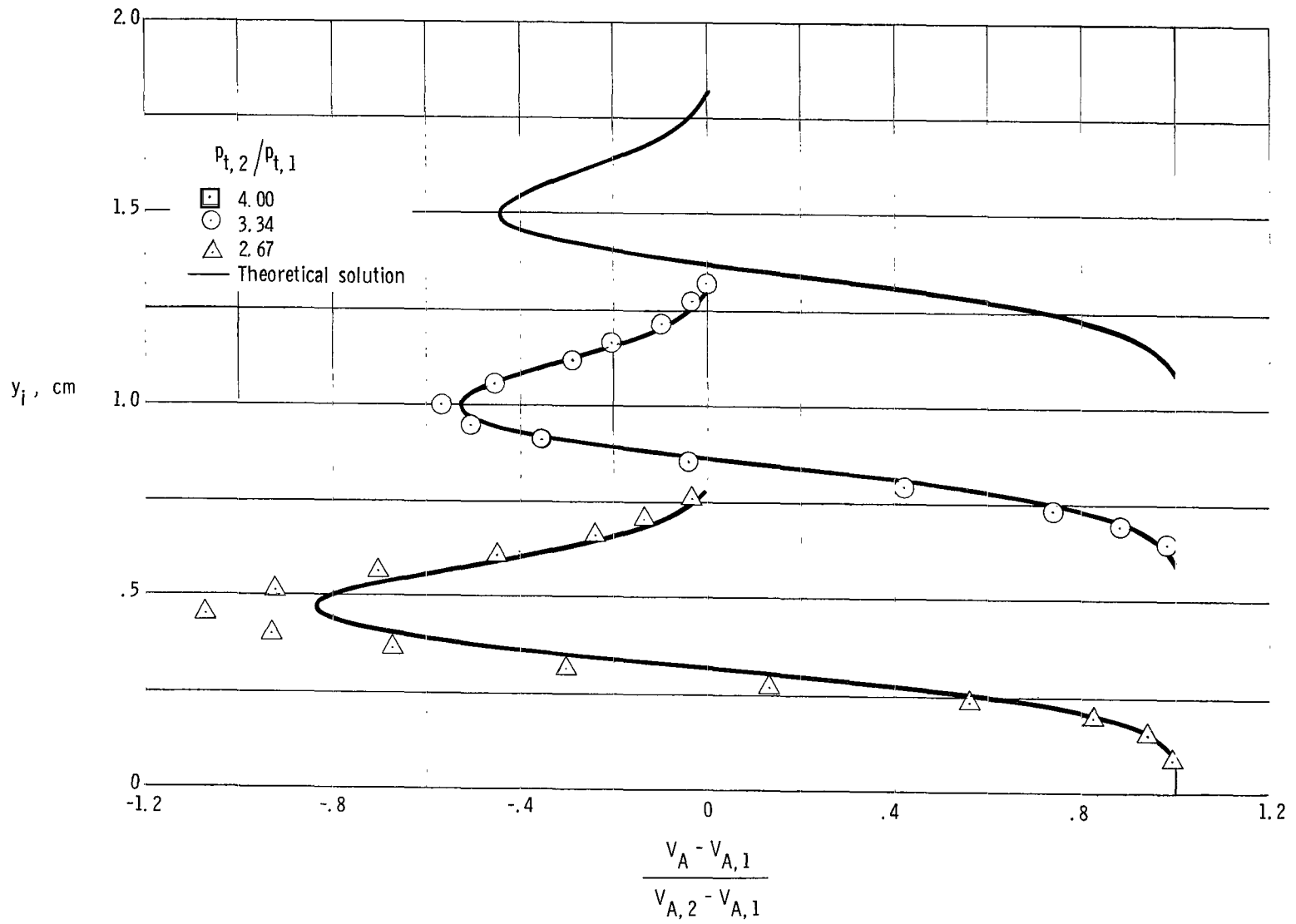
(b) x/d = 9.0.

Figure 15.- Continued.
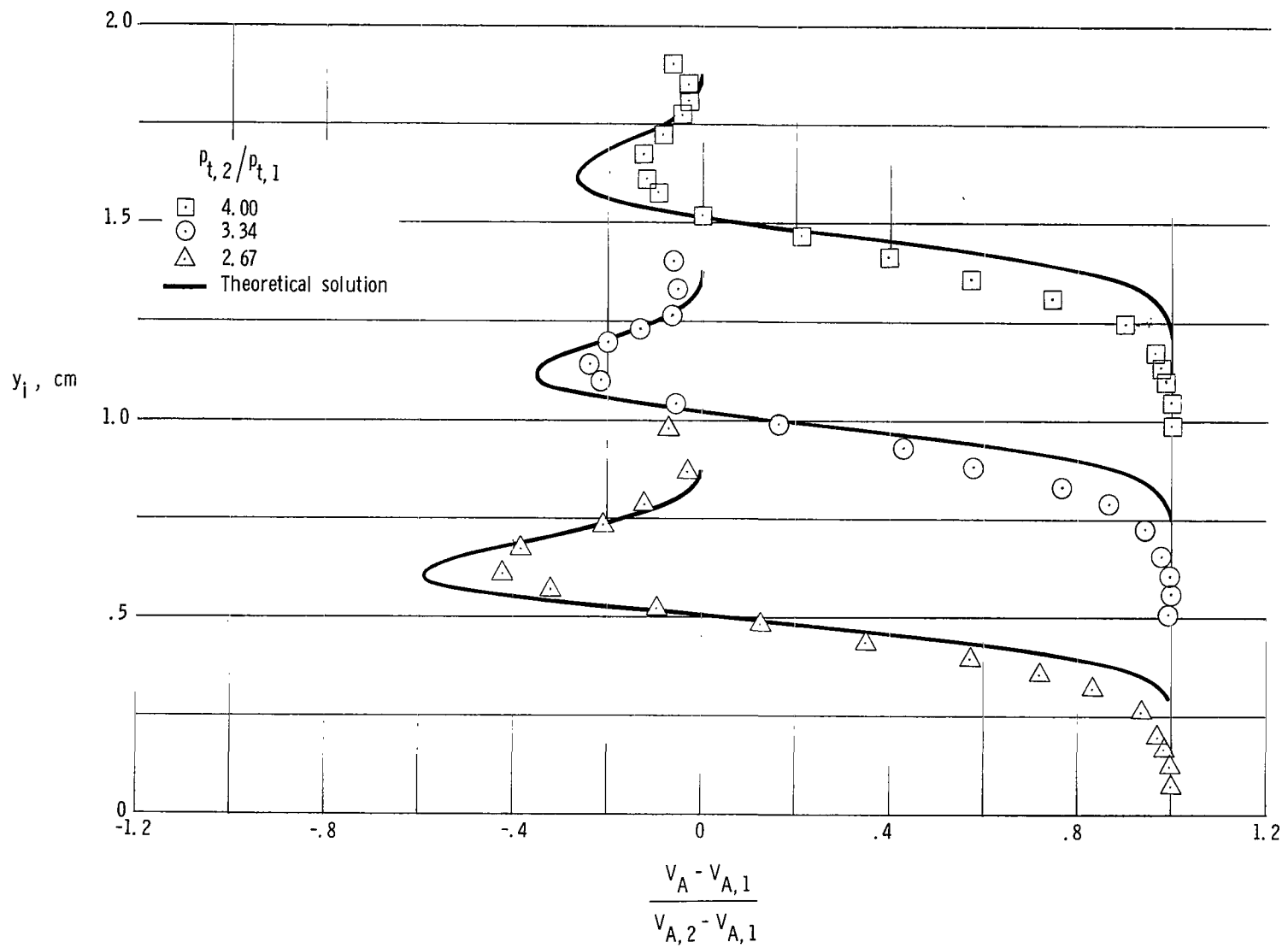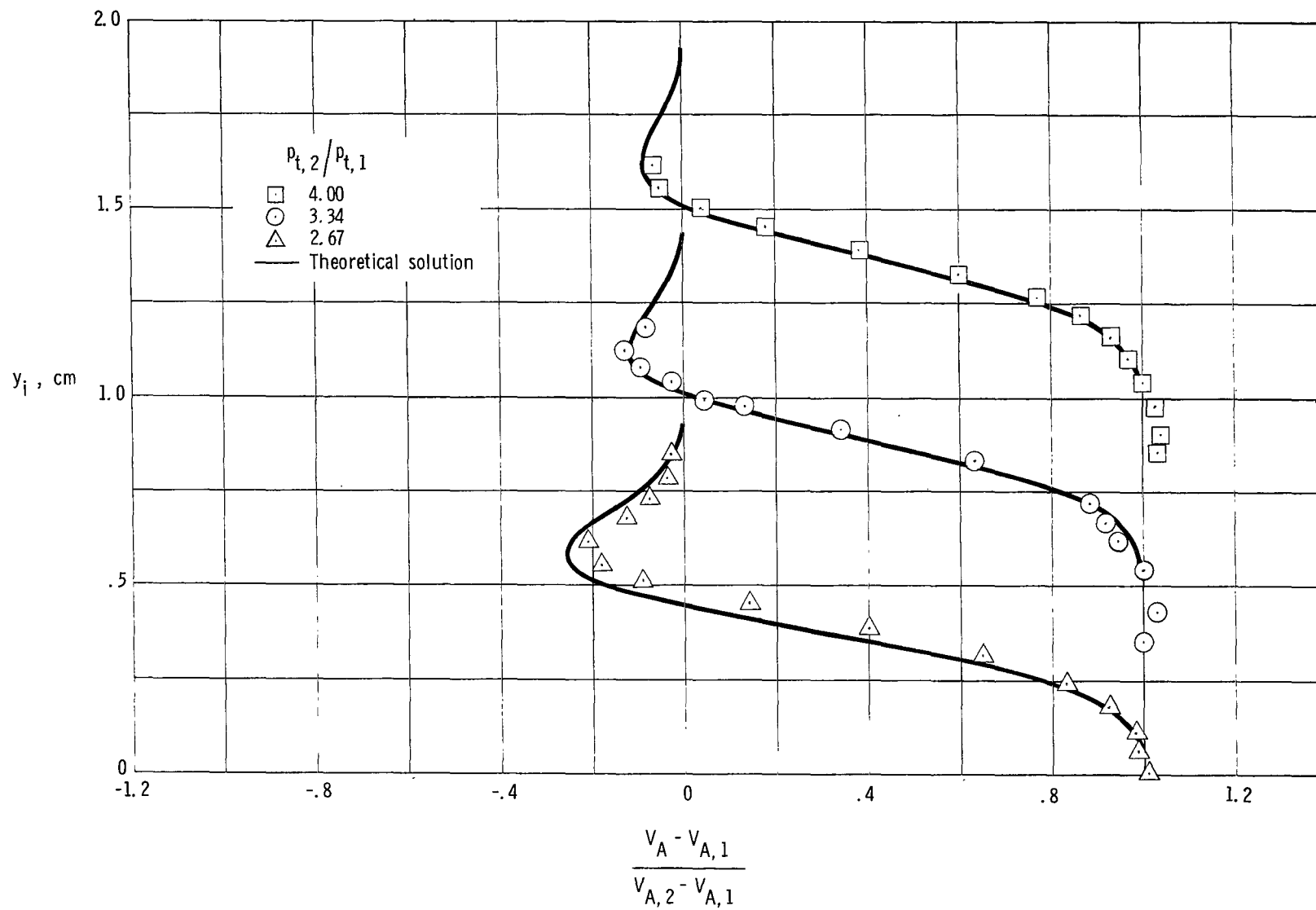
(c) x/d = 14.0.

Figure 15.- Continued.

$$\frac{V_A - V_{A,1}}{V_{A,2} - V_{A,1}}$$
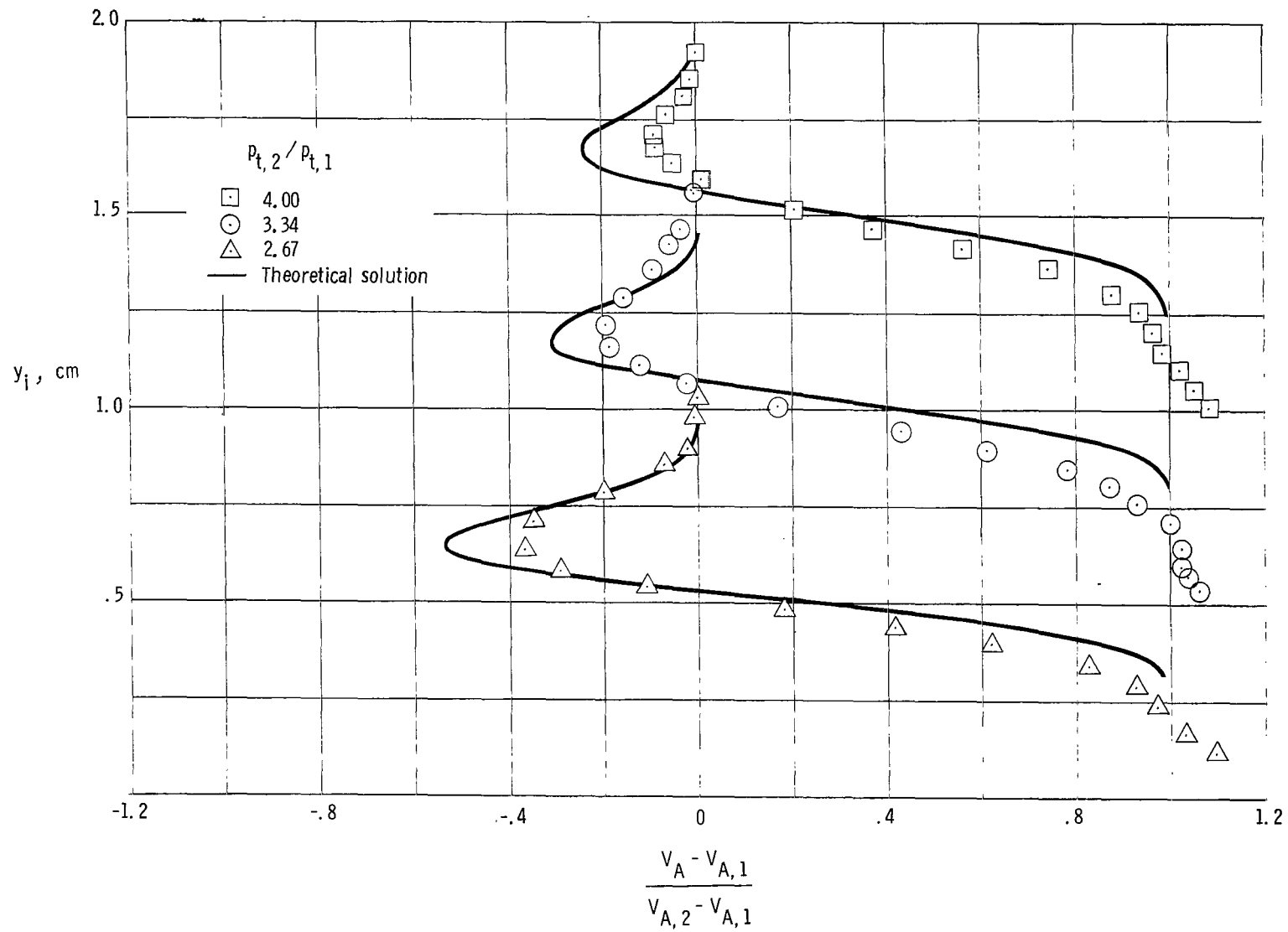
(d) x/d = 15.0.

Figure 15.- Continued.
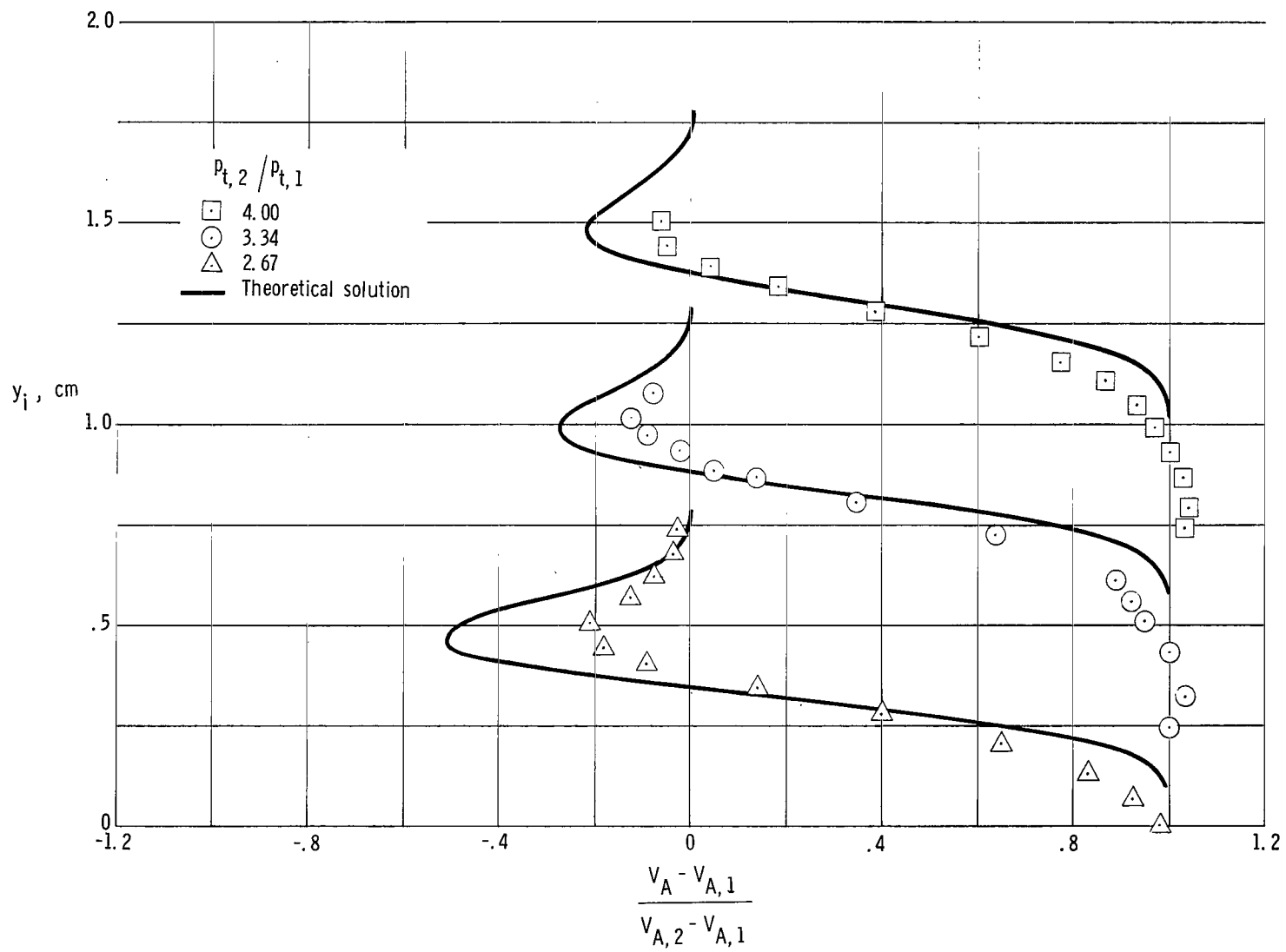
(e) x/d = 16.0.

Figure 15.- Concluded.
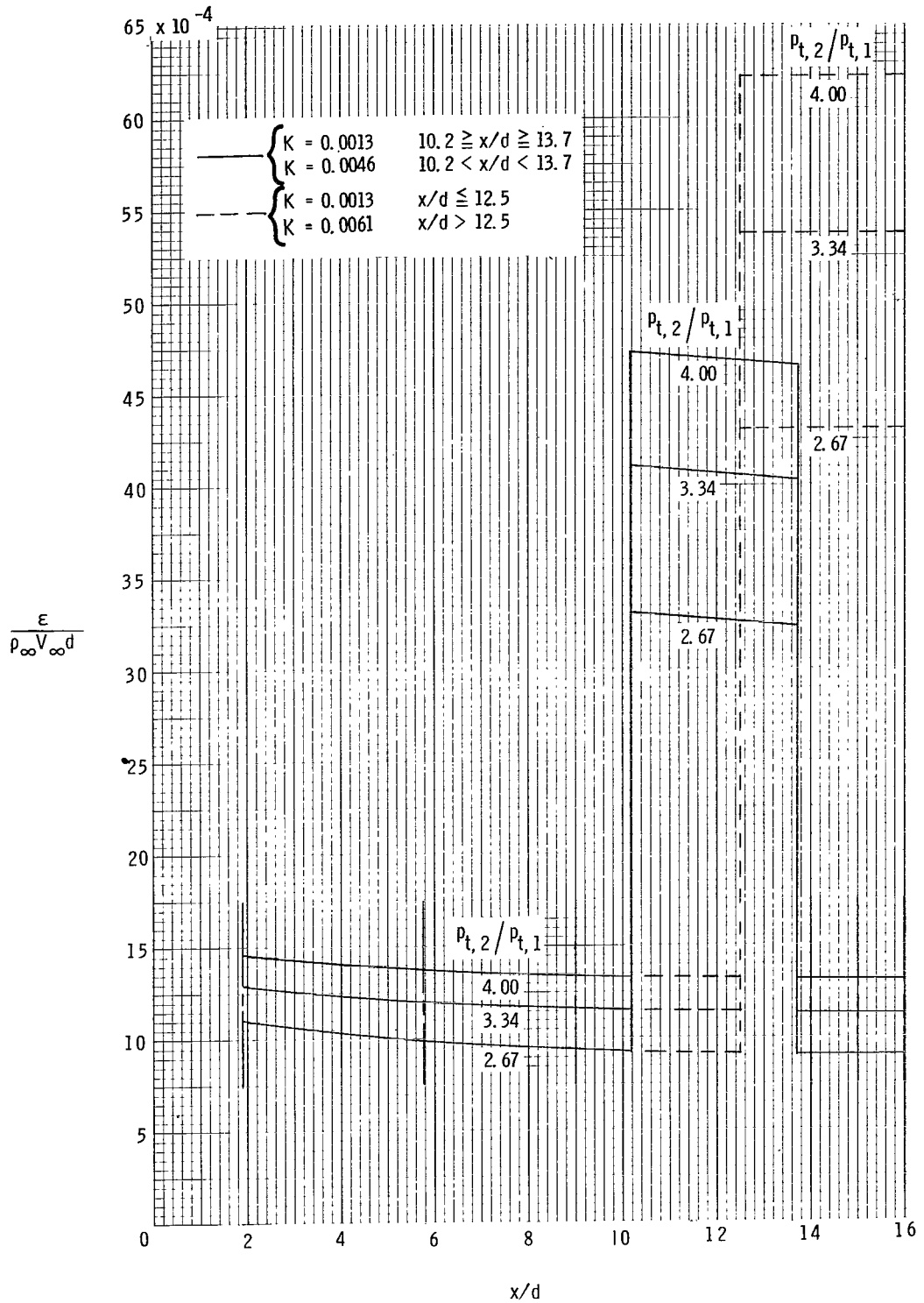
Figure 16.- Theoretical eddy-viscosity distributions. $\varepsilon = Kr_{1/2}(\rho V)_{\mathfrak{C}}$.

(a) x/d = 14.0.

Figure 17.- Correlation of theoretical velocity profiles with data behind shock system. $\varepsilon = Kr_{1/2}(\rho V)_t$, with K = 0.0061 starting at x/d = 12.5.
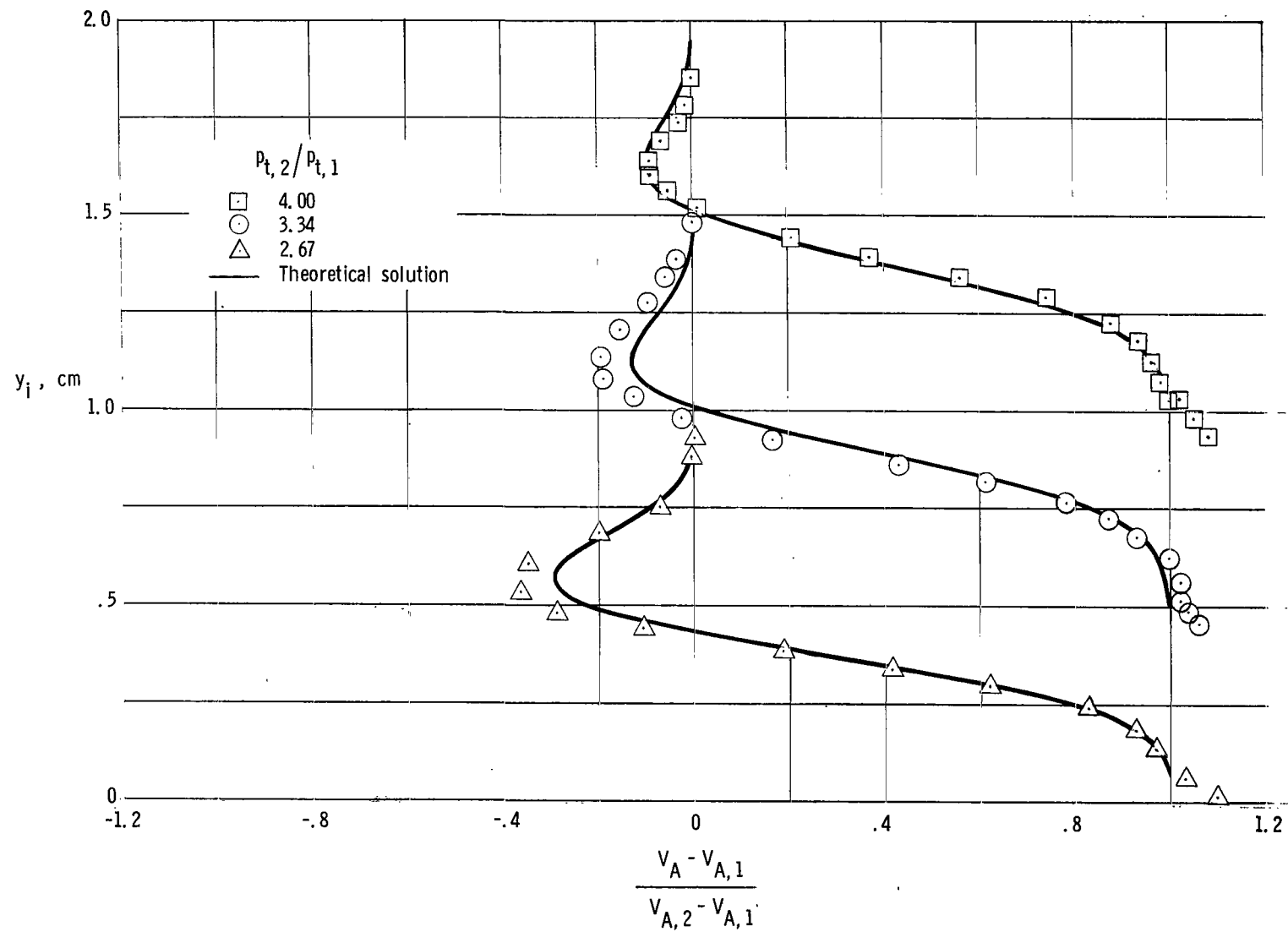
(b) $x/d = 15.0$.

Figure 17.- Continued.

Legend:

$p_{t,2}/p_{t,1}$

□ 4.00
○ 3.34
△ 2.67
— Theoretical solution

y-axis: y_i, cm

x-axis: $\dfrac{V_A - V_{A,1}}{V_{A,2} - V_{A,1}}$
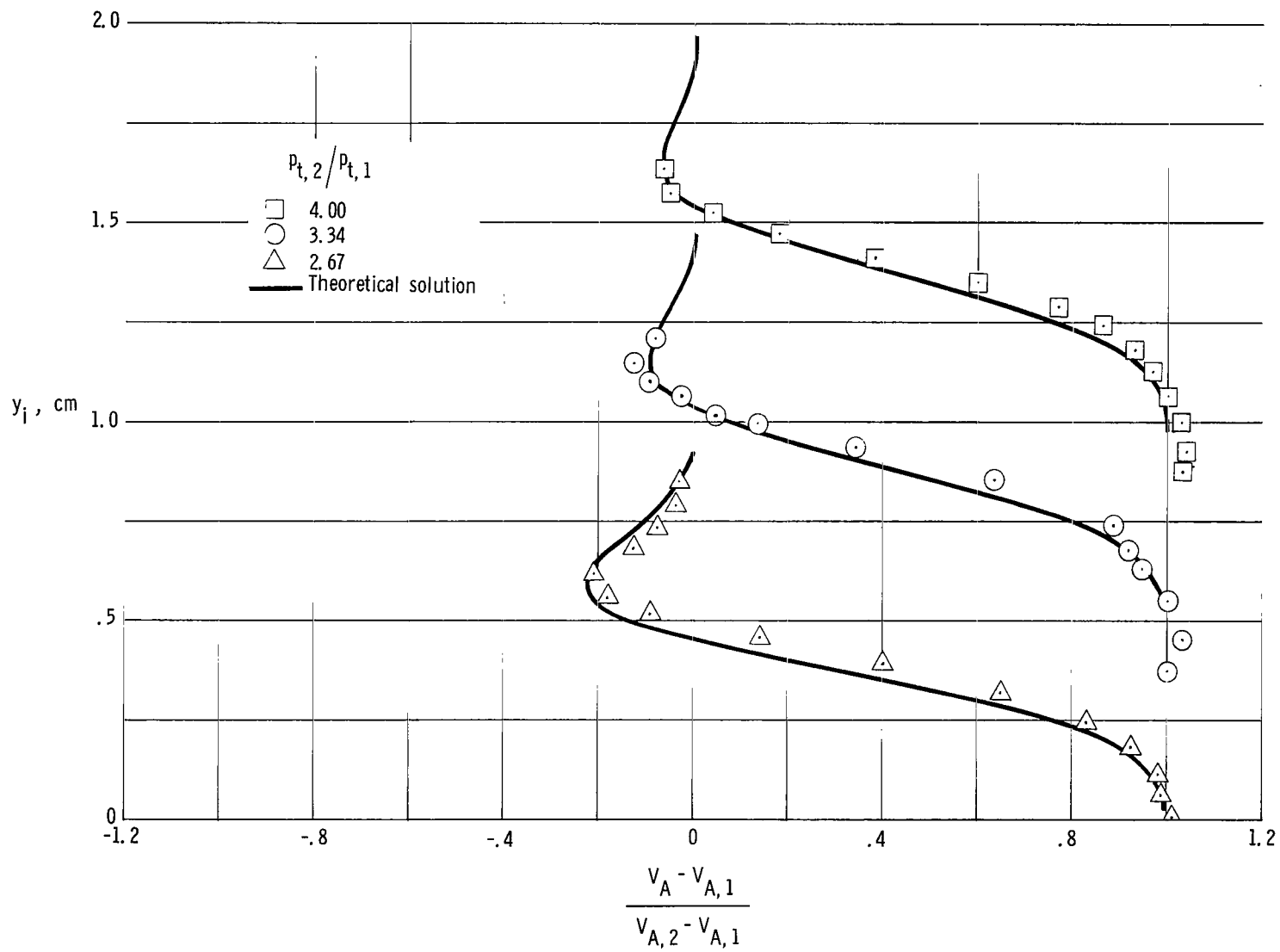
(c) x/d = 16.0.

Figure 17.- Concluded.
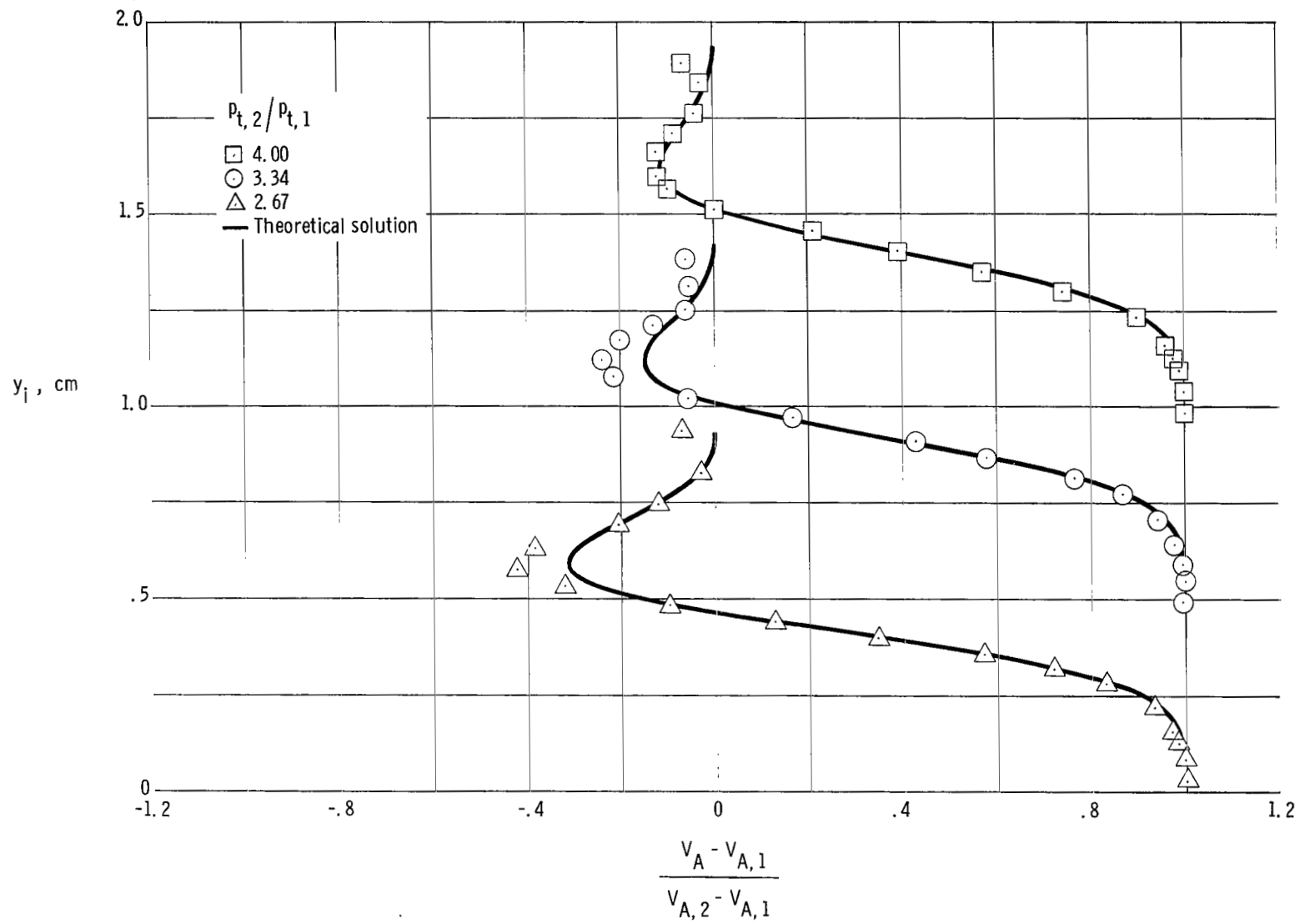
(a) x/d = 14.0.

Figure 18.- Correlation of theoretical velocity profiles with data behind shock system. $\varepsilon = Kr_{1/2}(\rho V)_{\text{¢}}$, with $K = 0.0046$ in the shock region followed by $K = 0.0013$.
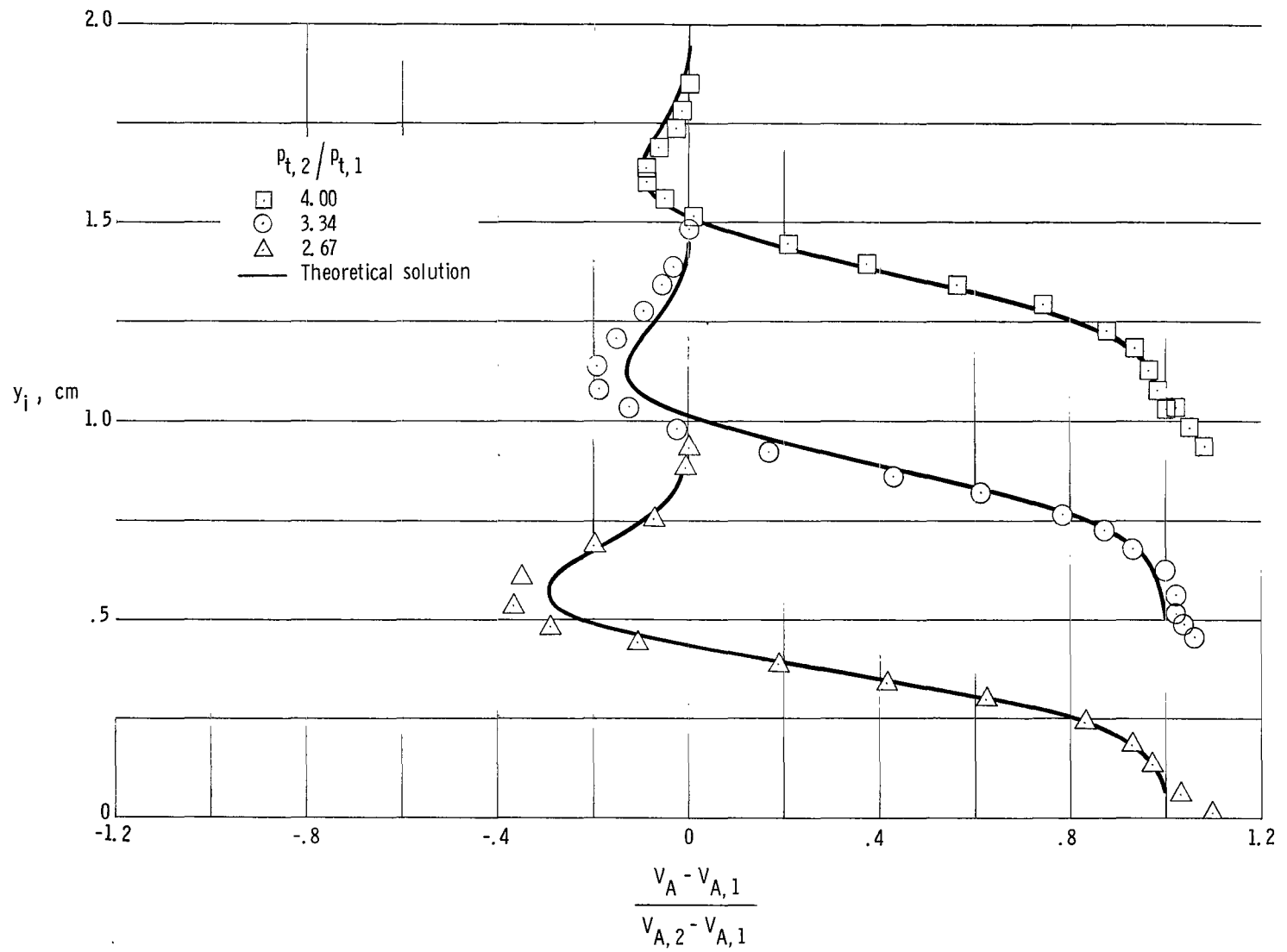
(b) x/d = 15.0.

Figure 18.- Continued.

$$\frac{V_A - V_{A,1}}{V_{A,2} - V_{A,1}}$$

(c) x/d = 16.0.

Figure 18.- Concluded.
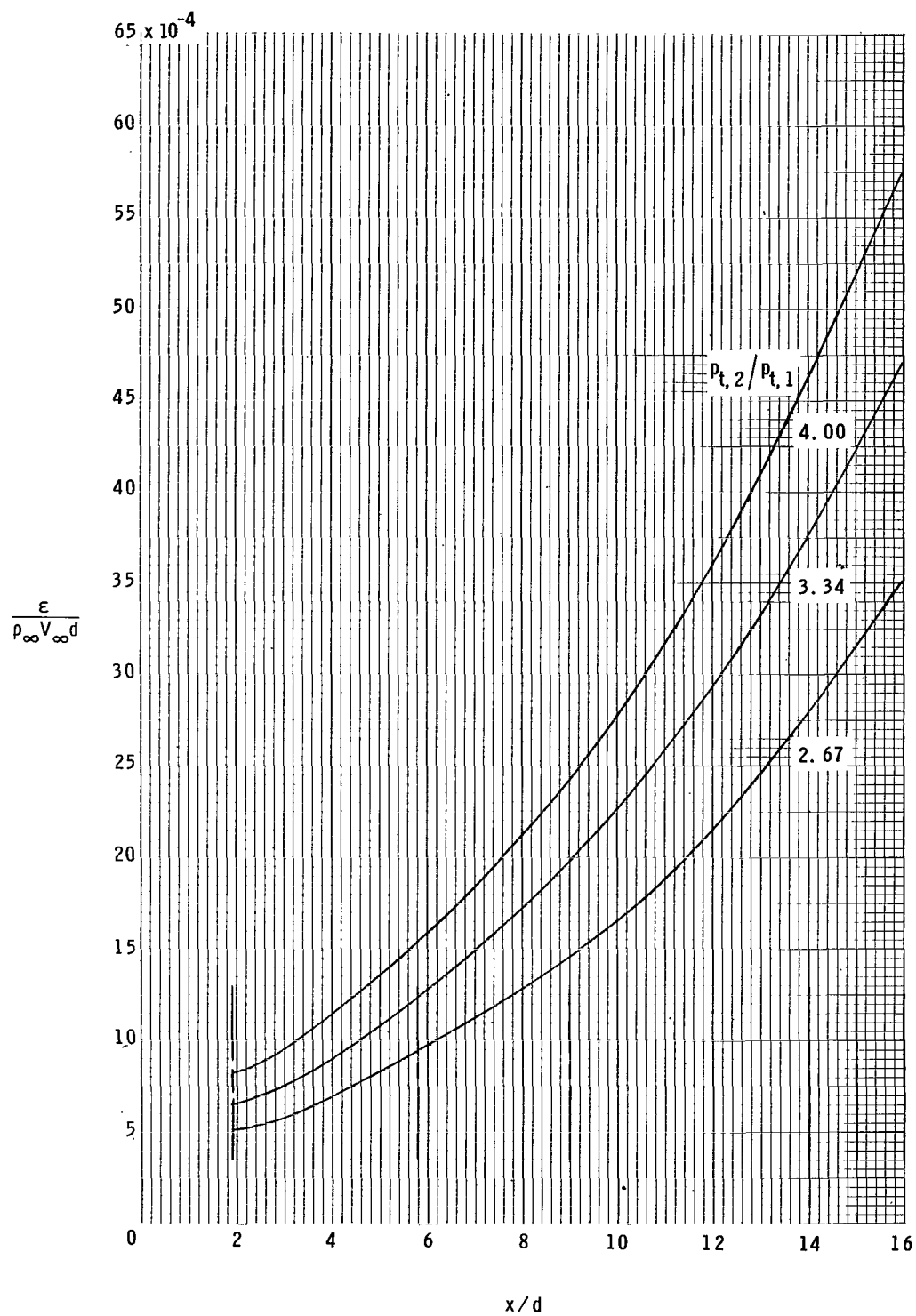
Figure 19.- Theoretical eddy-viscosity distributions. $\varepsilon = KJ(\rho V)_{\mathbb{C}}$, with $K = 0.0065$.
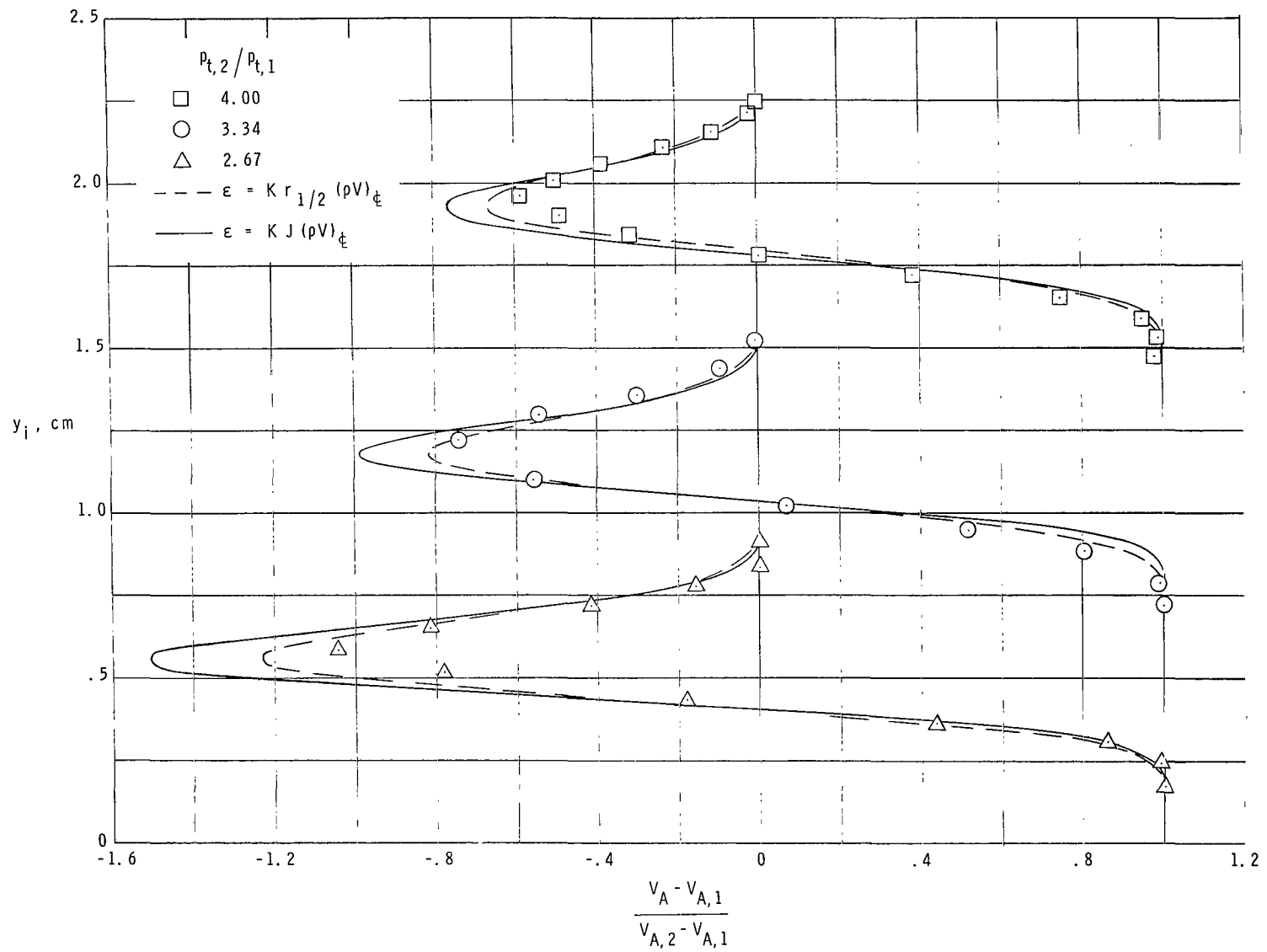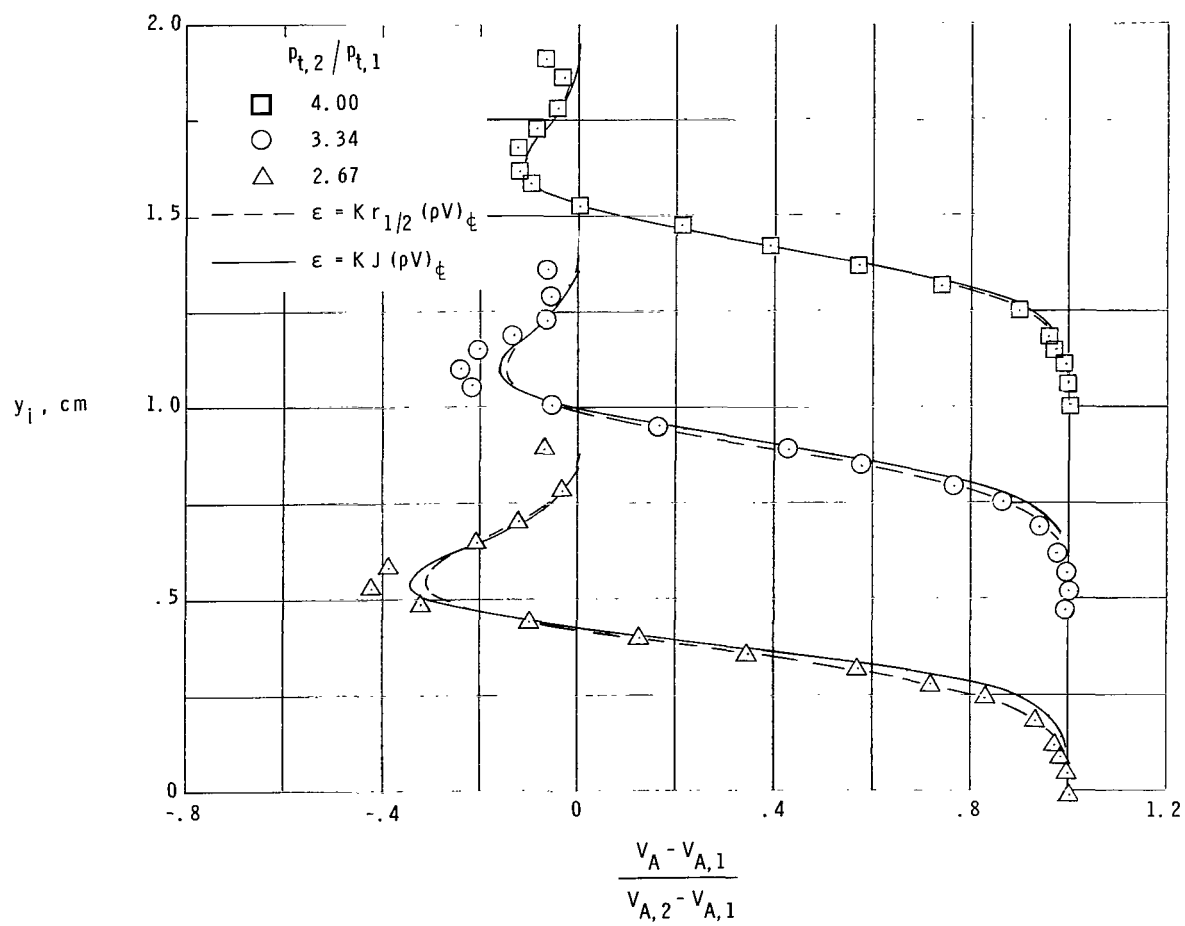
(a) x/d = 5.8.

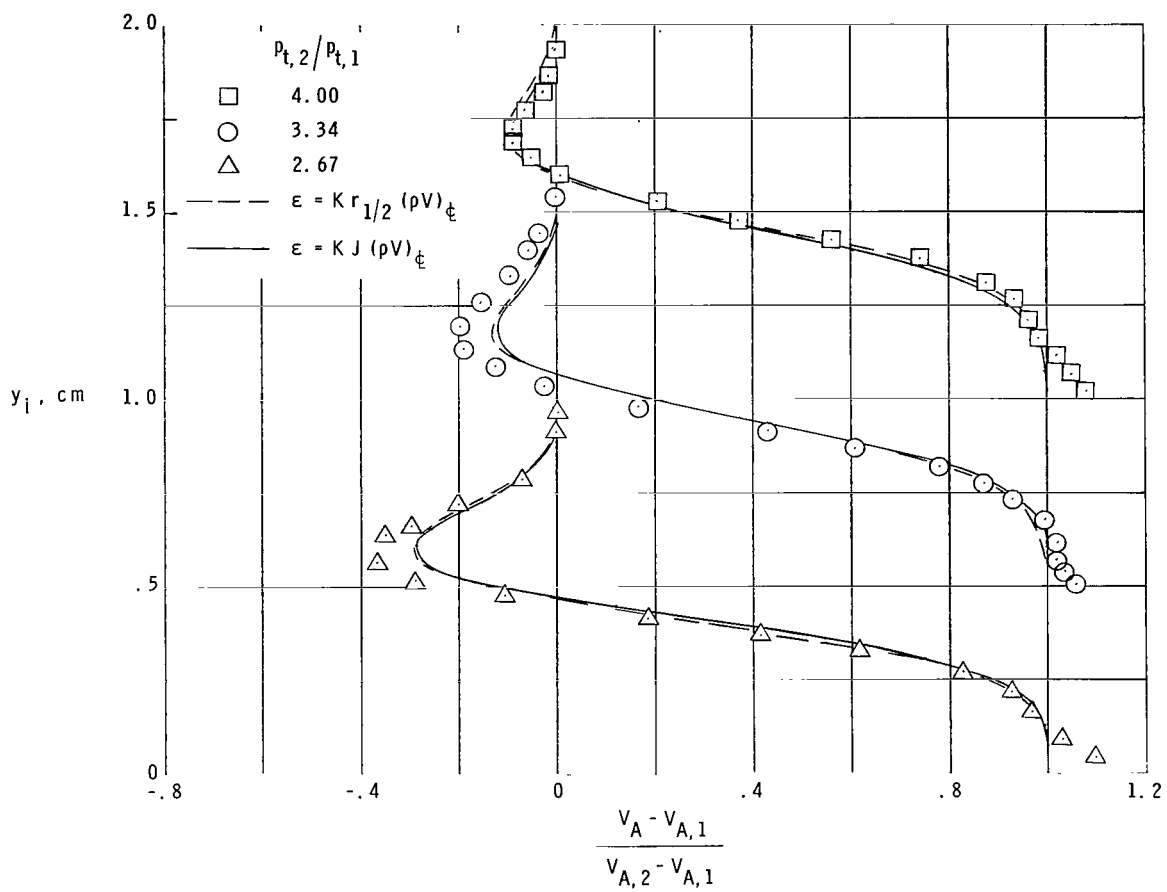Figure 20.- Comparison of theoretical solutions with data.

(b) x/d = 9.0.

Figure 20.- Continued.

y_i , cm

$p_{t,2} / p_{t,1}$

☐   4.00
○   3.34
△   2.67
- - - $\varepsilon = K\, r_{1/2}\, (\rho V)_{\,\mathcal{L}}$
——— $\varepsilon = K\, J\, (\rho V)_{\,\mathcal{L}}$
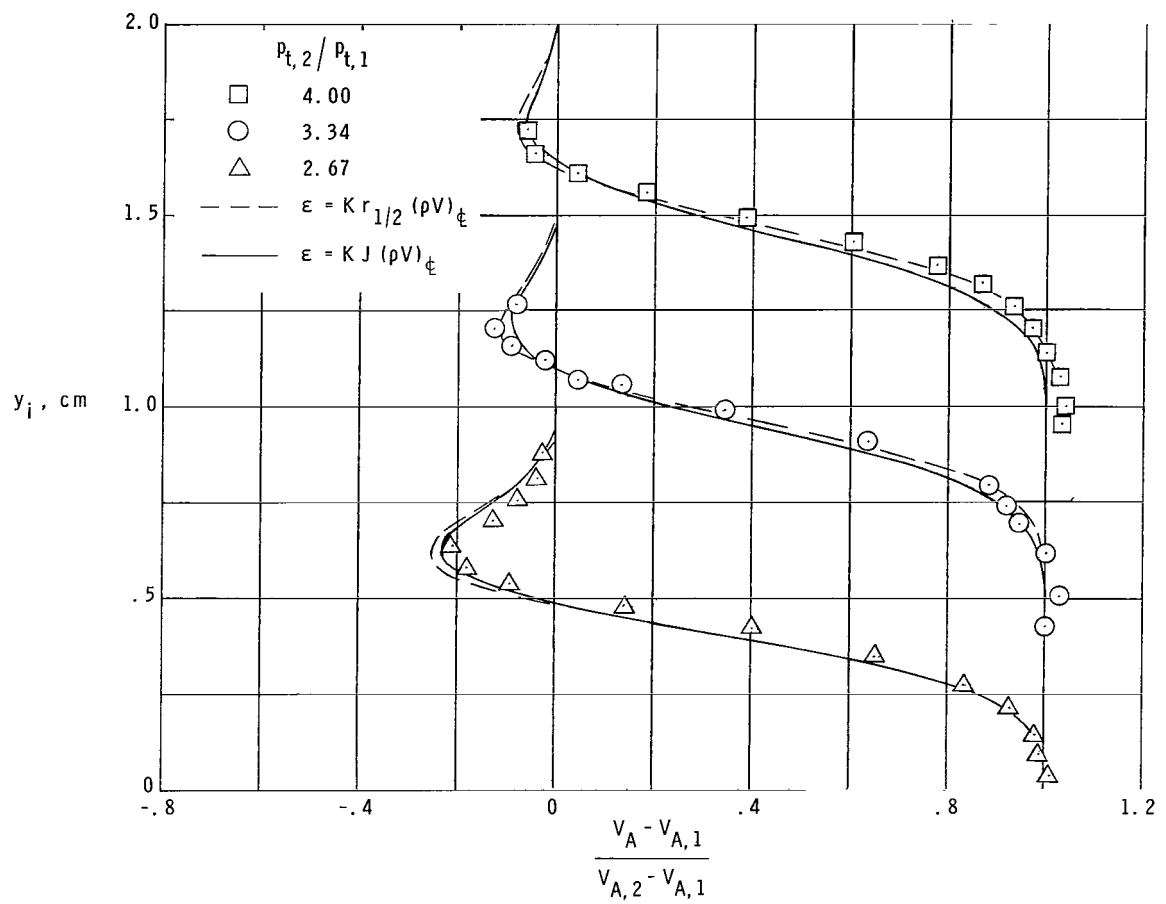
$$\frac{V_A - V_{A,1}}{V_{A,2} - V_{A,1}}$$

(c)   x/d = 14.0.

Figure 20.- Continued.

(d) $x/d = 15.0$.

Figure 20.- Continued.

(e) x/d = 16.0.

Figure 20.- Concluded.

$$\int_{\frac{x}{d}=1.9}^{\frac{x}{d}} \frac{\epsilon}{\rho_\infty V_\infty d} \, d\left(\frac{x}{d}\right)$$

400×10^{-4}

360

320

280

240

200

160

120

80

40

0

$\epsilon = K \, r_{1/2} \, (\rho V)_{\text{℄}}$ $\begin{cases} K = 0.0013 & 10.2 \geqq x/d \geqq 13.7 \\ K = 0.0046 & 10.2 < x/d < 13.7 \end{cases}$

$\epsilon = K \, J \, (\rho V)_{\text{℄}}$ $\qquad K = 0.0065$

320×10^{-4}

280

240

200

160

120

80

40

0

240×10^{-4}

200

160

120

80

40

$p_{t,2} / p_{t,1}$

4.00

3.34

2.67

x/d axis: 0 2 4 6 8 10 12 14 16

x/d
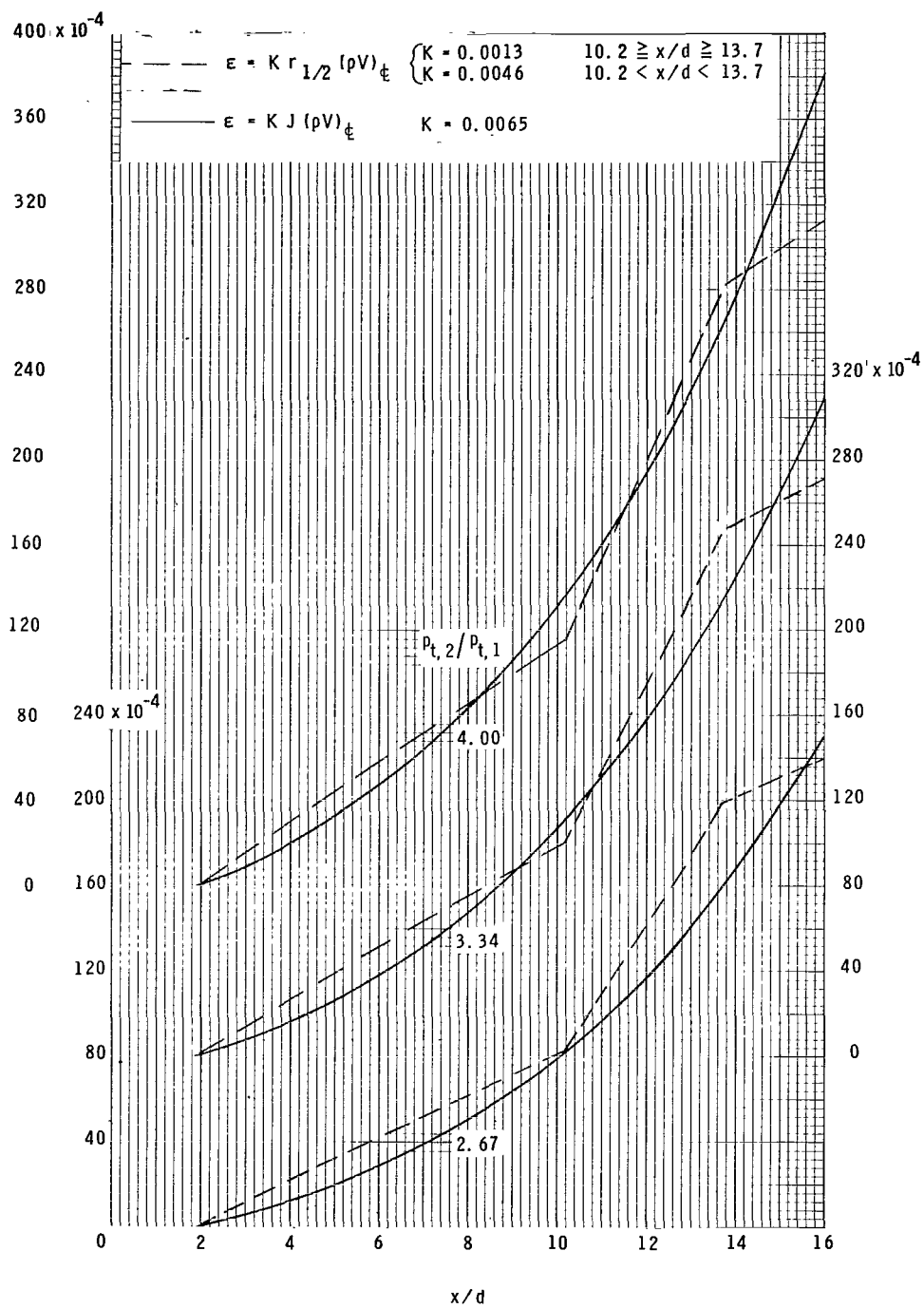
Figure 21.- Integral of eddy viscosity.

$$\textcircled{1} \quad \epsilon = K\, r_{1/2}\, (\rho V)_{\mathfrak{k}} \quad \begin{cases} K = 0.0013 & 10.2 \geqq x/d \geqq 13.7 \\ K = 0.0046 & 10.2 < x/d < 13.7 \end{cases}$$

$$\textcircled{2} \quad \epsilon = K\, J\, (\rho V)_{\mathfrak{k}}, \quad K = 0.0065$$

$$\textcircled{3} \quad \epsilon = K\, W\left[(\rho V)_{\mathfrak{k}} - (\rho V)_{min}\right], \quad K = 0.0031$$

$$\textcircled{4} \quad \epsilon = K\left(\frac{x}{d}\right)^{0.8}, \quad K = 0.00105$$

$$\textcircled{5} \quad \epsilon = K, \quad K = 0.0052$$

$$\int_{\frac{x}{d}=1.9}^{\frac{x}{d}} \frac{\epsilon}{\rho_\infty V_\infty d}\, d\!\left(\frac{x}{d}\right)$$

$$\frac{\epsilon}{\rho_\infty V_\infty d}$$

x / d

x / d
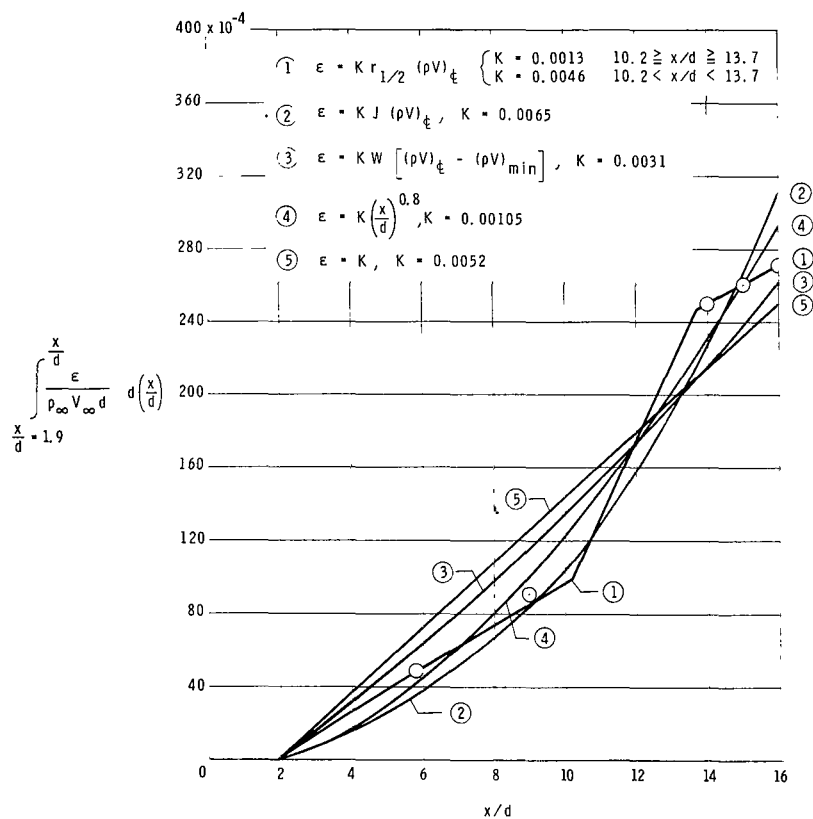
(a) Integral of eddy viscosities.
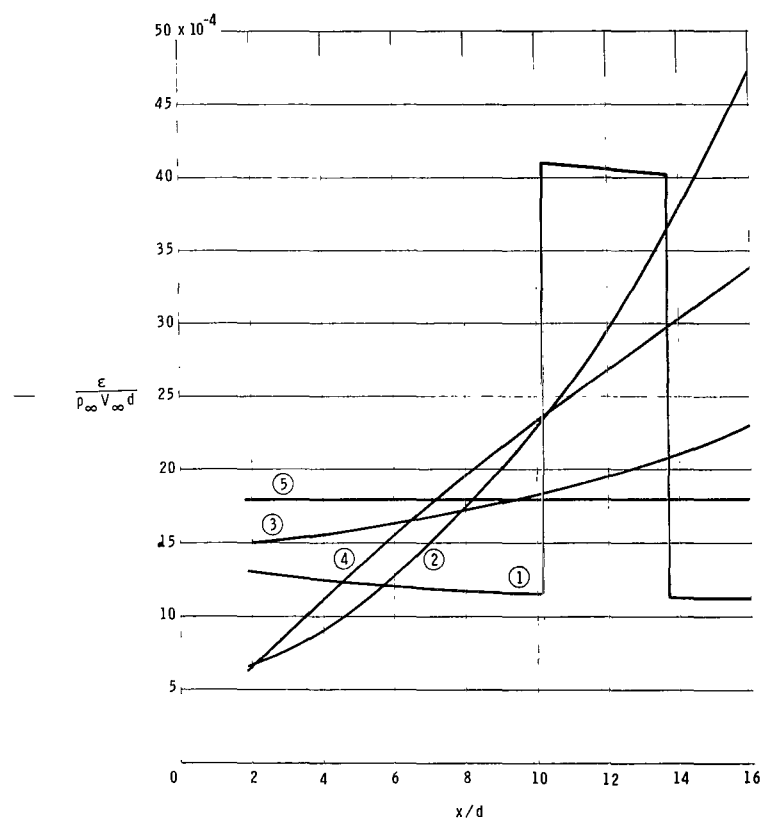
(b) Eddy viscosities.

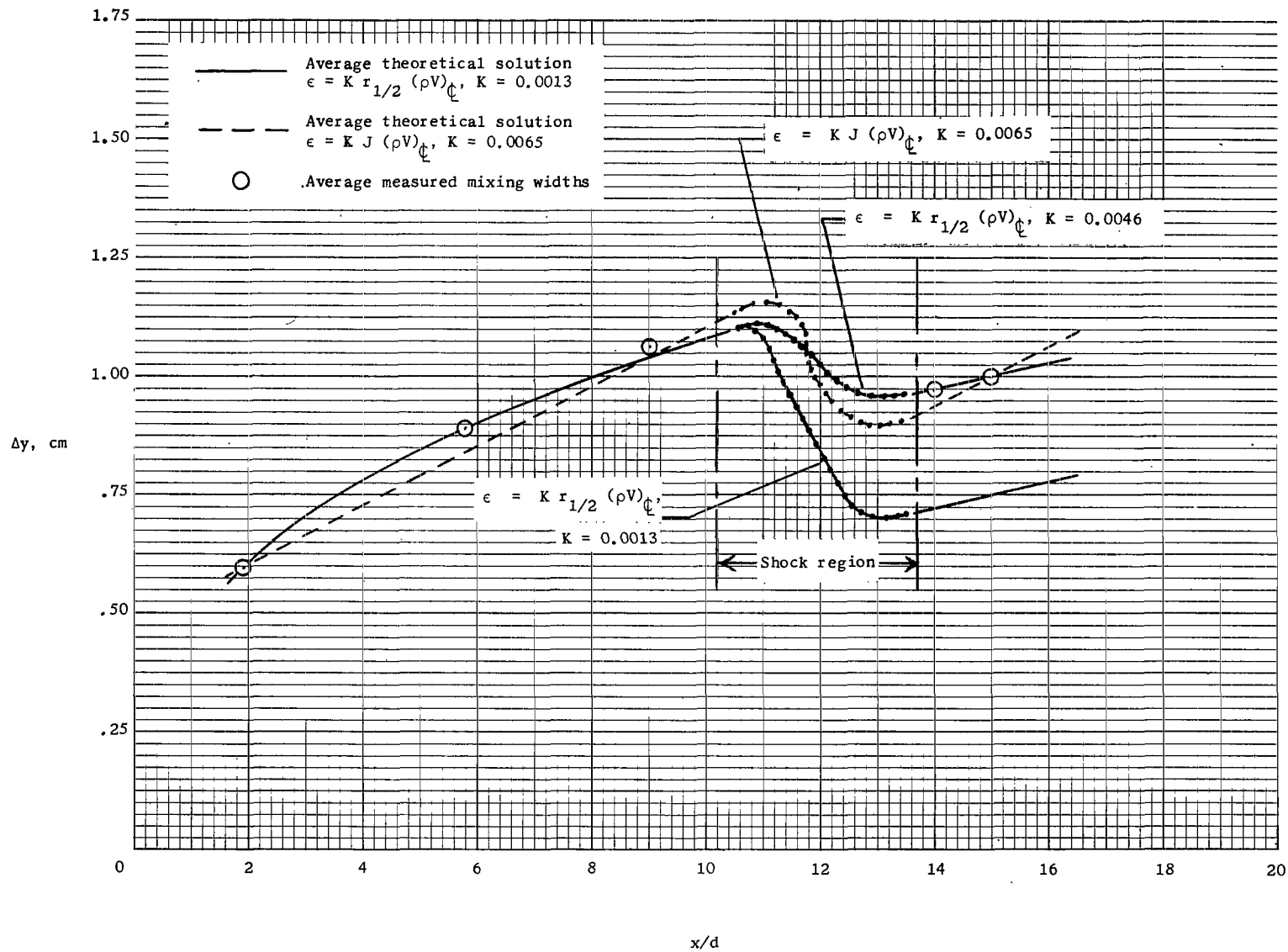Figure 22.- The results of several different viscosity models for $p_{t,2}/p_{t,1} = 3.34$.

Δy, cm

Figure 23.- Average mixing widths corresponding to constant values of static pressure on either side of the shock system.

x/d

FIRST CLASS MAIL

POSTMASTER: If Undeliverable (Section 15: Postal Manual) Do Not Retu

"The aeronautical and space activities of the United States shall be conducted so as to contribute . . . to the expansion of human knowledge of phenomena in the atmosphere and space. The Administration shall provide for the widest practicable and appropriate dissemination of information concerning its activities and the results thereof."

— NATIONAL AERONAUTICS AND SPACE ACT OF 1958

NASA SCIENTIFIC AND TECHNICAL PUBLICATIONS

TECHNICAL REPORTS: Scientific and technical information considered important, complete, and a lasting contribution to existing knowledge.

TECHNICAL NOTES: Information less broad in scope but nevertheless of importance as a contribution to existing knowledge.

TECHNICAL MEMORANDUMS: Information receiving limited distribution because of preliminary data, security classification, or other reasons.

CONTRACTOR REPORTS: Scientific and technical information generated under a NASA contract or grant and considered an important contribution to existing knowledge.

TECHNICAL TRANSLATIONS: Information published in a foreign language considered to merit NASA distribution in English.

SPECIAL PUBLICATIONS: Information derived from or of value to NASA activities. Publications include conference proceedings, monographs, data compilations, handbooks, sourcebooks, and special bibliographies.

TECHNOLOGY UTILIZATION PUBLICATIONS: Information on technology used by NASA that may be of particular interest in commercial and other non-aerospace applications. Publications include Tech Briefs, Technology Utilization Reports and Notes, and Technology Surveys.

Details on the availability of these publications may be obtained from:

SCIENTIFIC AND TECHNICAL INFORMATION DIVISION

NATIONAL AERONAUTICS AND SPACE ADMINISTRATION
Washington, D.C. 20546